



THE UNIVERSITY *of* EDINBURGH

This thesis has been submitted in fulfilment of the requirements for a postgraduate degree (e. g. PhD, MPhil, DClinPsychol) at the University of Edinburgh. Please note the following terms and conditions of use:

- This work is protected by copyright and other intellectual property rights, which are retained by the thesis author, unless otherwise stated.
- A copy can be downloaded for personal non-commercial research or study, without prior permission or charge.
- This thesis cannot be reproduced or quoted extensively from without first obtaining permission in writing from the author.
- The content must not be changed in any way or sold commercially in any format or medium without the formal permission of the author.
- When referring to this work, full bibliographic details including the author, title, awarding institution and date of the thesis must be given.

Increasing Knowledge Return from Data for Floating Tidal Energy

Jan Dillenburger-Keenan



THE UNIVERSITY
of EDINBURGH

Doctor of Engineering

THE UNIVERSITY OF EDINBURGH

2024

Abstract

Renewable energy is seen by many as the key to unlocking a future without fossil fuels for electricity generation. Tidal energy represents an untapped predictable energy source, the commercial exploitation of this resource is possible with decreased costs. Data are a key to further the understanding of design limitations and operations of a tidal turbine in order to reduce costs but data are often expensive to obtain.

The subject of this thesis is the O2, a 2 MW floating tidal turbine developed and installed by Orbital Marine Power. Four research studies in this thesis demonstrate how the implementation of data-based methods can reduce costs for the tidal sector. These studies pertain to: the streamlining of legacy data processing methods; reprocessing onboard, non-wave specific, data streams to calculate environmental wave statistics; validation of an existing computational model using operational field data; and the application of new sensors and techniques for incident flow measurement for tidal turbine power performance assessments.

A range of legacy data processing methods are streamlined to enable quick execution time or better access to data for the engineering team. Fast data processes are shown to reduce task person-hours by a factor of 10, while better access to data aided operational safety. A number of methods for calculating wave statistics are presented using onboard data streams. Wave heights accurate to ± 0.5 m were achieved using REDACTED. A loads model validation campaign demonstrated the accuracy of the drive train modelling software used by Orbital Marine Power in predicting loads at two different operational set points. Limitations around fatigue loading for a given wave height were shown as well as yield implications of setting controller based load limits for operation. Limitations in the current standard for incident resource measurement when applied to floating tidal energy were explored and outlined. The application of a horizontal rotor height ADCP enabled the turbine-relative profiling of incoming flow that could be used as an alternative to established incident flow measurement techniques.

Exploiting data sets for more than one use and applying sensors with a multi-use intention gives a low cost means of gaining more information about a system. This is important for a sector looking to reduce costs.

Lay Summary

Tidal energy is one of the only predictable forms of renewable energy from environmental flows. The resource, however, is yet to be exploited to a commercial level with cost being a key barrier. One method of reducing costs for the industry is the recycling of ‘expensive to obtain’ data sets. This thesis demonstrates how knowledge can be increased at low cost by analysing data that were recorded initially for another purpose or by using sensors with more than one purpose. The thesis is based around data from the O2, a 2 MW tidal turbine designed, deployed, and operated by Orbital Marine Power.

The first study took legacy data processes and updated them to make them faster. This allowed these processes to be applied over a longer time period. This not only increased access to data for the engineering team, but also increased safety for the operational team.

The second study looked at how to calculate wave statistics using data from physical motions of the turbine. Two methods are presented with the more complex method providing better results. The wave statistic code can calculate wave height and period applicable to a range of use cases.

The third study validated a computational model used by Orbital Marine Power in the design of their turbines. The model was validated at two different turbine maximum power levels demonstrating the applicability of the model software under a range of conditions. Going forward, this study is an important means of developing confidence in the modelling software as a tool which, in turn, allows for more accurate modelling and therefore reduced costs.

The final study looked at how the sector records incoming flow and how methods used for seabed mounted turbines are not necessarily directly transferable to the floating tidal sector. An alternative method was explored with limitations outlined. This section informs the standards makers of adaptations to standard practices needed to help floating designs combat cost associated with the recording of incoming flow.

Tidal resource is a constant for countries with the correct coastal topography. Cost is the only barrier in our ability to exploit the resource for electricity generation. Reducing cost from every facet of the technology brings commercialisation closer.

Acknowledgements

This EngD document was made possible by a range of people.

I would like to thank Calum Miller as my industrial supervisor for his support and technical guidance throughout my EngD work. Thanks also goes to Dr. Brian Sellar as my principal supervisor for his valued insights along with the rest of the supervisory team, Dr. Helen Smith and Dr. Erkan Oterkus.

I would like to thank the whole team at Orbital Marine Power for including me as a fellow employee for the three years I spent on my EngD. Particular thanks goes to Mark Byers, Lindsey Amos, and the rest of the hydrodynamics team for sharing their knowledge and expertise in all things tidal energy.

I would like to acknowledge all the people behind IDCORE for, not only their support, but for all they do to educate students to make a difference in the offshore renewable sector. A mention also for the 2020 IDCORE cohort who's cohesion helped to navigate online corona virus modules in the early days of IDCORE and for the sounding board they provided as we tackled our projects simultaneously. I would also like to acknowledge the funders of IDCORE, UK Research and Innovation as part of the EPSRC and NERC, Grant EP/S023933/1.

I would also like to thank Aimee and my parent for their unwavering support and for making the write-up period as pain free as possible.

Declaration

I declare that this thesis was composed by myself, that the work contained herein is my own except where explicitly stated otherwise in the text, and that this work has not been submitted for any other degree or professional qualification except as specified.

Jan Dillenburger-Keenan

Contents

Abstract	ii
Lay Summary	iii
Acknowledgements	iv
Declaration	v
Figures and Tables	xi
Nomenclature	xvi
Acronyms	xviii
1 Introduction to Tidal Energy	1
1.1 Green energy and the energy mix	1
1.2 Tidal energy	6
1.2.1 Tidal sites	7
1.2.2 Fall of Warness	10
1.3 Research gaps	14
1.3.1 Environment monitoring	14
1.3.2 Model validation	15
1.3.3 Velocimetry	15
1.4 Research aims and objectives	16
1.5 Thesis structure	19
2 Orbital Marine Power	21
2.1 Company philosophy	21
2.2 O2	21
2.2.1 Design Philosophy	22
2.2.2 Sensors on board the O2	23
2.2.3 O2 data wrangling	25
2.3 Future Orbital Marine Power data pipeline	26

CONTENTS

I	Increasing Knowledge-Return from Data by Re-Analysing Existing Data.	28
3	Data Handling Advancements for the Design and Operation of the O2	29
3.1	Introduction	29
3.1.1	Harmonic analysis for tide speed prediction on-site	29
3.1.2	Fatigue calculations for the analysis of turbine lifetime	30
3.2	Streamlining data processes for the analysis of O2 operational data	31
3.2.1	Forecasting tide speeds for operation and maintenance of the O2 using harmonic analysis	31
3.2.2	Efficiency savings in the calculation of fatigue parameters of the O2 for confidence in lifetime predictions	34
3.3	Application and Impact	37
3.4	Conclusion	38
4	Estimating Tidal Site Wave Statistics for the Design, Operation, and Maintenance of the O2 Using the Existing Onboard Sensor Suite	39
4.1	Wave statistics introduction	39
4.1.1	Wave theory	40
4.1.2	Recording oceanic waves	42
4.1.3	Simulating waves using modelling software	46
4.1.4	The wave climate in the Fall of Warness	47
4.1.5	Chapter aims	48
4.2	Materials used	48
4.2.1	Wave related time series data available from the O2	48
4.2.2	REDACTED	49
4.2.3	On-site wave statistics dataset	49
4.2.4	Statistical tests	50
4.3	Methodology 1: The Dispersion Relation Method for the calculating of Hs and Tp	51
4.4	Results 1: The Dispersion Relation Method for the calculating of Hs and Tp	53
4.4.1	Wave Height	53
4.4.2	Peak Wave Period	54
4.5	Methodology 2: REDACTED	56
4.6	Discussion	56
4.6.1	Methodology 1 Limitations	57
4.6.2	Methodology 2 Limitations	58

CONTENTS

4.6.3	Extending wave statistics to 3 dimensions	58
4.7	Application and impact	60
4.8	Conclusion	61
5	Validation of a Numerical Simulation Tool Used to Model O2 Drive-Train Loads	63
5.1	Introduction	63
5.1.1	Tidal Bladed	64
5.1.2	Tidal terminology	65
5.1.3	Aims and Objectives	66
5.2	Materials and Methods	66
5.2.1	Tidal Bladed model	66
5.2.2	Model run matrix	67
5.2.3	Data prepossessing	68
5.2.4	Blade coordinate system	70
5.2.5	Data post-processing	72
5.3	Results	75
5.3.1	Blade root My metrics	75
5.3.2	Blade root Mx metrics	75
5.3.3	Rotor thrust metrics	75
5.3.4	Rotor torque derived from blades loads metrics	76
5.3.5	Rotor torque from low speed shaft (LSS) sensor metrics	76
5.3.6	Generator speed metrics	77
5.3.7	Blade pitch angle metrics	77
5.3.8	Blade pitch motor metrics	77
5.4	Discussion	78
5.4.1	Tidal site horizontal flow shear	78
5.4.2	Leg shadow	78
5.4.3	Controller	78
5.4.4	Blade derived values	78
5.4.5	Outliers	79
5.4.6	Yield implications of load limit	79
5.4.7	Limitations	79
5.5	Application and Impact	80
5.6	Conclusion	80

CONTENTS

II Floating Tidal Turbine Incident Velocimetry and Increasing Knowledge-Return from Data through Novel Sensor Applications 82

6 Application of ADCPs for Floating Tidal Turbine Incident Resource Measurement	83
6.1 Introduction	83
6.1.1 ADCP principal of operation	83
6.1.2 The application of ADCPs in the full scale tidal sector	86
6.1.3 Research gaps	90
6.2 Incident flow measurement in accordance with TS 62600-200	91
6.2.1 Methodology	91
6.2.2 Results	93
6.2.3 Discussion	103
6.3 Application and impact	107
6.4 Conclusion	108
7 Application of a Horizontal Turbine Mounted Hub Height ADCP for Incident Resource Measurement	110
7.1 Introduction	110
7.1.1 Research gaps	111
7.1.2 Aims and objectives	111
7.2 Method	112
7.2.1 The ADCP	112
7.2.2 Introduction to dataset recorded by the horizontal ADCP and the corresponding operating and environmental conditions	114
7.2.3 Data quality control procedure	114
7.2.4 Single beam maximum range	116
7.2.5 Incident flow from divergent beams	117
7.3 Results	117
7.3.1 Single beam range	117
7.3.2 Incident flow from divergent beams	120
7.4 Discussion	121
7.4.1 Horizontal ADCP for power performance assessment	122
7.4.2 Additional applications of a horizontal hub height ADCP	125
7.4.3 Direct measurement of turbine blockage using a horizontal ADCP	126
7.5 Application and impact	129
7.6 Conclusion	129

CONTENTS

8	Conclusions	131
8.1	Thesis conclusion and novelty	131
8.1.1	Estimating tidal site wave statistics for the design, operation, and maintenance of the O2 using the existing onboard sensor suite . . .	132
8.1.2	Validation of a numerical simulation tool used to model O2 drive-train loads	133
8.1.3	Application of ADCPs for floating tidal turbine incident resource measurement	134
8.1.4	The application of a horizontal turbine mounted hub height ADCP for incident resource measurement	134
8.2	Research contributions	135
8.2.1	Key novelty	135
8.3	Further Work	137
8.3.1	Estimating tidal site wave statistics for the design, operation, and maintenance of the O2 using the existing onboard sensor suite . . .	137
8.3.2	Validation of a numerical simulation tool used to model O2 drive-train loads	138
8.3.3	Application of ADCPs for floating tidal turbine incident resource measurement	138
8.3.4	The application of a horizontal turbine mounted hub height ADCP for incident resource measurement	139
 Appendices		
A	Dissemination of works	141
	Bibliography	142

Figures and Tables

Figures

1.1	Map of potential UK tidal project sites including sites under development, sites previously under development, and speculative sites (Coles et al., 2021). . .	10
1.2	EMEC Fall of Warness tidal test site. The island of Eday shown top right. Map courtesy of openstreetmap.org, test site boundary courtesy of EMEC. . .	12
1.3	Holistic view of how O2 data are handled from data sources to processing and presentation to the end user. Areas where this thesis adds value are outlined in orange.	17
1.4	Data streams described in Figure 1.3 divided by thesis structure, Part I and II, and chapter.	20
2.1	Side profile of the O2 2 MW tidal turbine designed, built, and installed by Orbital Marine Power.	22
2.2	Schematic of the future data pipeline for Orbital Marine Power designed to handle large volumes of data from multiple turbines and multiple arrays . . .	26
3.1	Process involved in the streamlining of the tidal prediction forecasting including the identification of the thesis contribution in this task.	32
3.2	Sample of the Excel output from the streamlined tidal speed forecasting tool. .	33
3.3	Sample of the time series graphic output from the streamlined tidal speed forecasting tool.	34
3.4	Process involved in the streamlining of the damage calculation method including the identification of the thesis contribution in this task.	36
3.5	REDACTED	37
4.1	Oceanic waves classified by frequency (adapted from Munk (1950))	40
4.2	Wave recording trilemma (Story, Fu, & Hackett, 2011).	42
4.3	Directional spread of wave energy example (Holthuijsen, 2010).	45
4.4	Map of the Fall of Warness tidal test site showing its location relative to neighbouring islands. Map courtesy of OpenStreetMap.org, test site boundary courtesy of European Marine Energy Centre (EMEC).	47

FIGURES AND TABLES

4.5 ADCP dataset cumulative percentage with respect to wave height showing the range of wave heights recorded in the set. 49

4.6 Simple schematic of the O2 following the surface of a perfect sinusoidal wave. . 51

4.7 BA plot showing the difference between the seabed ADCP dataset wave height and the Dispersion Relation Method wave height against the mean of the two variables: where H_{SDP} is the significant wave height calculated from the dispersion relation and H_{SADCP} is the ADCP measure of significant wave height. A line of best fit, the mean difference, as well as the ± 1.96 *difference standard deviation limits are shown. 53

4.8 Cumulative probability distribution function of dispersion calculated significant wave height (H_{SDP}) and sea bed ADCP recorded significant wave height (H_{SADCP}). 54

4.9 BA plot showing the difference between the seabed ADCP measured peak period (T_{PADCP}) and the Dispersion Relation Method peak period (T_{PDP}) against the mean of the two variables. A line of best fit, the mean difference, as well as the ± 1.96 *mean difference limits are shown. 55

4.10 Cumulative probability distribution function of dispersion relation calculated peak wave period (T_{PDP}) and sea bed ADCP recorded peak wave period (T_{PADCP}). 55

4.11 Pitching period and tide speed against time. 59

5.1 Example of a typical power curve for a pitch regulated horizontal axis turbine for wind or tidal. This is not the power curve from any particular device and only serves as an example to enable discussion of flow speed region terminology. 65

5.2 Torque from LSS strain gauge measurement and nacelle temperature for starboard nacelle against time showing a temperature dependency of the sensor. . 70

5.3 Blade root coordinate system used for both the numerical model of the O2 and the O2 itself (DNV GL, 2016b). 71

5.4 REDACTED 79

6.1 ADCP profiling range divided into bins with a cell size. The blanking distance and end of profile are also shown (Nortek AS, 2018). 84

6.2 ADCP deployment regions following IEC/TS 62600-200 guidance for a power performance assessment. Both possible orientations are shown with lengths defined in equivalent rotor diameters (D_E). Image adapted from IEC (2013). . 90

6.3 Significant wave height on site for the duration of the September 2022 dataset. 92

FIGURES AND TABLES

6.4 O2 10-minute average operational location for 30 days with respective location of TS 62600-200 defined ADCP permissible deployment areas. 93

6.5 A_R against tide speed. Each tide speed value represents the middle of a 0.625 m/s speed bracket. Marker size represents the percentage of energy generated for ebb or flood in that tide speed bracket for this dataset. 95

6.6 O2 operational location 10-minute average for a month with respective location of ADCP boxes. 96

6.7 Representation of side lobe contamination limiting measurable water column in front of rotor to D^* , where $D^* = D - D_S$, with D being the rotor diameter and D_S being the region of rotor measurement distorted by side lobe contamination. ADCP not to scale. 98

6.8 Area of the Fall of Warness tidal test site where 30 m depth is exceeded. Map courtesy of openstreetmap.org, test site boundary courtesy of EMEC, and bathymetry courtesy of Orbital Marine Power. 98

6.9 Representation of blanking distance limiting measurable water column in front of rotor to D^* . Where $D^* = D - D_B$, with D being the rotor diameter and D_B being the region of rotor measurement omitted due to blanking distance. ADCP not to scale. 99

6.10 Map of the Fall of Warness showing the location of transect lines across which data were extracted from the TELEMAC 3D model. Map courtesy of openstreetmap.org, test site boundary courtesy of EMEC. 101

6.11 Four transects of the Fall of Warness showing the percentage of time, over a day, each location along the transect meets the IEC 10% threshold for horizontal shear between ADCPs in Orientation B. Data is shown for absolute speeds over 1.5 m/s with high resource indicating locations where absolute flow speed reaches above 2.5 m/s. 102

7.1 Leg ADCP location as viewed from aft of the O2 with distances to the hub center shown. 112

7.2 Leg ADCP location as viewed from the port side of the O2 with distance to the hub center shown. 113

7.3 Leg ADCP coordinate system used in this chapter 113

7.4 Significant wave height for duration of non-generation dataset. 114

7.5 Mean amplitude of Beam 4 against distance in front of the horizontal ADCP showing sea surface strike around 17 m. 118

FIGURES AND TABLES

7.6 Percentage of data removed in Beam 5 after filters applied, as a function of distance in front of the horizontal ADCP for a range of flow speed brackets. Each sub-figure represents a different filter with each line representing a 0.5 m/s speed bracket with the bracket centre indicated. The total filter affect is shown in the bottom right sub-figure. 119

7.7 Z velocity from beam combinations compared to Beam 5 against distance from horizontal ADCP binned by flow speed. 121

7.8 Significant wave height for duration of generation horizontal ADCP dataset. . 126

7.9 Flow speed binned by beam-wise average (between 20 m and 30 m for 4 days in August 2022 during 2 MW rated power. Each plot is normalised by flow speed at 20 m in front of the horizontal ADCP. 127

7.10 OrcaFlex Location of Beam 5 from the horizontal ADCP in relation to the mooring lines when the turbine is under generation thrust. 128

7.11 Flow speed binned by beam-wise average (between 20 m and 30 m for 4 days in August 2022 during no power generation. Each plot is normalised by flow speed at 20 m in front of the turbine. 128

Tables

1.1 Grid connected tidal energy converters hosted by EMEC in the Fall of Warness (EMEC, 2023c) 13

4.1 Standard oceanic wave statistics of interest. 44

4.2 KS test results for comparison of dispersion derived wave height and seabed ADCP measured wave height. 54

4.3 KS test results for comparison of dispersion derived wave Period and seabed measured wave Period. 54

5.1 Mean and standard deviation of difference between Power Weighted Rotor Average (PWRA) and single hub height bin for forward and aft downward facing ADCPs on board the O2 over a 30 day period covering speeds from -4 to 4 m/s. 68

FIGURES AND TABLES

5.2 Loads related data tags and the associated calculated statistics for the validation of Tidal Bladed including whether a tag was duplicated for Port Side (PS) and Starboard (SB) symmetry. The results sections for each of the metrics are also shown for ease of navigation through this document. 72

6.1 Typical blanking distances for ADCPs using different transmission frequencies. Adapted from Teledyne RD Instruments (2011a). 85

6.2 A_R for dataset divided into ebb and flood for Orientation A and B and into port and starboard for Orientation B. 94

6.3 Percentage of transect span whereby 10% horizontal flow shear limit is met for the entire dataset. This is the percentage of Figure 6.11 where percentage time compliant across the transect is at 100%. 102

7.1 Beam filters applied to horizontal ADCP dataset 115

7.2 Transformed Filters 116

7.3 Horizontal ADCP range in meters for a given acceptable data loss percentage and flow speed. 120

7.4 Range of three horizontal ADCPs deployed on full scale tidal turbines along with manufacturer stated range including the Nortek Signature 500 studied in this paper (Harrold, Ouro, & O’Doherty, 2020; McNaughton, Harper, Sinclain, & Sellar, 2015; Nortek AS, n.d.-a). 123

Nomenclature

η	Wave surface elevation
$\hat{U}_{i,j,n}$	Power weighted current velocity
κ	Wave number
λ	Wave length
ω	Angular frequency
ω_I	Incident wave frequency
ω_R	Resultant wave frequency
ϕ	Pitch angle
ψ	Blade pitch angle
θ	Wave direction
A	Constant ADCP box area
A_C	Coincident area
A_k	Area of location bin
A_R	Percentage area remaining
A_w	Trigonometric wave amplitude
A_{rot}	Rotor area
D	Rotor diameter
D^*	Rotor diameter remaining after removal of contaminated distance
D_1	Diameter of rotor 1
D_2	Diameter of rotor 2
D_B	Rotor diameter distorted by blanking distance
D_E	Equivalent diameter
D_j	Miner's rule damage
D_S	Rotor diameter distorted by side lobe contamination
DEL_j	Damage equivalent load
f^{eq}	Damage equivalent load selected frequency
g	Gravitational acceleration
H	Wave height
h	Water depth
$H_{S_{ADCP}}$	Significant wave height measured from ADCP
$H_{S_{DP}}$	Significant wave height calculated from the dispersion relation

NOMENCLATURE

L^{MF}	Mean load
L^{ult}	Ultimate load
L_i^R	Load range for cycle i
m	S-N curve exponent
N	Number of values inside the 10-minute time window
N_i	Number of allowable cycles at a load range
N_j^{eq}	Number of allowable cycles at the Damage Equivalent Load
n_j^{eq}	Equivalent cycles
T	Wave period
T_j	Damage equivalent load time period
Tp_{ADCP}	Peak period measured from ADCP
Tp_{DP}	Peak period calculated in the dispersion relation
U	Velocity along shear profile
u	Tidal stream velocity
$U_{i,j,k,n}$	Instantaneous tidal current velocity at time j , location bin k , and speed bin i for data point n .
U_{ref}	Shear profile reference velocity
y	Height above sea bed
y_{ref}	Shear profile height reference
Z_5	Z-axis velocities from Beam 5
$Z_{1,2,3,4}$	Z-axis velocities from Beam 1,2,3,4
$Z_{1,3}$	Z-axis velocities from Beam 1 and 3
H_s	Significant wave height
T_p	Peak wave period

Acronyms

ADCP	Acoustic Doppler Current Profiler
AR4	Auction Round 4
AR5	Auction Round 5
BA	Bland-Altman
BEM	Blade Element Momentum
BST	British Summer Time
C-ADCP	Convergent-beam Acoustic Doppler Current Profiler
CFD	Computational Fluid Dynamics
CfD	Contracts for Difference
D-GPS	Differential Global Positioning Systems
DEL	Damage Equivalent Load
EMEC	European Marine Energy Centre
FORCE	Fundy Ocean Research Centre for Energy
GMT	Greenwich Mean Time
GPS	Global Positioning Systems
IEC	International Electrotechnical Commission
IMU	Inertial Measurement Unit
JONSWAP	Joint North Sea Wave Observation Project
KS	Kolmogorov-Smirnov
LSS	Low Speed Shaft
OEMs	Original Engineering Manufacturers
PPA	Power Performance Assessment
PS	Port Side
PTEC	Perpetuus Tidal Energy Centre
PWRA	Power Weighted Rotor Average
QARTOD	Quality Assurance / Quality Control of Real-Time Oceanographic Data
ReDAPT	Reliable Data Acquisition Platform for Tidal energy
RMS	Root Mean Squared
ROC	Renewables Obligation Certificate
SB	Starboard
TS	Technical Specification

NOMENCLATURE

UK United Kingdom

Introduction to Tidal Energy

1.1 Green energy and the energy mix

Energy is an unavoidable requirement for human survival in a modern world, but social responsibility for where this energy comes from has seen an unprecedented shift in recent years. The political sphere has caught up with the scientific world in realising that fossil fuels are finite and their use adds an unsustainable quantity of greenhouse gasses into the atmosphere.

The Kyoto protocol was one of the first internationally concerted attempts to do something about greenhouse emissions (United Nations, 1997). This protocol implemented a system to monitor the emissions from signatory countries allowing for the setting of legally binding targets. Over successive years, countries have come together at numerous conventions to try to ratify change and avoid effects of a warming global temperature.

An overarching theme in these conventions is the need for reduction in reliance on fossil fuels in the energy mix of each country. This reduction in fossil fuel consumption is juxtaposed against an increasing population and increasing energy demand. As a result, not only is there a need for reduction in polluting forms of energy, there is also a requirement to replace this energy with clean alternatives.

Domestic energy usage comes under three main categories; transport, electricity, and space-heating. Traditionally, these energy uses have been serviced by different fuel sources like oil, gas, and coal. Instead of producing fuels for different technologies, there has been a shift to creating technologies depending on the fuel available. An abundance of clean electricity has seen an increase in electrification of the transport and space-heating sectors. While electrification has allowed these sectors to decarbonise, it has also resulted in a huge increase in electricity demand for the adopting countries.

1.1. Green energy and the energy mix

Green energy technologies have seen a rapid uplift in electrical generation capacity with global wind energy installed capacity growing by 891 GW, or 120-fold, to the year 2022 since the Kyoto Protocol in 1997 (IRENA, 2020, 2023). Fossil fuel-based electrical generation has now been largely displaced in a number of countries. In 2020, Scotland produced 95.9% of electricity from renewables sources with the majority percentage coming from offshore wind (Scottish Government, 2021). Norway produces 98% of yearly electrical power needed from renewable sources with the majority share from hydropower (Ministry of Petroleum and Energy, 2016). Norway even produces enough renewable energy to export electricity in winter months.

The global future of green energy shows no sign of slowing down. Major economies like the United States and Europe have passed legislation to help pay for an increase in renewables energy technologies (Congress.gov, 2022; European Commission, 2019). Large multi-country deals like the European Green Deal (European Commission, 2019) require individual countries to play their part in both increasing renewable energy market size and incentives to attract private funds to help accelerate the deployment of renewable energy technologies.

UK Green energy targets

Since the Kyoto protocol, the United Kingdom (UK) has set successive climate targets. The 2008 Climate Change Act was seen globally as a leading piece of legislation (GOV.UK, 2008). This set a target for net zero by 2050 applicable to carbon dioxide and all other targeted greenhouse gasses. The act also outlined how the UK would achieve these targets for greenhouse gas emissions by 2050 (GOV.UK, 2008). The act created legally binding targets for the present government and successive governments enabling the policy to survive for longer than the 4-year election cycle. The legislation created accountability for climate action by forcing the incumbent Secretary of State to address parliament regularly to outline how the government intended to meet the carbon reduction targets. A key part of The 2008 Climate Change Act was the avenue for judicial review if the government failed to meet targets (GOV.UK, 2008). Despite this avenue, no material penalty was created for failure to miss targets with reputational damage being the only consequence (Lockwood, 2021). The Climate Change Act 2008 was a commitment that spanned a longer time frame than set out in the Kyoto protocol of 5% below 1990 levels by 2012 (United Nations, 1997). The Climate Change Act 2008 also set out a framework for carbon budgeting as a means to record progress and provide a backdrop for accountability towards the 2050 target.

1.1. Green energy and the energy mix

The Paris agreement was another key international treaty signed by the UK for action on climate change. In 2015, the Paris agreement used an international collective goal as a means to focus minds to implement change rapidly. This goal was to keep the global rise in temperature to below 2°C (United Nations, 2015). In having a collective target rather than country specific carbon targets, the psyche of the global decision makers could shift to the realisation of the truly global impact of inaction.

For many years, the idea of greenhouse gas reduction targets have been hindered by the corresponding high costs of implementation. However, delay in action only serves to increase costs to meet targets (UNEP, 2016). While costs are clearly involved in meeting climate change targets, the UK government has realised the potential benefits. Fully embraced climate change targets allows for the creation of new sectors as well as export opportunities. The UK has dubbed these opportunities as, ‘The Green Industrial Revolution’, setting out a plan for how the value can be captured (GOV.UK, 2020). The Ten Point Plan for a Green Industrial Revolution outlines the ability for the manufacturing industry within the UK to benefit from early adoption. The ability to create jobs, draw in investment, all while reducing greenhouse gas emissions, provides a compelling argument for a green industrial revolution (GOV.UK, 2020).

UK funding for green energy

In order to take advantage of the indigenous supply of green energy within the UK, and to therefore meet green energy targets, the government needs to provide subsidies. As with all technology, the early stage of renewable energy could not compete on price with existing and established energy generation using oil and gas.

The first utility scale renewables subsidies created by the UK government was the Renewables Obligation Certificate (ROC) in 2002. The ROCs scheme worked by allocating certificates to renewable energy generators based on their capacity. These contracts were then traded to energy suppliers who are given a legal requirement to demonstrate a proportion of their energy was created using renewable energy sources (GOV.UK, 2002).

Selling ROCs represented an additional revenue stream for the renewable energy companies enabling renewable projects to be profitable and attractive for investors. The ROCs scheme was successful in bringing investment to renewable energy technologies with the capacity of wind power under the scheme increasing from 513 MW to 18,779 MW between 2002 and 2020 (Shao, Chen, Li, & Liu, 2022). With this increase in capacity, the ROC

1.1. Green energy and the energy mix

scheme was also able to reduce the cost of wind generated electricity by £1.28/MWh for each 1 GW of capacity added (Shao et al., 2022). This cost race-to-the-bottom reduced prices for suppliers, so much so, that it resulted in the ROCs scheme no longer benefiting consumers and the scheme was closed in 2017.

The ROCs scheme was replaced by Contracts for Difference (CfD). The first stage of CfD involves the government allocating a capacity of renewables required. Companies then compete on price to fill this capacity. The capacity is filled with projects in order of cost. The capacity is filled cumulatively with the most expensive project that fills the capacity required setting the strike price, the price for all projects. To allow for different technologies at different cost points, the projects entered are divided into a number of ‘pots’. The CfD auction process is then run in each pot separately. The strike price is a fixed price of electricity guaranteed by the government: when the electricity wholesale price falls below the strike price the government makes up the difference, similarly, if the wholesale price goes above the strike price the difference is paid back to the government by the generator (GOV.UK, 2014). CfD completely protects a renewables project from the volatility of the wholesale energy market and allows for investor confidence in a project.

CfD represented a shift from consumer funded subsidies to direct government funding. This gives increased control for the UK government in setting targets for renewable capacity as well as diversity of generation and price.

The auction rounds for CfD were originally planned every two years, however, as of 2022 the rounds take place every year. This change to a yearly process did not see a doubling of funds available, but rather the division of funds between two years (GOV.UK, 2022, 2023). Once allocated a contract, projects have defined milestone dates they must meet in the progression to electricity export.

UK indigenous renewable energy

The ability for the UK to meet its green targets is aided by the volume of renewable energy resource that can be exploited within the UK land area and surrounding waters. The physical location of the UK results in exposure to strong Atlantic and North Sea weather systems that create a high energy environment from which to extract power.

1.1. Green energy and the energy mix

Wind energy is an ever-growing part of the energy mix of the UK. Onshore wind made up 11% of the UK's electrical generation in 2020 (Office for National Statistics, 2021). Onshore wind power requires appropriate sites often at higher altitude where the wind is stronger, but is aided by ease of access as technicians can walk up to the turbine in order to execute an operation.

Onshore wind, while being one of the cheapest forms of renewable energy, has seen difficulties in obtaining a social licence to operate. With the re-election of the Conservative Party to power in 2015, the renewable industry saw a ban on public subsidies for onshore wind and the effective halt to the development of new projects within England (The Conservative Party, 2015). Environmental groups have since successfully campaigned to reverse this policy.

The wind resource for onshore wind is inherently hampered by high surface friction from objects on land leading to slowed speeds at hub height. Placing a turbine offshore results in almost no surface friction as the wind travels across water before reaching the turbine. This results in a better resource and placing the turbines far offshore reduces negative visual affects while allowing turbines to become bigger. The UK has a vast offshore wind resource; a result of having high wind speeds and shallow near-coast waters (Cavazzi & Dutton, 2016). The UK government is aiming for an installed capacity of 39 GW of fixed bottom offshore wind and 1 GW of floating offshore wind by 2030, accelerating an industry that has already seen a 715% increase between 2009 and 2020 (GOV.UK, 2020; Office for National Statistics, 2021).

Despite the relatively high latitude of the UK, solar energy presents another potential renewable energy solution. The south of England has areas that could accommodate solar energy with as much as 3,500 GW of potential based on appropriate land area (Palmer, Gottschalg, & Betts, 2019). Solar energy, like wind, is a non-dispatchable renewable energy posing the issue of intermittence for the national grid.

Hydroelectric energy represents a dispatchable renewable energy as well as an energy storage solution. Pumped hydro allows for excess renewable energy to be stored as potential energy. The UK does not have many locations where hydropower is feasible with most schemes located in either Scotland or Wales. As a result, hydro power only represented 5% of electricity produced from renewables in 2019. However, the real value of the technology comes from the ability to change power output quickly as this aids the National Grid in balancing the UK electricity demand and supply (Department for Business energy & Industrial Strategy, 2020).

1.1. Green energy and the energy mix

The coastal nature of the UK lends itself well to wave energy as another form of renewable energy. It is estimated that as much as 50 TWh/year could be extracted from wave energy in the UK surrounding waters which equates to approximately 1.7% of the global extractable wave energy (Carbon Trust, 2006). Wave energy, like a number of other renewable energy types, struggles with proximity to the grid. In general, the energy present in waves is larger further from the coast. This results in long distances of cabling needed to bring energy back to shore adding to costs.

Tidal energy is another renewable energy indigenous to the UK waters, however, it is highly site specific as the resource is only available under certain conditions. Tidal energy is a predictable energy making it useful for grid management within an increasingly variable power energy mix (Coles et al., 2021). The UK has a large capacity for tidal stream energy with as much as 18 TWh/year available equating to 10-15% of the global resource (Carbon Trust, 2006). This would be enough energy to completely displace the electricity generated from coal and oil in the UK in 2019 (Department for Business energy & Industrial Strategy, 2020). The specific topography required for a site to have tidal stream energy has the added benefit that the energy is close to shore. This removes the need for long sub-sea cables and also ensures maintenance teams do not have far to travel.

1.2 Tidal energy

Tidal energy is a form of renewable energy that is entirely predictable. This is because it is based on orbits of celestial bodies that can be calculated. As the moon and the sun move around relative to the Earth, their gravitational pull acts on the surface water of the Earth. This pull generates the tides that are well known to everyone. The limited volume of water in the oceans dictates that high tide and low tide must occur at different times at different locations around the world. This, therefore, requires the transport of water from one point to another. When this transport of water is impeded by landmass, the water must move around and, in doing so, is accelerated to form tidal currents. The cyclic nature of tides means that these points of accelerated flow experience a directional change that can be predicted (Ahmad, Kumar, & Ranjan, 2022). Along with the gravitational pull of the sun and moon, the tides on Earth are affected by the spin of the Earth itself. The Coriolis affect results in the acceleration of tides at the more extreme latitudes.

1.2. Tidal energy

1.2.1 Tidal sites

As for any renewable installation, resource dominates the feasibility and cost of a project. Tidal energy is much more limited for global potential sites than the likes of wind and solar. This is not only due to the need for a coastline, countries also have to have correct coastal topography for the creation of fast tidal currents. As well as high flow speeds, potential tidal sites have to be deep enough for the implementation of tidal devices.

North America

North America has a number of strong tidal current locations. The strongest of which, also the strongest in the world, is located at Minas Passage in the Bay of Fundy, Nova Scotia, Canada. The Minas Passage has flow speeds in excess of 4 m/s in some locations and depths of over 100 m in others (Hagerman, Fader, Carlin, & Bedard, 2006; Karsten, 2011). The site also benefits from a small wave climate as large swell waves are blocked from the site by the surrounding landmass. The potential for tidal energy in the Minas passage and surrounding waters has led to extensive study of the site. Early estimations for the tidal resource in the Minas passage suggest that as much as 166 MW could be captured by in-stream tidal energy converters at the site with a further 165.9 MW available at adjacent sites (Hagerman et al., 2006). The volume of tidal energy available at this site also warranted the creation of a purpose built research centre, the Fundy Ocean Research Centre for Energy (FORCE).

North America is also host to potential tidal sites on the west coast. The Salish Sea in the Pacific North West of the United States contains as many as 16 viable tidal energy sites representing a high tidal resource near a population centre spread between Canada and the United States (Yang, Wang, Branch, Xiao, & Deb, 2021). The United States is poised to accelerate the implementation of tidal stream energy after the creation of the Bipartisan Infrastructure Law. This document releases up to \$45 Million for investment into tidal energy projects to help set up tidal sites and fabrication centres within the U.S. (U.S. Department of Energy, 2023).

1.2. Tidal energy

South America

South America has a number of potential tidal stream energy sites in countries towards the south. Chile is recognised as having the largest tidal stream capacity in the region (Shadman et al., 2023). The Magallanes Strait and the Chacao Channel in the south of Chile can reach speeds of up to 5 m/s according to Shadman et al. (2023). The tidal stream energy resource in South America shares a common dilemma with sites around the world. Given the resource is often in the extreme latitudes, tidal energy in Chile is located far from the demand hub and transmission line systems of the highly populated regions in Chile (Shadman et al., 2023).

Asia

A number of countries throughout South-East Asia have the natural resource to allow for the extraction of tidal stream energy. Indonesia has numerous sites of suitable depths with tide speeds of up to 2 m/s giving a realistic capacity for tidal stream energy of 4.8 GW, while the Philippines also has a large capacity of up to 60 GW of practically extractable power (Quirapas, Lin, Abundo, Brahim, & Santos, 2015). Other countries in the area have capacity for tidal stream energy converters to be applied in a river current setting (Quirapas et al., 2015).

In countries with archipelagos of island communities, tidal energy gives the opportunity to displace unreliable diesel generators with clean tidal energy. This would aid in energy security for the community but would require added cable infrastructure should the tidal energy be intended to service the countries' national grid.

China has a large number of highly energetic tidal sites located throughout its 18,000 km coastline (Liu et al., 2021). As a result of this vast coastline, China sees a range of tidal energy forms from tidal inlets to straits and headlands. China's dense coastal population lends itself well to the utilisation of tidal energy as the demand centres are close to supply.

Oceania

Tidal energy sites are not uncommon in Australia with a number of sites in the north-west, south, and east of the country (Lyne, Condie, & Hallegraeff, 2005). One of the most viable tidal stream energy sites for the country is located at the Banks Strait on the coast of Tasmania. The Banks Strait is a low energy site compared to other global sites with

1.2. Tidal energy

flows of up to 2.5 m/s (Cossu et al., 2021). As higher energy sites begin to fill with tidal energy converters, subsequent generations of tidal turbines will have to be designed for slower speeds. Not only would this open the Banks Strait as a more viable tidal site, it would also open up many more sites globally (Lewis, Neill, Robins, & Hashemi, 2015).

Slower speed sites are a feature in New Zealand’s tidal sector. Only four sites are identified by Huckerby and Johnson (2008) as having flow speeds over 1 m/s with a range of site-specific difficulties identified including depth and exposure (Nasab, Kilby, & Bakhtiaryfard, 2020). Another avenue for tidal energy in New Zealand is tidal flows around harbours. Harnessing energy around a harbour guarantees close proximity of a load to consume the energy produced (Moore & Boyle, 2014).

Europe

A large proportion of the European tidal energy resource is created by the interaction of the Atlantic Ocean and the North Sea. As the North Sea fills and empties, the position of the UK causes water to accelerate around the land mass. As a result, large tidal stream resources can be found at the northerly and southerly extremities of the UK. A number of tidal sites can be found in the French waters of the English channel as a result of this phenomenon. The Alderney Race situated in North-West Normandy, France, is a particularly high energy site with maximum flow speed of over 5 m/s and average speeds of over 2 m/s (Du Bois et al., 2020). French waters also host tidal stream resource to the western edge of Brittany as well as large tidal range energy at La Rance.

The UK has as many as 49 potential tidal sites dispersed throughout its coastal waters (Coles et al., 2021). Not only is the tidal resource large for the UK, it is also dispersed along the coast (see Figure 1.1). This dispersion leads to tidal resources being as much as 6-hours out of phase with each other, in turn, creating the possibility of a continuous tidal energy output for the UK (Todeschini et al., 2022). Four of the most commercial ready sites in the UK are separated by long distances and include the Perpetuus Tidal Energy Centre (PTEC) off the coast of the Isle of Wight on the south coast of England, Morlais in Anglesey, Wales, and MeyGen and the Fall of Warness both in the Orkney Islands in the north of Scotland.

1.2. Tidal energy

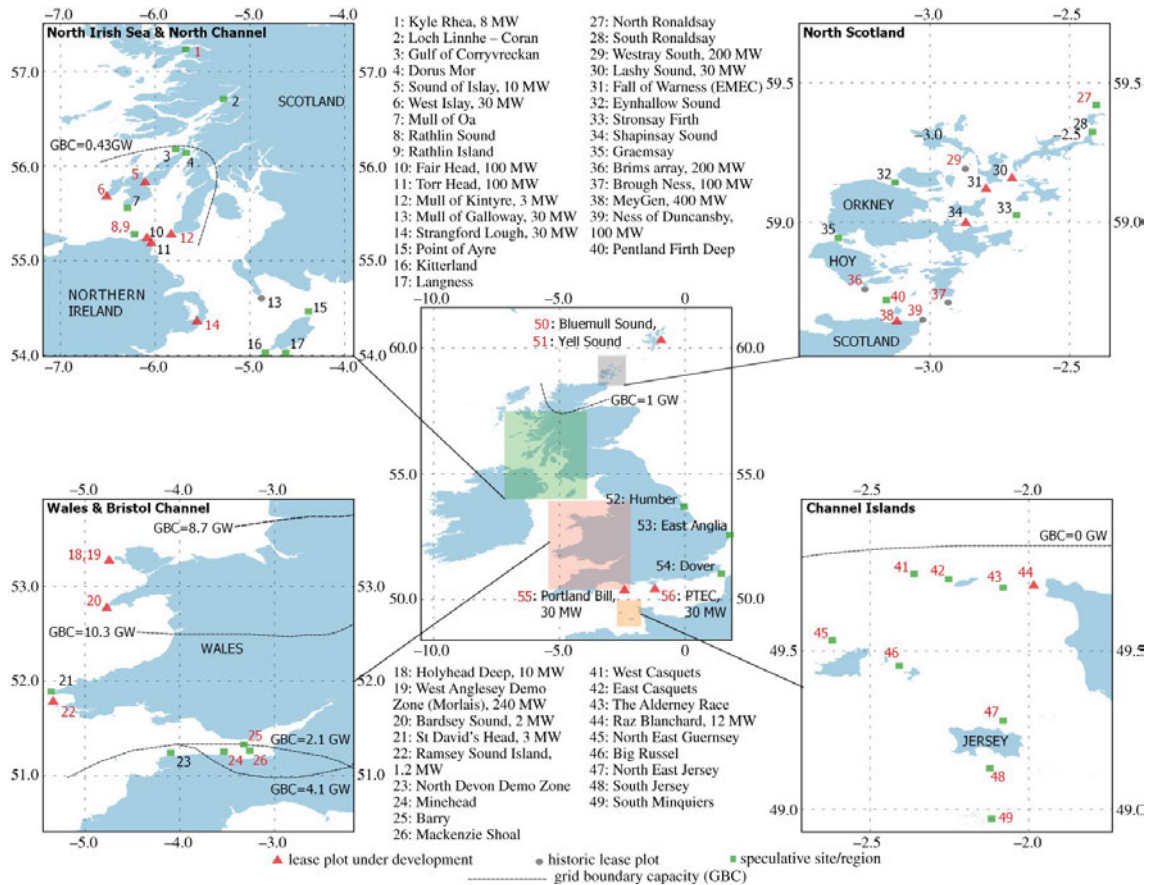


Figure 1.1: Map of potential UK tidal project sites including sites under development, sites previously under development, and speculative sites (Coles et al., 2021).

1.2.2 Fall of Warness

The Fall of Warness is an energetic tidal site located in the Orkney Islands operating as a tidal test site for developers under the ownership of European Marine Energy Centre (EMEC) since 2006 (EMEC, 2023b) (see site 31 in Figure 1.1). The primary purpose of the site is as a facility for the testing of tidal energy converters allowing progression from pre-commercial to commercial. Since its inception, the site has played host to eight different companies and 11 different tidal turbines. Having a test bed for the tidal sector allows companies to de-risk their design without the expense of gaining site approval and grid connection as both are provided by EMEC.

1.2. Tidal energy

Resource

The Fall of Warness is the second most energetic tidal site in Orkney after the Pentland Firth with maximum spring tide speeds of 4 m/s. The resource at the Fall of Warness is a subject of extensive study primarily by technology developers, as the resource is key to the financing of a project, but also by academia (Lawrence, Kofoed-Hansen, & Chevalier, 2009; Sellar, Wakelam, Sutherland, Ingram, & Venugopal, 2018; Waldman et al., 2017). The good tidal resource that is present at the site lends itself to being studied, however, the site is also studied as it is operated by EMEC. EMEC is a centre for research as well as an aid to technology developers and so are able to support research institutions to record data as well as recording in-house data for dissemination or for technology developers.

Fall of Warness Test Site

EMEC operate seven tidal turbine berths in the Fall of Warness with a grid connection via the substation on the island of Eday (see Figure 1.2). Each berth has a preinstalled 11 kV electrical cable running along the seabed. The Eday substation acts to transform electricity to 33 kV before it is sent to the mainland via a 4 MW grid connection (EMEC, 2023a). Given the success of the test site and its popularity as well as increased funding in recent CfD rounds for tidal energy, this grid connection is being upgraded to 7.2 MW (EMEC, 2023a). In addition to transformers, the substation on Eday also houses a large vanadium flow battery storage unit capable of storing 1.5 MWh (EMEC, 2023a). This battery allows the electricity going into the substation to be stored and released at another point in time enabling a smoother power to the grid output from the substation. The Eday substation also contains a 0.67 MW electrolyser to transform excess electricity into hydrogen (EMEC, 2023a). This hydrogen is stored in tube trailers at the site before being ferried to the main island in Orkney where it is used for hydrogen cars. The ultimate goal for the hydrogen is to use it as the fuel-of-choice for heavy plant propulsion in Orkney. Plans are underway to convert the ferry fleet in Orkney to run on hydrogen and initial trials have already taken place to convert the inter-island aircraft to operate on hydrogen as a fuel.

1.2. Tidal energy

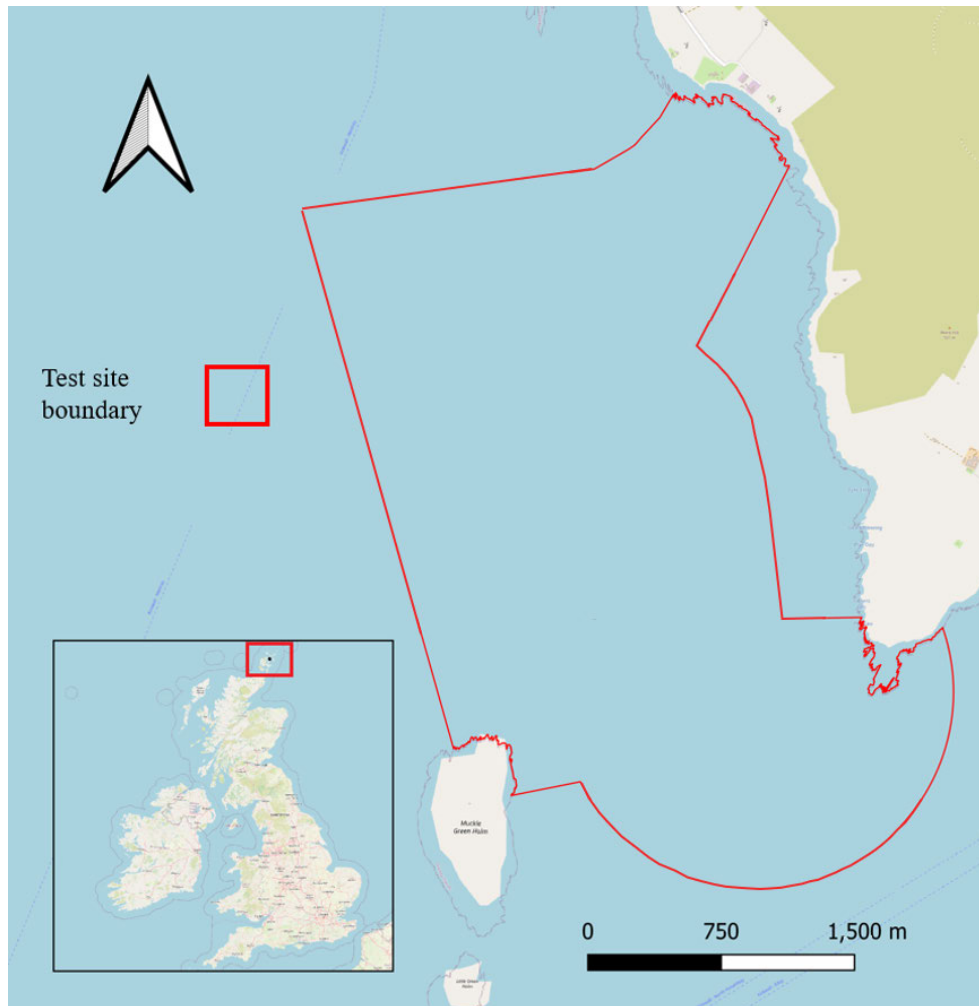


Figure 1.2: EMEC Fall of Warness tidal test site. The island of Eday shown top right. Map courtesy of openstreetmap.org, test site boundary courtesy of EMEC.

Tidal energy converters in The Fall of Warness

The Fall of Warness has hosted a number of tidal turbines since 2006 (see Table 1.1). Open Hydro was the first turbine to be installed at the site and was the first grid connected tidal turbine in the UK. Since Open Hydro, the Fall of Warness has continued to be an important test bed for the tidal industry allowing technology developers to connect to the grid.

Tidal turbines, unlike wind, have yet to converge on a standard shape and design. As a result, different technologies have chosen different methods for capturing tidal energy. All of the tidal energy converters in Table 1.1, with the exception of Open Hydro, use horizontal axis turbines with a central shaft each with a varying number of blades attached. This is common with standard wind turbines. Using lessons learned from the

1.2. Tidal energy

Table 1.1: Grid connected tidal energy converters hosted by EMEC in the Fall of Warness (EMEC, 2023c)

Company	Technology name	Power rating (MW)	Deployment Period
Open Hydro	n/a	0.25	2006-2018
Alstom	DeepGen-III	0.5	2010-2013
Andritz Hydro Hammerfest	HS1000	1	2011-2015
Atlantis	AR1000	1	2011-2012
Orbital Marine Power	SR250	0.25	2011-2013
Alstom	DeepGen-IV	1	2013-2016
Voith Hydro	HyTide	1	2013-2015
Orbital Marine Power	SR2000	2	2016-2018
Tocado	T2	0.275	2017-2017
Magallanes Renovables	ATIR	1.5	2019-Present
Orbital Marine Power	O2	2	2021-Present

wind sector avoids duplication of expensive learning. A key engineering problem for tidal turbines is the design and configuration of the turbine super structure. This is evidenced by the variety of superstructures on which turbines are deployed. The early turbines placed in the Fall of Warness, with the exception of the SR250, all had seabed mounted superstructures and looked similar to a wind turbine scaled for higher density fluid interactions. Since 2016, all new tidal turbines deployed in the Fall of Warness have used a floating superstructure to attach to the power take-off system. This shows a trend away from seabed mounted turbines. One of the main drivers for this is access for operation and maintenance. Removing the need for heavy lift vessels for a maintenance intervention vastly reduces the cost of each operation and negates the need to design in expensive redundancies and large tolerances in the hope of avoiding maintenance all together.

Scale and power rating of the devices deployed at the Fall of Warness have trended upwards with time (see Table 1.1). The Fall of Warness has seen smaller scale test devices and is now hosting full scale utility devices up to 2 MW. In total, 10.8 MW of cumulative tidal stream devices have been installed and tested in the Fall of Warness since 2006 making it the most tidal stream technology rich body of water in the world (EMEC, 2023c). The volume of tidal stream technology deployed in the Fall of Warness is as a result of the testing environment created by EMEC at the site as well as the large energy resource available.

1.3 Research gaps

Research within tidal energy Original Engineering Manufacturers (OEMs) is a high priority as the industry seeks to bring down costs and become competitive with other established renewable energy technologies. Current learning rates, the percentage cost reduction per doubling of capacity, for the tidal sector are thought to be around 10% (Callaghan & Boud, 2006; Walker & Thies, 2021). A tool at the disposal of the developer is access to data. Better, faster sensors, along with increased storage, with the development of cloud based storage platforms, risk large quantities of data being recorded without the means to leverage the data for enhanced understanding of a system. This is a problem realised by the wind industry who are increasing the use of ‘Big Data’ techniques to aid operation and maintenance programs (Bouqata, 2018).

In tidal energy, the low number of staff per company and the need for development on every aspect of the design, manufacture, deployment, operation, and maintenance, results in the inability to realise all learning available from data without the use of adequate data techniques. A review of the current data techniques used in tidal energy and how they can be streamlined and improved is a significant research gap for tidal energy in the wider context. This gap is predominantly due to the commercial sensitivity of such a topic and therefore the inability to compare techniques used by different companies. Instead, companies review their data handling and processing internally without the development of an industry standard.

1.3.1 Environment monitoring

A significant gap, and one that can be filled by the correct application of data, is environment monitoring. The tidal environment is highly energetic and, therefore, the ability to correctly record wave and tidal climates enables comparison to loads for limit state analysis and or maintaining within the operating envelope of a device. According to the International Electrotechnical Commission (IEC), the wave climate of a tidal site is important for loads on the device and so are a key part of the resource assessment carried out before a turbine is placed at a site (IEC, 2015b). A limitation in the current method for wave climate recording is the need for external measurement equipment. This limits the longevity of recording often due to battery life for the instrument. Instead, being able to use sensors onboard the turbine which has a grid connection would remove the need for expensive marine operations to deploy sensors and solves the issue of limited battery life. Recording wave climates from onboard a tidal turbine is relatively new due to the sensors

1.3. Research gaps

required. Sellar and Sutherland (2015) is one case where an Acoustic Doppler Current Profiler (ADCP) was placed on an operating tidal turbine with the ability to record waves via surface tracking and pressure signals. With a trend towards floating tidal turbines in recent years (see Table 1.1), this method may only have limited application in the future. Wave recording from a floating tidal turbine is a different challenge as there is no fixed datum to record displacement or pressure from. Arguably, the accurate recording of wave statistics is of greater importance to floating tidal energy compared to fixed bottom tidal energy as the sea surface sees the most energetic wave climate. Wave recording from a floating platform has been studied for the application of wave statistics for large dynamic positioning vessels (Brodtkorb & Nielsen, 2023; Brodtkorb, Nielsen, & Sørensen, 2018a, 2018b; Iseki & Ohtsu, 2000; Mounet et al., 2023), however, the direct applicability of the method discussed in these papers to a fast tidal environment, moored, thrust producing tidal turbine is unknown. Instead, other avenues must be explored to calculate accurate wave statistics.

1.3.2 Model validation

Design within the tidal turbine industry is often done using computational software as a means for rapid design and load modelling for lower cost than physical modelling (Kangaji, Orumwense, & Abo-Al-ez, 2022). Models created by developers can range from tidal flow models to full scale, multi-element, models of entire tidal turbine systems (Pacheco, Ferreira, Carballo, & Iglesias, 2014; Parkinson & Collier, 2016). Model validation is a key way tidal turbine developers can apply data to reduce costs. A calibrated and validated model enables confidence in model outputs allowing for smaller safety factors to be applied. In order to validate a model, realistic data must be obtained (Draycott et al., 2019). Confidence in this comparative dataset increases with scale with full scale testing resulting in the most realistic dataset. The validation of a model is a research gap for any unvalidated model.

1.3.3 Velocimetry

Kinetic energy within tidal streams is an important environmental factor creating loads on a floating tidal turbine. Knowledge of the tide velocity is of major importance from both a loading perspective as well as a financing and power production prediction perspective. Recording of tide velocity for the tidal sector is traditionally done by seabed mounted ADCPs (IEC, 2013, 2015a). Issues arise when trying to measure the flow field from onboard a floating tidal turbine as the set location of a seabed ADCP may become non-optimal

1.3. Research gaps

due to floating platform movement with the changing tide. One solution is to place the ADCP on the floating platform pointing downwards, however, the distance away from the rotor plane becomes an issue as it is limited by the size of the floating platform. Another option is to place an ADCP at hub height pointing horizontally into the flow (Harrold et al., 2020; RealTide Consortium, 2021; Sellar et al., 2018). As well as control, a horizontal ADCP would enable the study of flow structure features on approach to a tidal turbine. Ranging forward of the rotor could also open up the measurement of incident flow to the rotor replacing seabed ADCPs in the power performance of the turbines (IEC, 2013; TIGER, 2022). In order for this application to be realised, knowledge of ADCP range when placed horizontally must be known. Once the range of the instrument is recorded, the application of data from a horizontal ADCP are numerous.

1.4 Research aims and objectives

This thesis uses data to deliver cost savings for the operation of the O2, the tidal turbine operated by Orbital Marine Power, by reprocessing existing datasets in a novel way and developing new approaches to acquiring new data. The value associated with the new data techniques presented are quantified and their applicability to the wider tidal energy industry showcased. This engineering doctoral thesis follows a portfolio approach whereby a number of studies are tackled individually, with data handling for the O2 connecting them together.

Figure 1.3 shows the data infrastructure of the O2 and where this thesis adds value. Data are collected at the turbine level with a suite of sensors, these data then pass through a processing level where data analysis techniques are applied in order to glean further knowledge. The data at this level are also used for bespoke analysis programs to allow for learning at a system and component level in order to inform engineering of future generations of turbines. The processing level progresses into the user level. At the user level, data are presented based on use case; this can range from dash boarding for instantaneous turbine status reporting to fleet level maintenance system where spares and operation and maintenance staff are managed.

Figure 1.3 shows the area of the O2 data infrastructure where this thesis adds value circled in orange. The thesis adds value to the processing level of the O2 data infrastructure (see Figure 1.3) by accelerating data access and processes like fatigue monitoring and tide speed forecasting. The ability to use existing data to record environmental parameters is also

1.4. Research aims and objectives

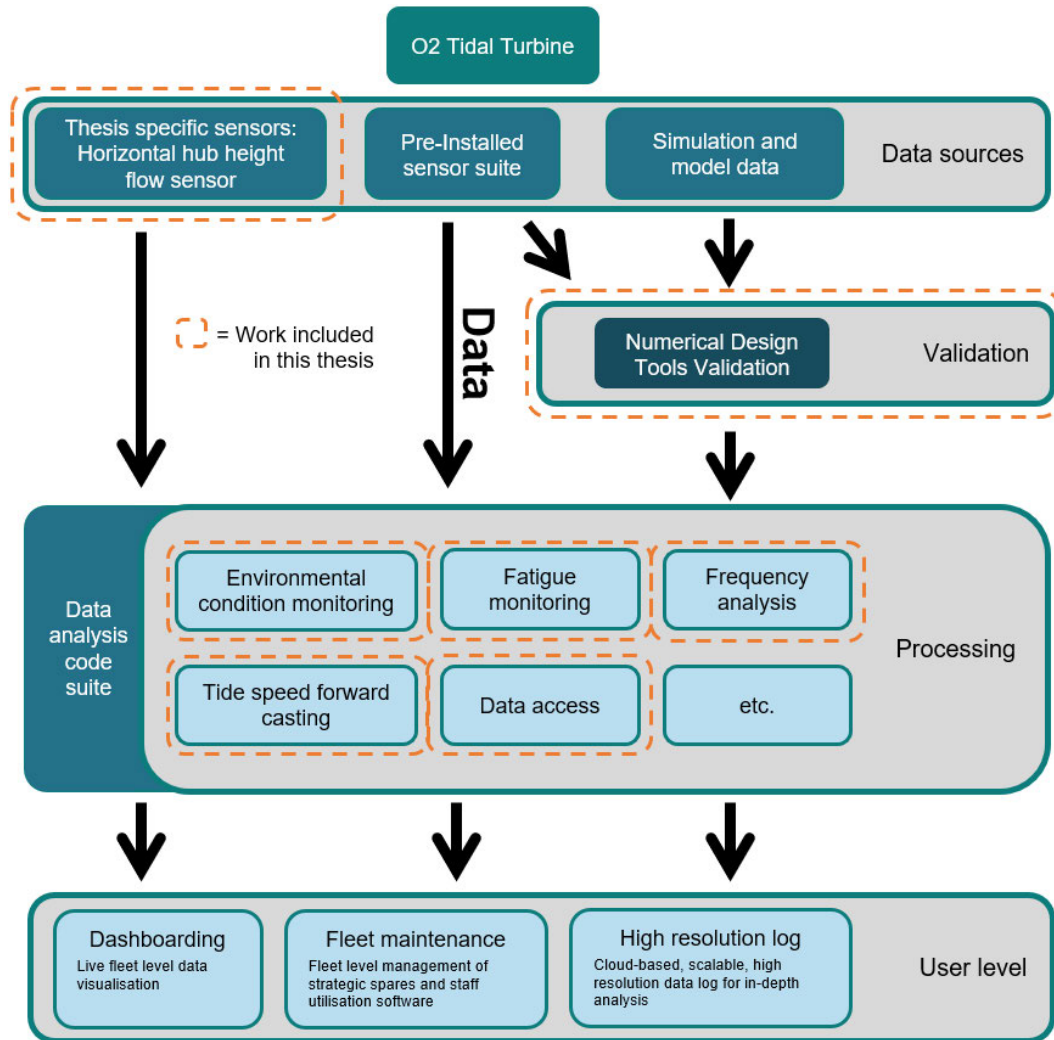


Figure 1.3: Holistic view of how O2 data are handled from data sources to processing and presentation to the end user. Areas where this thesis adds value are outlined in orange.

presented and the value added quantified. The validation of the loads model used in the design of the O2 is also presented adding valuable data to the turbine data infrastructure. Finally, the thesis makes the case for a horizontal incident flow sensor and deploys and validated its use on the O2. How data from this additional flow sensor can be used by the O2 is then demonstrated.

Key research aims and objectives are:

1. Reduce person-hours involved in O2-standard data processes.
 - Identify legacy processes where a reduction in processing time could be most impactful.

1.4. Research aims and objectives

- Showcase impact of process streamlining by both time reduction quantification and ability to apply the process over a longer time period.
 - Demonstrate how this has changed Orbital Marine Power’s working practice.
2. Generate a real-time, reliable, and uninterruptible measure of wave height and period at the O2 location that is accurate to a level defined by use case.
 - Identify a number of candidate methods for calculating wave height and period from turbine motion.
 - Quantify the accuracy of each method by comparison to a dataset of known accuracy to determine the extent of usefulness of each method given use-case requirements.
3. Validate the numerical drive-train model used extensively in the design of the O2 and subsequent future turbine designs against a robust dataset of full scale field data.
 - Identify loads of interest on the O2 drive-train.
 - Ensure like-for-like comparison for loads on the O2 and in the numerical model and execute comparison.
 - Analyse discrepancies and reasons for them.
 - Demonstrate the impact of a validated numerical drive-train model.
4. Quantify barriers to the use of ‘IEC Technical Specification (TS) 62600-200 electricity producing tidal energy converters - power performance assessment’ (IEC, 2013) in measuring incident flow for a floating tidal turbine.
 - Identify factors unique to floating tidal energy that could impede the use of standard inflow measuring practices.
 - Quantify how turbine motion affects optimal seabed positioning for a fixed ADCP used for incident flow measurement.
 - Quantify how O2-specific features impede the ability to record inflow in accordance TS 62600-200.
5. Deploy and critically analyse a horizontally mounted hub height 5-beam ADCP to assess suitability for use as the principal incident flow measurement instrument in a power performance assessment for a floating tidal turbine.
 - Use data quality filters and data remaining after filter application to assess the range of the single central horizontal beam.
 - Compare and assess the difference in incident flow measurement between single horizontal beam measurement and measurement using a combination of divergent beams on the ADCP.

1.4. Research aims and objectives

- Outline O2-specific limitations to determine the feasibility of a horizontal hub height ADCP as a long-term incident flow measurement for turbine control or for a power performance assessment.

1.5 Thesis structure

This thesis introduces the tidal developer Orbital Marine Power and their latest device, the O2, the research subject. The document then presents the research conducted pertaining to data collected over three years of operation of the O2 across many systems and sensors as well as model data created by the wider Orbital Marine Power engineering team. The thesis is divided into two parts: Part I, Increasing Knowledge-Return from Data by Re-Analysing Existing Data; Part II, Floating Tidal Turbine Incident Velocimetry and Increasing Knowledge-Return from Data through Novel Sensor Applications. Figure 1.4 shows where each of the thesis relevant sections described in Figure 1.3 are tackled in this document.

Part I tackles a number of projects using existing data. They include: Chapter 3, Data handling advancements for the design and operation of the O2; Chapter 4, Estimating tidal site wave statistics for the design, operation, and maintenance of the O2 using the existing onboard sensor suite; Chapter 5, Validation of a numerical simulation tool used to model O2 drive-train loads. Chapters 3 and 4 add to the ‘processing level’ described in Figure 1.3, with Chapter 5 presenting a model validation that adds to overall turbine understanding.

Part II of this thesis pertains to the addition of horizontal hub height sensor to add a new source of data to be used by the ‘processing level’ in Figure 1.3. This part is divided into two chapters: Chapter 6, Application of ADCPs for floating tidal turbine incident resource measurement; Chapter 7, The application of a horizontal turbine mounted hub height ADCP for incident resource measurement. Chapter 6 outlines the rationale for the application of a new incident flow sensor by describing difficulties for floating tidal developers using TS 62600-200 in conducting a power performance assessment. Chapter 7 presents an alternative sensor deployment that alleviates some of the issues incurred by floating tidal developers in using TS 62600-200.

1.5. Thesis structure

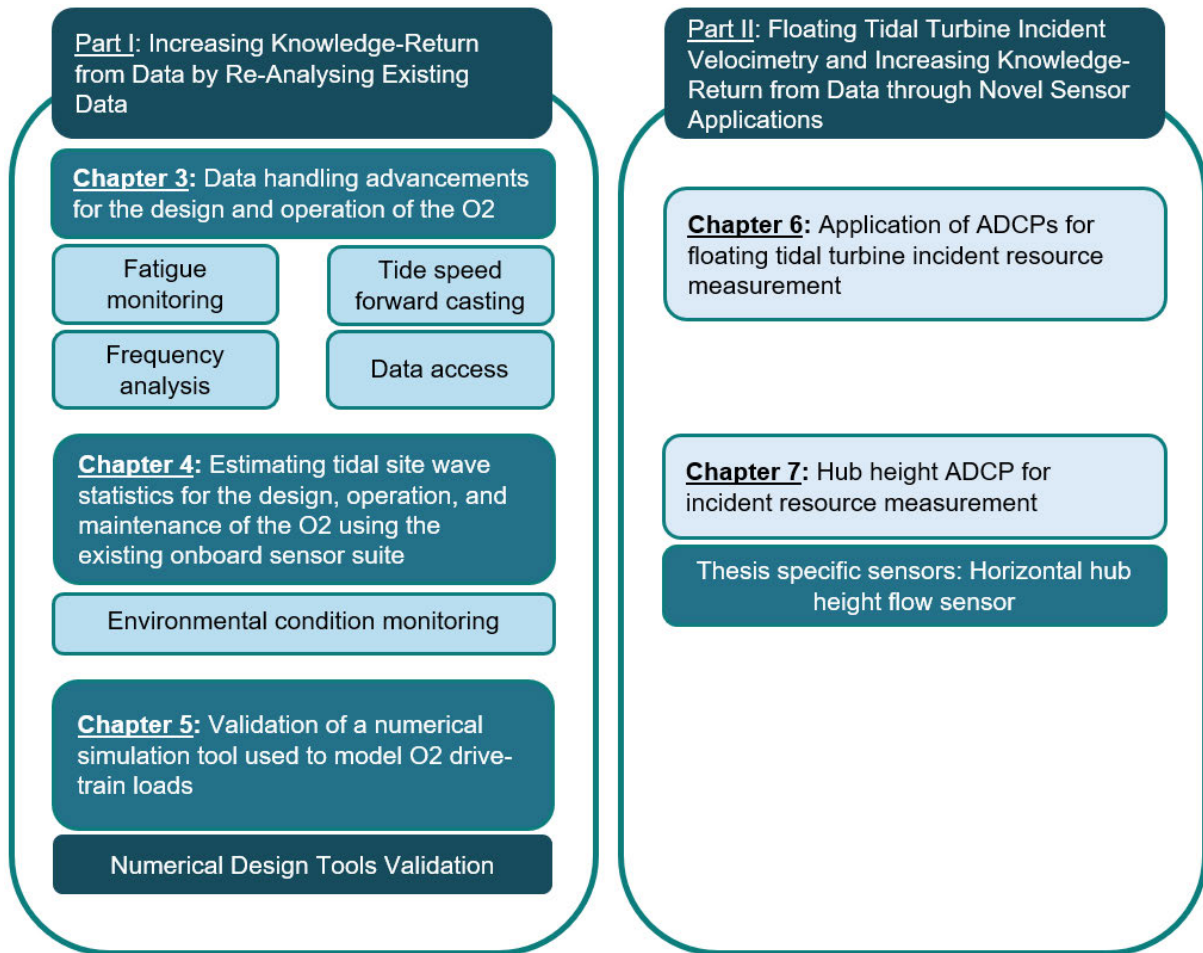


Figure 1.4: Data streams described in Figure 1.3 divided by thesis structure, Part I and II, and chapter.

The rationale behind each chapter is identified before the method, results, discussion, and conclusions are outlined. The impact on Orbital Marine Power and the wider sector is explicitly defined for each chapter to show the objectives were met. Finally, the thesis concludes with an overview of overall impact and an outline of possible avenues for future work.

The research in this thesis reduced levelised cost of energy for the O2 by creating learning from legacy data collected by the O2 as well as introducing new sensors and data techniques to further this reduction. Although only marginal savings are possible for a device that is already deployed, the learning presented serves to enhance the information available to Orbital Marine Power for the development of future devices in order to bring down costs.

Orbital Marine Power

2.1 Company philosophy

Orbital Marine Power was founded in Orkney in 2002 as a specialist in floating tidal energy. The company deployed and tested the SR250 and SR2000 under their previous name, Scotrenewables. Since then, Orbital Marine Power designed and built the O2, the new generation of their 2 MW tidal turbine. The O2 was designed in keeping with the general design philosophy of the previous turbines but with a number of additions, namely, a new design of the structure and mechanism attaching the nacelles to the main hull structure, and also the introduction of pitching blades for improved power take-off at high flow speeds.

Since the deployment of the O2, Orbital Marine Power acquired 14.4 MW of installed capacity in Auction Round 4 (AR4) and Auction Round 5 (AR5) to be serviced by the next generation of Orbital Marine Power's tidal turbines (GOV.UK, 2022, 2023). Moving forward, the company sees this as a first step towards the goal of large arrays of turbines eventually around the globe.

2.2 O2

The O2 is a 2 MW floating tidal turbine deployed in Berth 5 at the EMEC tidal test site, the Fall of Warness (see Figure 1.2) and can be seen in Figure 2.1. The device consists of a 72 m long cylindrical hull that sits on the sea surface with two legs extending into the water, one on either side. At the end of each leg is a single nacelle that holds the power-take-off for the turbine. The legs can be raised to the water line and are positioned symmetrically. The turbine is kept in position by semi-compliant catenary moorings, two forward lines and two aft lines. The catenary nature of the mooring allows the turbine to align slightly to the oncoming tide but the device does not vane between tides. Each

2.2. O2

power-take-off nacelle holds a 1 MW generator and a gearbox and is connected to a pitching hub with two blades. The pitching hub allows the full individual 360° control of the blades and is the reason the device does not have to vane between tides as the rotors can change direction. The electricity is exported from the turbine via a single dynamic cable umbilical that extends from the main hull to the seabed before travelling along the seabed to the export substation.

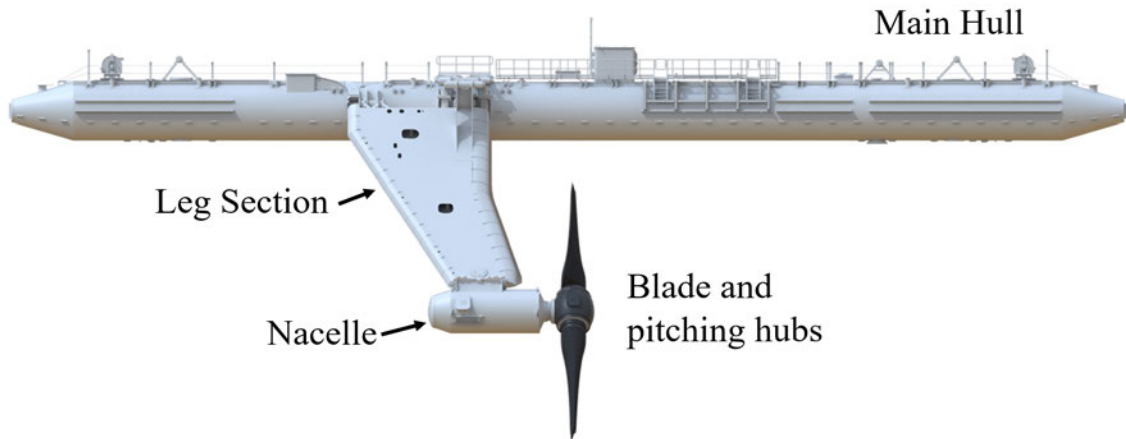


Figure 2.1: Side profile of the O2 2 MW tidal turbine designed, built, and installed by Orbital Marine Power.

2.2.1 Design Philosophy

The issue of maintenance is a key driver of Orbital Marine Power’s floating design philosophy. Maintenance is less expensive if it can be done from the level humans are on i.e., land or sea surface. Wind turbine structures have their base structure on ground level allowing for human access through the tower. For a tidal turbine to have its base structure on ‘human level’, the whole device must be floating. The philosophy of maintenance from sea level enables the use of small vessels for interventions. Avoiding heavy lift vessels from the design stage enables low cost maintenance further down the line. This floating approach was adopted by a number of tidal turbine developers as outlined in Table 1.1. For many of the floating tidal turbines deployed in the Fall of Warness, including Orbital Marine Power’s previous two editions the SR250 and SR2000, the only part accessible from the sea surface was the main hull containing the major electrical systems. The O2 goes one step further, articulated legs allow the nacelles and blades to be brought to the surface allowing for access to key components including the gearboxes.

2.2. O2

The other major generation progression for the O2 is the ability for individual blades to pitch. Pitching blades with a control system enables Orbital Marine Power to extract more power out of the environment as the blades can be angled depending on the flow speed. The pitching blades are also used to allow the O2 to remain geo-stationary on compliant moorings with the blades changing direction between tides. This application simplified the mooring system reducing costs.

Floating tidal energy comes with some areas of added complexity. Placing a turbine on the sea surface makes the hydrodynamics of the structure a key part of the design. This is less of an issue for seabed mounted turbines where the structure can be heavy and designed only for loads. An added complexity is the addition of a dynamic cable acting as the umbilical for the export of electricity from the turbine. Dynamic cable design has been a hindrance to the development of floating offshore wind energy, a sector with much more money than tidal energy (Marcollo & Efthimiou, 2024). This is another example where learning from the wind sector can have benefits to the tidal industry.

2.2.2 Sensors on board the O2

The O2 has numerous sensors onboard designed to measure loads and the environment. The data from these sensors allows Orbital Marine Power to gain knowledge around what the O2 is doing as well as how the environment is affecting the device.

Main Hull

The main hull of the O2 (see Figure 2.1) is a 72 m long, 3.5 m diameter, steel tube housing many of the main electrical components as well as the hydraulic system for operating the rams used to articulate the legs. The main hull contains sensors monitoring the state and health of each of these main components. The main hull also houses an Inertial Measurement Unit (IMU) located close to the centre of gravity.

The main hull also holds two acoustic flow measurement sensors. Two RDI Workhorse 4-beam ADCP's are positioned one at the front and one at the rear of the main hull pointing downwards. Both ADCPs are orientated so that their axis is lined up with the axis of the main hull resulting in a beam angled forward, aft, port, and starboard. The O2 does not vane between tides so these ADCPs are positioned to record flow coming into the rotors and flow behind the rotors with the roles of each switching depending on the tide direction. Each downward looking ADCP is capable of measuring the flow at 1 m bin depths below the sea surface allowing for flow measurement from the top of the rotor

2.2. O2

plane to the bottom. These ADCPs are located on the main hull of the O2 and point downwards, they are unable to measure the direct incoming flow to either rotor as they are not above either rotor. Instead, they measure the flow between the two rotors. This is an unavoidable limitation of placing the ADCPs on the main hull, however, their position enables access for maintenance and being turbine mounted means the flow measured is relative to the turbine irrespective of global motion.

Leg

The leg of the O2 (see Figure 2.1) has a number of sensors recording loads on the retraction system. This includes four load cells on either side measuring an x and y load component. These load cells were positioned to enable the measurement of loads at the joints in the legs. Having access to these data enables the load response of the legs to be monitored under different environmental and operational load scenarios.

The port-side leg has another flow sensor. On the leg is a Nortek Signature 500 ADCP placed close to the Port nacelle pointing aft horizontally. This 5-beam ADCP can measure horizontal flow speeds approaching the port side rotor during ebb tide in bins of 1 m. The working of this ADCP forms the basis for Chapter 7. Like the main hull ADCPs, the leg ADCP suffers from an incapacitated compass due to proximity to the large steel structure.

Nacelle

The port and starboard side nacelles on the O2 (see Figure 2.1) are instrumented in the same way. Both sides have multiple sensors recording gearbox parameters. These include vibrations and condition monitoring systems as well as sensors on the oil pumps measuring pressure and ferrous sensors at the oil filters measuring oil contamination.

In addition to the gearbox sensors, the nacelles also contain a number of sensors on the rest of the drive-train. On the drives, the speed of rotation is logged. Alongside this, there are two independent measurements of torque logged, one using strain gauges on the slow speed shaft and one as an output from the drives.

2.2. O2

Blades and pitching hubs

The blades and pitching hubs of the O2 (see Figure 2.1) are well instrumented. The blades have strain gauges measuring the edgewise and flatwise bending of each of the four blades. This allows for blade bending to be measured but also for rotor torque and hub bending to be calculated.

The pitching motors have torque sensors and can record the pitch azimuth angle. This feeds back to the controller for blade pitch control and also allows the health of the pitch motors to be monitored.

2.2.3 O2 data wrangling

Raw data format

The data from the O2 sensors must be logged in order to be of use to the engineering team. The data are logged to a number of different locations. The first form of logging is via .csv files. This logging format represents the basis of all logging and there are a number of different .csv files logging related data.

Cloud data storage

The .csv files recorded are logged to a computer onboard the turbine. Working with large datasets using .csv files is cumbersome and so the raw files are automatically transferred to a cloud data storage system. This system logs the data at the resolution contained within the .csv files. The data can then be accessed through the internet. This form of data logging allows data to be securely shared with third parties as account specific restrictions to data visibility can be set.

Low resolution data log

The turbine has an additional low resolution log of data. This data storage, supported by EMEC, logs all data tags as well as the tags owned by EMEC. The software also provides a service whereby the data can be displayed as a graph giving the Orbital Marine Power team quick access to live data. The addition of EMEC data tags allows for additional analysis.

2.3. Future Orbital Marine Power data pipeline

2.3 Future Orbital Marine Power data pipeline

As Orbital Marine Power aims to increase their turbine fleet and expand to multiple locations, the volume of data being logged will grow dramatically. It is, therefore, important to have a robust data pipeline in place before scaling up.

Figure 2.2 shows the proposed future data pipeline for Orbital Marine Power. Orbital Marine Power looks to deploy an array-level data handling package with the ability to clearly present useful data at the point of need as well as access to raw data for enhanced scrutiny. This will reduce analysis time and fault-finding enabling operations and maintenance teams to ensure high levels of up-time. The package will also use data analysis algorithms trained on legacy data to feed into the data log. This will give an advanced level of understanding and will aid controller performance at an individual turbine and the full array scale. This will help optimise power production from the entire farm. Orbital Marine Power will expand on the use of a maintenance management tool currently used for a single turbine. The deployment of this software on an array level will represent a step change in the ability to optimise the allocation of assets for the operations and maintenance teams. An automated feedback of turbine and array data will look to enhance the sophistication of this platform further, giving the ability to deploy predictive maintenance techniques rather than time windowed regular maintenance. This will reduce overall maintenance costs and reduce the offshore person-hours.

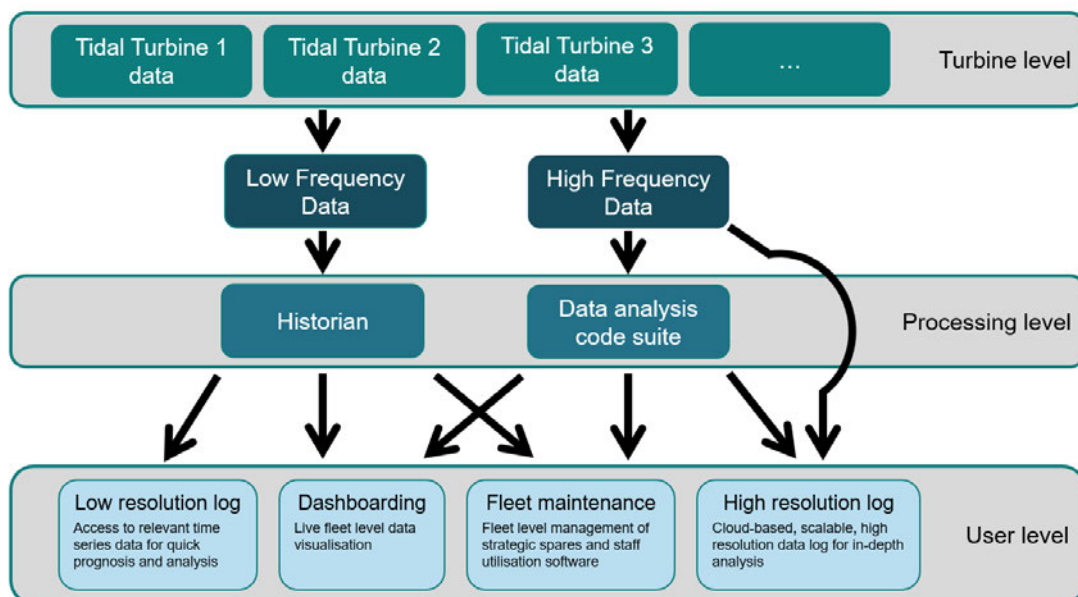


Figure 2.2: Schematic of the future data pipeline for Orbital Marine Power designed to handle large volumes of data from multiple turbines and multiple arrays

2.3. Future Orbital Marine Power data pipeline

Large volumes of input data are filtered through processing levels before being presented to an end user in a format based on use case. At the user level, a low-resolution log of the data will be made available allowing for quick time series analysis of short- and long-term processes. This data log will be fed by low frequency data flowing into a historian where the data is compressed using appropriate algorithms.

A suite of algorithms based on models trained using legacy data and simulation data will be created. This suite will use machine learning as well as other large dataset analysis methods and will enable pre-emptive fault finding as well as provide information like wave and environmental statistics that cannot be measured from a floating platform directly. This code suite will feed new data streams into a number of end user platforms including looping back into the array controller in order to optimise array power production.

The visualisation of live data is important for alarm recognition as well as having a system performance overview. The whole system array data will be condensed to data relevant to live operation and displayed on a user-friendly interface. The majority of the data displayed on the array dashboard will come from the low frequency data log, however, a number of data streams will be fed directly from the data analysis code suite.

The maintenance software used by Orbital Marine Power will be expanded to accommodate multiple turbines. The software will primarily use the low-resolution log of data from the turbines but will also incorporate data streams created by the analysis code suite to help plan for maintenance jobs. The system will also have access to a maintenance inventory in order to implement a strategic spares plan and, therefore, will be critical to efficient maintenance planning.

A high-resolution log will create a platform for in-depth array level analysis. The log will be hosted by a scalable cloud server with the ability to assign access rights for different data streams to different third parties. Initially, the data from this log will be used to train the machine learning algorithms and other code present in the data analysis code suite. The easy access of the high-resolution log will be pivotal in analysing and reporting array performance as well as in-depth fault finding.

The work of this thesis acts as a precursor to sections of the data framework just outlined. The progression from single turbine to fleet level can be seen in the comparison of Figures 1.3 and 2.2. It is important that the framework works on a single turbine level before it is applied to a fleet level.

PART I

Increasing Knowledge-Return from Data by
Re-Analysing Existing Data.

Data Handling Advancements for the Design and Operation of the O2

3.1 Introduction

The logging of data without meaningful ways to process and interpret it is pointless, as the mere accumulation of data does not provide insights. Often, methods for data interpretation and analysis are slow only because they are not meant to be repeatable and are only used on an ad hoc basis. Well thought-out and structured data processing enables fast extraction of information from the data that can be repeated for other datasets. The streamlining of a number of data processes previously used by Orbital Marine Power on a single-use basis are developed in this chapter to enable repeatability and low processing time.

3.1.1 Harmonic analysis for tide speed prediction on-site

The standard way a tidal resource is determined for a site is through a harmonic analysis. The link between the tides and the orbits of celestial bodies allows tidal cycles to be broken into multiple sinusoidal constituents with differing wavelengths and amplitudes. Calculating these parameters for a particular site enables the forecasting of the tide. This calculation is done, in essence, by a fast Fourier transform of a small time period of recorded tide speeds at the location. The accuracy of the tidal constituents calculated is, in part, a function of the period of time over which the initial data recording takes place (Xu, Haas, & Gunawan, 2023).

3.1. Introduction

Orbital Marine Power have deployed numerous seabed ADCPs to collect data for harmonic analysis and forecasting of tide speeds. These calculations are important for financing of a tidal site as the predicted electricity generated is calculated using this resource calculation and the power curve of the tidal device. Harmonic analysis calculations are often done in isolation as they are only intended for a single use.

Knowledge of the future tide state is not only important for calculating predicted energy production, it is also useful for the operations and maintenance of a tidal turbine. The floating design of the O2 enables maintenance to be carried out during slack tide where no generation happens. This enables short maintenance procedures to be carried out without the need for any downtime from a production perspective. In order to take advantage of this floating design benefit, the operations team need a reliable prediction of when these slack tides will occur.

Maintenance procedures that are larger and require a longer period of time are carried out during neap tides. This is a period of time when the tidal speeds are less intense. Using neap tides also mitigates the affect of any necessary downtime that lasts longer than a slack tide as the flow speeds are lower and so the amount of energy missed is low. Harmonic analysis can also play a part here where the spring and neap cycles can be observed and maintenance can be planned accordingly.

Harmonic analysis is one area identified where streamlining could be applied to great affect within this body of work. Another area of interest is fatigue loads and their quantification.

3.1.2 Fatigue calculations for the analysis of turbine lifetime

The O2 is designed with a lifetime of 25 years over which it will experience a number of high load events due to storms. The majority of the loads experienced in this lifetime will be much lower than these high load cases and so it is important to monitor fatigue as a potential failure mechanism.

Fatigue is studied in the literature from model data, however, often due to the need for companies to protect their intellectual property, fatigue data is not made open access and so only a number of studies have been conducted looking at tidal turbine fatigue using real data including Ahmed, Apsley, Afgan, Stallard, and Stansby (2017) and Mullings and Stallard (2021). Operational fatigue data is of high importance within Orbital Marine Power as the dynamic tidal environment can cause large cycles on a number of components.

3.1. Introduction

Damage is a commonly used parameter to quantify fatigue for any industry. Damage is given by the Miner's rule and indicates the proportion of fatigue life remaining in a material (Antolovich et al., 2013). For Orbital Marine Power, the calculation of damage is only performed for a set number of target components which were instrumented in the design phase to record fatigue.

Damage Equivalent Load (DEL) is a common method of presenting fatigue loads. A DEL is a means of collapsing all cycles into a single load value by calculating the load, with a predefined frequency, that would generate the same damage as the cumulative real-load real-frequency damage recorded (Freebury & Musial, 2000). Calculating a DEL enables time domain analysis of damage as a value can be calculated in time steps. It also facilitates comparisons of damage to modelled data as the values being compared can be like-for-like.

3.2 Streamlining data processes for the analysis of O2 operational data

3.2.1 Forecasting tide speeds for operation and maintenance of the O2 using harmonic analysis

Tide speed forecasting is a key tool for operations and maintenance that insures site conditions are appropriate for the safe execution of tasks. It also ensures that the turbine is offline at appropriate times to minimise electricity production downtime as discussed earlier. The ability to forecast tides is a common process for a range of marine users. The way the data are displayed, however, is key to the usability of a prediction.

Previous tidal speed forecasting for operations and maintenance

The initial tide speed forecasting for the O2 was done using flow sensor data collected by EMEC as well as flow sensor data collected from onboard Orbital Marine Power's previous device, the SR2000, when it was on site. These two datasets were processed using the MATLAB code UTide in order to calculate the tidal constituents (the updated version authored by Codiga (2023)). This UTide prediction was then outputted as a time series graph and given to the operations team.

3.2. Streamlining data processes for the analysis of O2 operational data

Limitations of previous tidal speed forecasting for operations and maintenance

The legacy method used by Orbital Marine Power for operations and maintenance tidal predictions was slow and cumbersome. This is because a limited amount of data could be displayed on a single graph. The method was also hindered by the need to produce a new graph for each time period of interest, a highly laborious task.

Consultation with the operations and maintenance team outlined a number of user-based limitations. The key user-based limitation was the inability to balance the volume of data that could be displayed on one graph while maintaining the ability to read off exact times of interest. This is important as some tasks can only be performed when the tide magnitude is below a certain value.

Streamlined tidal speed forecasting for operations and maintenance

The streamlining of the tidal speed forecasting tool addressed the limitations from processing as well as from a user perspective. Figure 3.1 shows the process involved in streamlining the tidal forecasting tool.

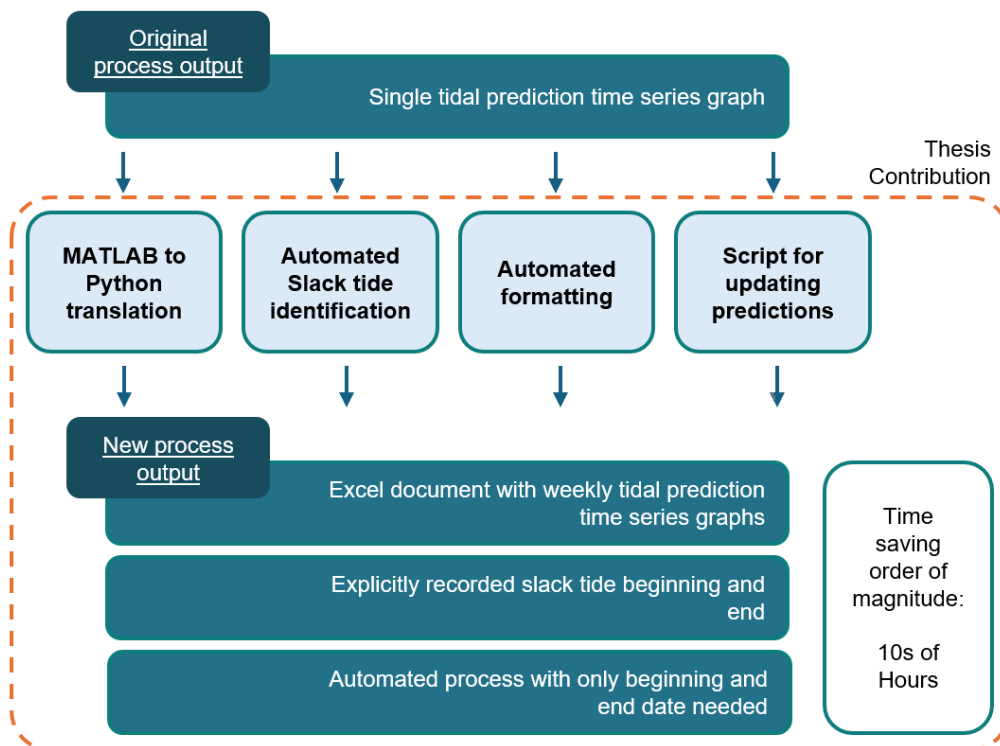
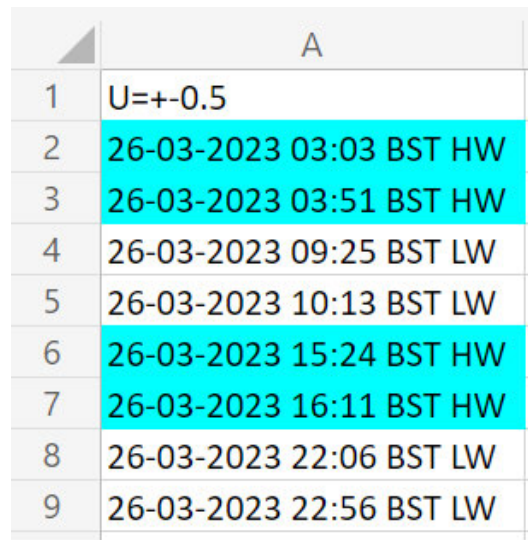


Figure 3.1: Process involved in the streamlining of the tidal prediction forecasting including the identification of the thesis contribution in this task.

3.2. Streamlining data processes for the analysis of O2 operational data

User limitations were addressed by supplementing the time series graphs of tide speed with a spreadsheet of slack water times. Slack tide was indicated by absolute tide speeds of less than 0.5 m/s. Time series data were processed for beginning and end of the slack tide, each slack tide pair was then coloured the same for ease of visuals. The outputted spreadsheet can be seen in Figure 3.2. Each slack tide pair is also labelled with either ‘HW’ or ‘LW’ to indicate if the slack tide corresponds to a high or low water slack.



	A
1	U=+-0.5
2	26-03-2023 03:03 BST HW
3	26-03-2023 03:51 BST HW
4	26-03-2023 09:25 BST LW
5	26-03-2023 10:13 BST LW
6	26-03-2023 15:24 BST HW
7	26-03-2023 16:11 BST HW
8	26-03-2023 22:06 BST LW
9	26-03-2023 22:56 BST LW

Figure 3.2: Sample of the Excel output from the streamlined tidal speed forecasting tool.

The time series graphic was also altered after consultation with the operations and maintenance team. Figure 3.3 shows a sample graphic for one week of tidal predictions. Lines for $y = \pm 0.5$ m/s were included as well as an indication of which side was flood and ebb. This allows for a large amount of data to be inferred without the need to study the graphic in detail. One of the benefits of the $y = \pm 0.5$ m/s lines is that periods of spring tides and neap tides can be seen very clearly.

The tidal prediction was split into week long sets with an accompanying Excel sheet of each slack tide pair in that week and a time series of the entire week (see Figures 3.2 and 3.3). In the same Excel document, each week was collated on a new page allowing for a compact accumulation of a long term multi-week tidal prediction that could be used effectively for operations and maintenance.

The laborious nature of creating these predictions was also a target of this work. The entire process was moved from MATLAB to Python as part of the company shift to the open source code platform. The Python code used a start date and an end date as well as a binary function indicating Greenwich Mean Time (GMT) or British Summer Time

3.2. Streamlining data processes for the analysis of O2 operational data

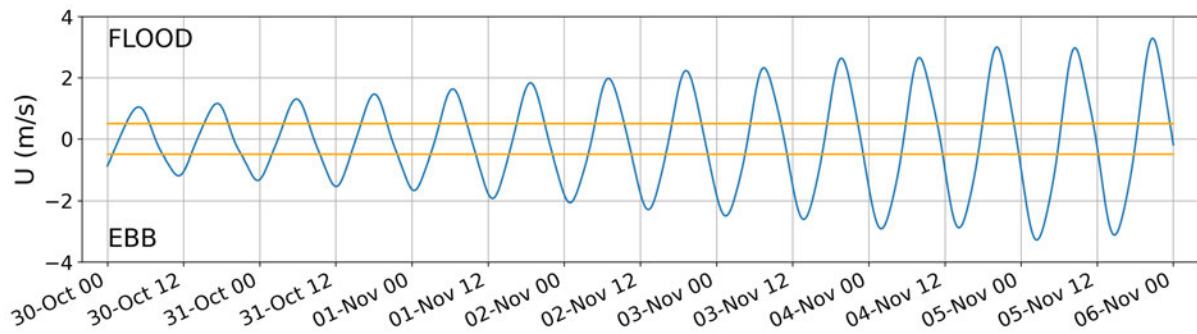


Figure 3.3: Sample of the time series graphic output from the streamlined tidal speed forecasting tool.

(BST). The output was a self-contained Excel spreadsheet with each full week between the start and end date split into separate Excel pages. In automating this process with a Python script, time taken to perform tidal predictions has decreased from a number of hours to under a minute.

Harmonic analysis has the ability to drift in accuracy as the prediction moves away from the initial time period of recording from which the tidal constituents were calculated. To account for this drift, a supplementary Python script was created that allows for an updated harmonic analysis based on O2 mounted downward facing flow sensor data. This data source is grid connected and always live, therefore giving a long term reading of the tide speed at site. Using this data source at regular intervals ensures that the accuracy of the tidal prediction for operations and maintenance is maintained.

3.2.2 Efficiency savings in the calculation of fatigue parameters of the O2 for confidence in lifetime predictions

Orbital Marine Power use both the actual Miners rule value of damage as well as the DEL when quantifying damage on the turbine (Antolovich et al., 2013). The damage value is primarily used when comparing damage on a time-step by time-step basis, whereas DELs are used in comparing model predicted damage to real damage experienced by the O2.

3.2. Streamlining data processes for the analysis of O2 operational data

Previous calculation of fatigue parameters

One key focus of fatigue monitoring for Orbital Marine Power are the two leg joints on the turbine. This is because large load cycles are experienced here due to the moment created by the rotor thrust and the length of the leg. Prior to process streamlining, the fatigue calculation for the legs was a two-step process. Firstly, the time series data were rainflow-counted in order to obtain the cycles and amplitudes. The rainflow table was then inputted into an Excel spreadsheet set up with appropriate fatigue curves to calculate damage. This process was time consuming and took two members of staff, one experienced in obtaining the rainflow table from the time series data and one experienced in using the Excel spreadsheet.

DEL was a common output from the software used to model loads on the turbine. This allowed for comparison of fatigue between different runs of the model, however, the calculation was not implemented on Python within Orbital Marine Power and so comparison between model DELs and measured DELs using Python was not possible.

Limitations of previous calculation of fatigue parameters

The main limitation in the previous calculation of fatigue parameters was the time consuming nature of the calculation. Leg load fatigue calculations were particularly time consuming whereas the DEL calculation had not yet been implemented on Python within Orbital Marine Power.

Streamlined calculation of fatigue parameters

The fatigue calculations for Orbital Marine Power were streamlined by converting the existing process to a Python function. This process is described in Figure 3.4. Having the calculation in a Python function acted as an enabler for fatigue studies that would have otherwise been overtly time consuming.

One such application of the new fatigue function was to analyse the effect of the tide state on the damage experienced by the leg joints. This study was instigated by a concern that the majority of the damage might have been occurring when the turbine was not experiencing thrust and waves were present, i.e., slack tide with waves.

3.2. Streamlining data processes for the analysis of O2 operational data

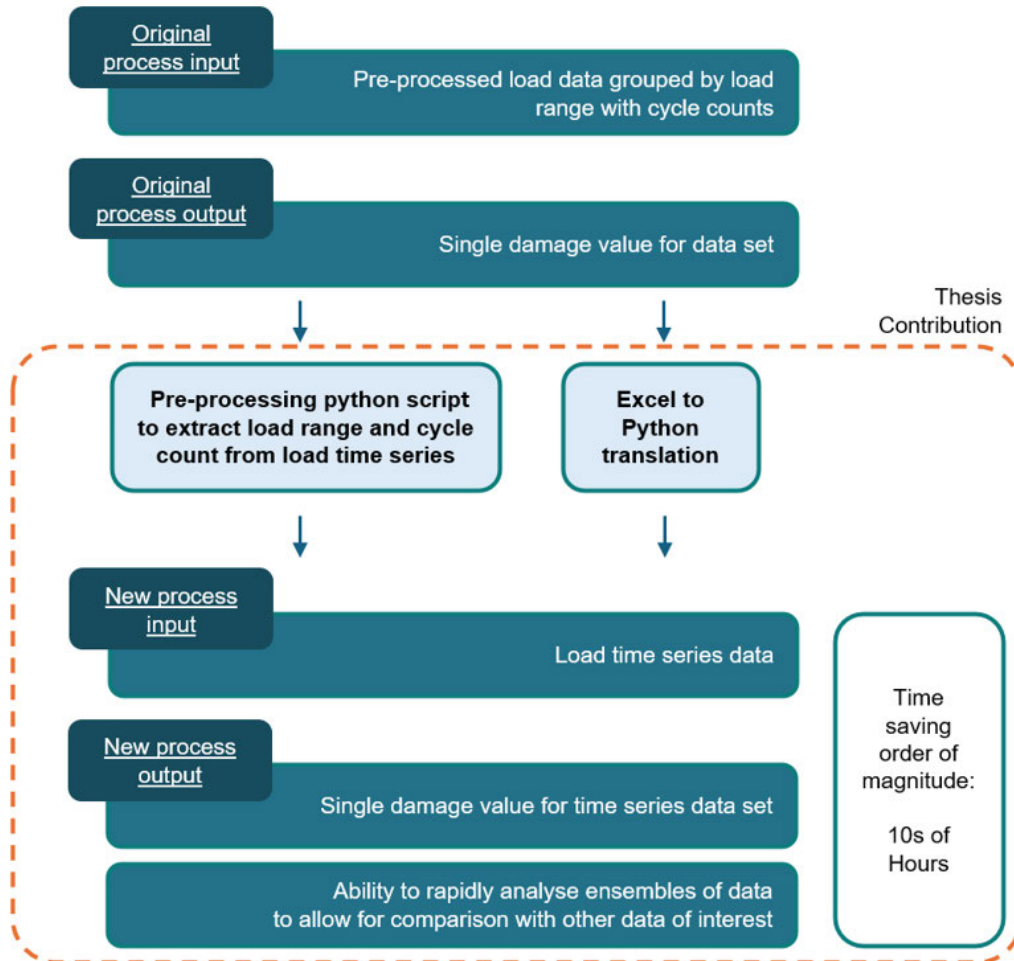


Figure 3.4: Process involved in the streamlining of the damage calculation method including the identification of the thesis contribution in this task.

This study divided 6 months of leg load data into slack tide, flood tide, and ebb tide. For each tide period the following were calculated: wave height, wave period, power generated, tide magnitude maximum, and leg load damage for port and starboard using the new Python tool. Collating the data in this way allowed for easy analysis of a number of different factors affecting leg joint loads.

The first comparison made was the effect of tide state on the leg joint damage. Naturally, the tide state was not the direct cause of the damage, but rather, coincided with other physical phenomenon that would occur at the same time. Figure 3.5 shows that more damage occurred during slack tides, followed by non-operating periods of either flood or ebb tide.

An understanding of where the most damage occurs in a tidal cycle enables Orbital to make informed operational decisions. Figure 3.5 shows REDACTED

3.2. Streamlining data processes for the analysis of O2 operational data

The dataset was analysed further to correlate wave height and tide speed with damage, however, the focus of this chapter is the efficiency savings of streamlining the processes and so this further-understanding developed is not in the scope of this chapter.

The creation of the DEL function also streamlined the comparison of recorded O2 data to model data. This function was used extensively in Chapter 5 where it is discussed in detail.

Figure 3.5: REDACTED

3.3 Application and Impact

The streamlining of data processing described in this chapter fulfilled Aim 1 set out in Section 1.4. The objectives were met by large savings of both computational time as well as human resource hours.

The automation of the harmonic analysis for operations and maintenance planning:

- Eradicated the effort and hours needed for the production of tidal predictions.
- Created an ‘easy to interpret’ data format for the operations team.
- Ensured longevity by developing a script to update tidal predictions.
- Created an easy to run and edit master script for further edits as required.

In doing this, time for other work was created. The ability to output processed data faster enabled more data to be created. The time period over which the tidal predictions were outputted increased from two-week blocks, to half a year in each Excel file. Increasing this volume of data allowed the operations and maintenance team to plan further into the future with greater confidence which reduces operational risk.

The translation and adaption of the fatigue and DEL calculations in conjunction with data access all within a Python environment:

- Enabled in-depth fatigue analysis to be conducted faster.
- Allowed ensemble data to be analysed in order to compare with other data streams like environmental conditions.
- Reduced the number of data processes required to be executed.
- Ensured code remained accessible for future edits as required.

Developing a method with a shortened time requirement enables more learning to be generated as time becomes less of a constraint.

3.3. Application and Impact

The work done for this chapter also had longer term, less directly tangible, impacts. Data streamlining enabled the progression of other research at a faster rate than would have otherwise been possible. The translation and automation of other Orbital Marine Power work allowed for efficient use of time throughout the completion of studies pertaining to the entirety of this thesis.

3.4 Conclusion

Data handling and data processing form the basis for any data driven research. The ability to streamline this first stage acts as an enabler for downstream processes. This is true for most data applications but is very relevant for a resource limited sector like tidal stream.

Two examples where streamlining a process had a large effect on the volume of data and information that could be conveyed were presented in this chapter. These examples were harmonic analysis for operations and maintenance, and the streamlining of the fatigue calculation used to analyse leg joint fatigue.

Streamlining the harmonic analysis process to enable the fast extraction of tide states key to the operations and maintenance team allowed important data to be conveyed clearly to the team. The human-hours needed for the process were greatly reduced freeing up time for other work.

Fatigue calculations are important for the tidal sector. This work showed how streamlining allowed for more data to be processed at a faster rate enabling more understanding to be taken from recorded data.

The work conducted in this chapter saw a large reduction in time needed for the completion of processes. It also generated a basis for functions applied throughout the work conducted in this thesis as well as other work within Orbital Marine Power. Data access, along side streamlined functions, generated the ability to quickly analyse datasets for fault finding, operational insights, as well as stand alone knowledge building studies.

Estimating Tidal Site Wave Statistics for the Design, Operation, and Maintenance of the O2 Using the Existing Onboard Sensor Suite

4.1 Wave statistics introduction

Environmental data are key to understanding the loading regime and response of a tidal turbine on site. Waves represent a significant load case as they introduce more load cycles to the device, affecting fatigue of the turbine itself as well as ancillary structures (Thies, Johanning, Harnois, Smith, & Parish, 2014). Larger waves can also act as an ultimate load state for tidal turbines (McCann, 2007). Given this ultimate and fatigue load duality attributable to waves, tidal developers are keen to record waves accurately in order to correlate to load data.

The ability for turbine access forms one of the underpinning principles for floating tidal turbines. Generating an access envelope based on wave height and tide speed for safe operations and maintenance requires the recording of wave parameters. This access envelope can be paired with local wave height statistics to estimate accessibility for operations and maintenance teams, something already done in the wind industry (Rowell, Jenkins, Carroll, & McMillan, 2022).

The loading implications, along with platform access limits, generates a need case for the recording of wave parameters for floating tidal energy. The requirement to understand how waves impact turbine motion, loads, and access is continuous, and therefore the measurement of waves should be uninterrupted.

4.1. Wave statistics introduction

4.1.1 Wave theory

Oceanic waves can be generated from a range of different sources creating waves of varying periods (see Figure 4.1). The majority of oceanic waves are wind generated, with energy contained within the waves dependant on the fetch. The fetch is the distance over which the wind is in contact with the sea surface and therefore represents the distance energy can be imparted into the waves. A short fetch generates capillary waves. Increasing the fetch sees the waves develop into ripples and then fully developed seas and swell. A fully developed sea is when the wind can not impart any more energy into the waves. Once waves become swell waves, or ordinary gravity waves (see Figure 4.1), they are sustained by gravity alone. Ordinary gravity waves are the most energetic wind generated waves and so will have the greatest effect on a tidal turbine (see Figure 4.1).

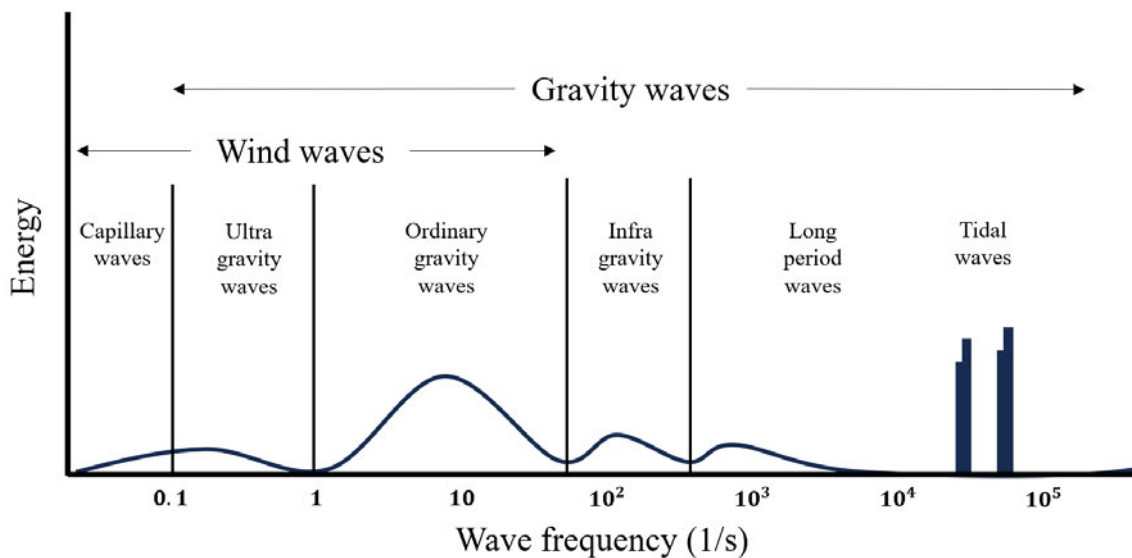


Figure 4.1: Oceanic waves classified by frequency (adapted from Munk (1950))

Swell wave

A fully developed single frequency swell wave, assumed to be sinusoidal, will have a surface elevation given by Equation 4.1 where η is the surface elevation, H is the wave height, λ is the wave length, T is the wave period, x is the axis of travel, and t is time (Brown, 2016).

$$\eta = \frac{H}{2} \cos \left(\frac{2\pi x}{\lambda} - \frac{2\pi t}{T} \right) \quad (4.1)$$

4.1. Wave statistics introduction

Dispersion relation

Waves are dispersive as their velocity varies with wavelength. This phenomenon is described by Equation 4.2 where ω is the angular frequency given by $\omega = \frac{2\pi}{T}$, κ is the wave number given by $\kappa = \frac{2\pi}{\lambda}$ and h is the water depth (Brown, 2016).

$$\omega^2 = g\kappa \tanh(\kappa h) \quad (4.2)$$

Equation 4.2 can be simplified by making assumptions on the water depth in relation to the wave length. In deep water where h is much larger than λ and so the value of κh is much greater than 1. As a result, the hyperbolic term $\tanh(\kappa h)$ equates to approximately 1. This simplifies the dispersion relation to Equation 4.3 (Brown, 2016).

$$\omega^2 = g\kappa \quad (4.3)$$

The shallow water assumption is when the water depth, h , is much smaller than λ . This results in κh being much smaller than 1. As a result, the hyperbolic term $\tanh(\kappa h)$ is approximately equal to κh and so the dispersion relation simplifies to Equation 4.4 (Brown, 2016).

$$\omega^2 = gh\kappa^2 \quad (4.4)$$

Wave spectra

In a real world environment, the sea state will never be a single frequency wave. The description of a single frequency wave as a sinusoidal wave (see Equation 4.1), however, allows for superimposition of numerous waves of different amplitudes and frequencies to generate a sea state more inline with recordings from an oceanic wave measurement device (Brown, 2016).

Superimposition allows a sea state to be classified by a spectrum of frequencies and amplitudes. The physics of waves causes sea state spectra to follow similar patterns irrespective of location. Particular increases in wave amplitude at specific regions of the wave spectrum can be used to identify locally generated wind waves as well as fully developed swell waves. Traditional spectra used to represent the real sea state include the ‘Pierson-Moskowitz’ and ‘Joint North Sea Wave Observation Project (JONSWAP)’ spectra (Hasselmann et al., 1973; Pierson & Moskowitz, 1964).

4.1. Wave statistics introduction

4.1.2 Recording oceanic waves

The recording of oceanic waves is highly important for a range of marine applications and so numerous measurement techniques are deployed. These measurement techniques are at a range of scales measuring different variables.

Oceanic wave measurement instruments

Measurement instruments for recording oceanic wave parameters can be divided into in-situ and remote sensing systems as suggested by Story et al. (2011). Each category provides strengths in differing areas. Figure 4.2 visualises the trilemma experienced by each measurement technique currently in use, whereby each single instrument can only obtain two of the three desirable criteria. In a number of cases an array of identical sensors can be used to tackle all three criteria, however, this comes at a considerable increase to cost.

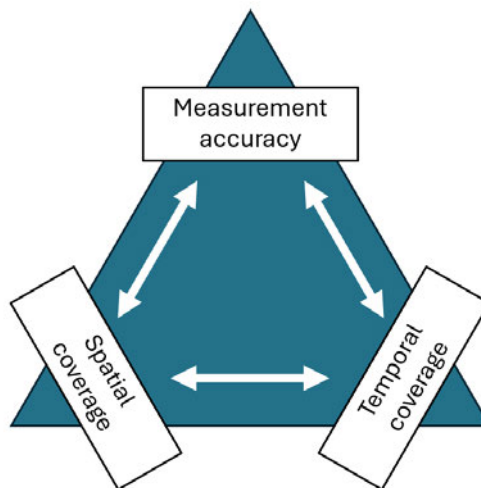


Figure 4.2: Wave recording trilemma (Story et al., 2011).

A common, in-situ, long term, recording technique for wave data is the deployment of wave rider buoys. The physical motion of these buoys are translated into wave parameters. These buoys are a point measure of the wave conditions and so have a low spatial coverage, but can be used in conjunction with other datasets. One example is the Met Office wave forecast which uses a range of data sources as input for a model (Valiente et al., 2023).

4.1. Wave statistics introduction

Another in-situ point measurement technique for waves is the deployment of ADCPs. These devices can record the orbital velocity of particles within a wave as well as the change in surface elevation and the change in pressure as a wave passes through, all in order to measure key wave statistics. While ADCPs offer poor spatial coverage as they are a point measurements, they are able to record wave parameters in high tidal velocities where wave buoys can not due to drag on their structure effecting the motion relied upon for accurate wave recording.

Satellites are a remote method of wave recording and can be used to obtain wave height and period data through altimeters and directional spectra using Synthetic Aperture Radar (Krogstad & Barstow, 1999). Satellite data are often intermittent as measurements can only be taken when the satellite orbit moves over the target location. As a result, this method can not be taken as a continuous source. Satellites, therefore, comply with measurement accuracy and spatial coverage from the instrument trilemma in Figure 4.2, but fall short on temporal coverage.

Other remote sensing techniques include X-band radar (Story et al., 2011), with accuracy benefiting from the addition of a reference wave buoy in the measurement area (EMEC, n.d.), and HF radar, which can record from land. Both radar methods average over a relatively large area and so are less accurate than a point measurement.

For an IEC compliant resource assessment of waves for a wave energy converter, the required accuracy of measurement is dependent on the class of study. The IEC divide studies in to Class 1, 2, or 3: reconnaissance, feasibility, and design (IEC, 2015a; Ramos, Carballo, & Ringwood, 2016). The spatial coverage, temporal coverage, and measurement accuracy needed from the sensor is therefore on a case by case basis. Beyond the Class of study, financial constraints can have an affect on the equipment exploited during an oceanic wave measurement campaign.

Oceanic wave measurement parameters

The stochastic nature of real oceanic waves states lends itself to the recording of statistical parameters rather than instantaneous deterministic values. Some of the key wave parameters measured by wave measurement techniques are listed in Table 4.1.

This statistical approach enables probabilistic significant wave heights to be recorded. The statistical average wave as well as the 50-year or 100-year return wave can also be calculated. These extreme wave values are important in the design of a tidal turbine for ultimate loads and survivability.

4.1. Wave statistics introduction

Table 4.1: Standard oceanic wave statistics of interest.

Wave Parameter	Abbreviation	Definition
Significant wave height	Hs	Four times the standard deviation of of the sea surface elevation (Young, 1999) which is approximately equivalent to the average wave height of the largest one-third of waves present, as coined by Sverdrup and Munk (1946).
Peak wave period	Tp	The wave period at the spectral maximum energy of a sea state (Dalphinnet et al., 2023).
Wave direction	θ	The bearing to which the waves are traveling.

Wave direction is usually described as a third dimension in a frequency-energy graph. The direction of each wave form that makes up the sea state is identified with its respective energy and frequency (see Figure 4.3) (Holthuijsen, 2010). It is potentially not useful for an average wave direction to be reported. In cases where two distinct peaks of wave energy direction are present, it is possible for the mean direction to have no discernible energy present. In this case, mean direction can be misleading.

Other methods for describing wave period exist other than the peak period. The zero crossing period describes the average time between the surface elevation crossing the mean water level. Other methods discretise the energy spectrum in to separate peak or moments and reports these periods separately (Dalphinnet et al., 2023). For the purpose of this chapter, reference to wave period will indicate peak period (Tp).

Recording waves for tidal energy applications

For a tidal site it is common to record significant wave height, peak wave period, and wave direction during the resource assessment phase of a project using a seabed mounted ADCP as other recording methods struggle in the extreme tidal environment. This measurement activity is costly as it requires a deployment and retrieval operation with accompanying weather windows along with equipment rental and the risk of unmonitorable system failure due to the offline nature of data recording.

4.1. Wave statistics introduction

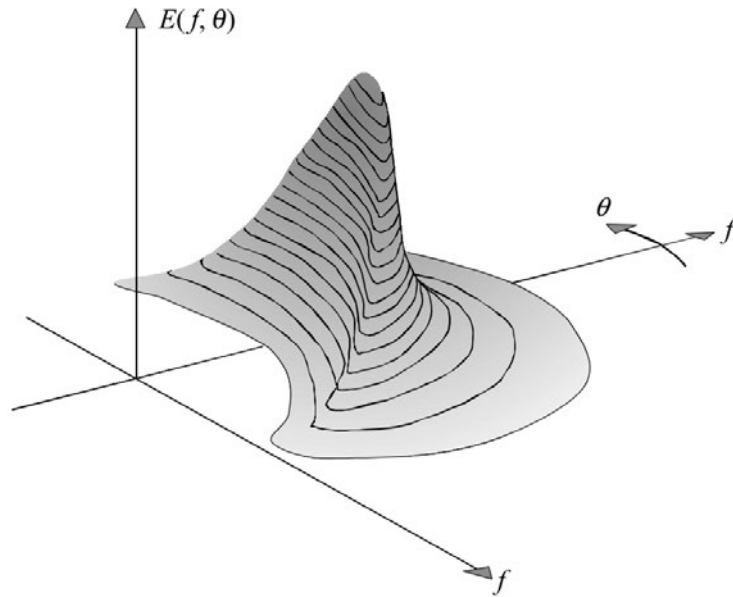


Figure 4.3: Directional spread of wave energy example (Holthuijsen, 2010).

One solution that would enable continuous wave statistic measurement without the need to deploy added sensors is to use the sensors already onboard the O2. Research into using a ship transfer function to convert heave, pitch, and roll of dynamic positioning vessels to wave parameters has been done, however, these methods assume the vessel is geostationary (Brodtkorb & Nielsen, 2023; Brodtkorb et al., 2018a, 2018b). Although the O2 is technically geostationary to within tens of meters, this assumption relates to the doppler shift affect of wave parameters when coupled with forward motion of the vessel. Given the relative motion between the water and the O2 due to tidal currents, the stationarity assumption does not hold in the case of the O2. Attempts have been made, however, to incorporate the forward velocities of ships using transfer functions (Iseki & Ohtsu, 2000). The ship transfer function method for wave height measurement as outlined in Brodtkorb and Nielsen (2023) requires the ship transfer function as a function of the wave frequency (ω) and wave direction (θ). For the O2, the transfer function will also be a function of tide speed as the mooring and trim dynamics changes depending on the tide speed which in turn affect the hydrodynamic response to incident waves. These added factors complicate this method further for the O2. Methods for converting platform motion of floating tidal energy devices into a wave height measurement is a research gap, owing manly to the few number of floating tidal turbines deployed in a significant wave environment.

4.1. Wave statistics introduction

4.1.3 Simulating waves using modelling software

The study of waves for the tidal sector goes beyond direct field measurement techniques. Fast, accurate modelling of tidal turbines in realistic conditions requires the simulation of waves by computational modelling software. In regularly used computational models like Tidal Bladed and OrcaFlex, waves can be inputted into the domain in order to model the turbine response to waves of varying magnitude.

Tidal Bladed is an industry standard numerical software tool used to model tidal turbine drive-train loads. Tidal Bladed is a software package built from Blade Element Momentum (BEM) theory with a number of relevant corrections to enable accurate results while maintaining efficient computing (DNV GL, 2016a). The initial BEM software saw the addition of structural dynamics capabilities to enable the modelling of entire tidal turbine structures. The comparison of field data to Tidal Bladed forms the basis for Chapter 5 where it is used extensively. Tidal Bladed wave distributions can either be defined as a JONSWAP function or by a user-defined look-up table (DNV GL, 2016a). Using the JONSWAP function, users enter values for significant wave height (H_s), peak period (T_p), and the, “ratio of the maximal spectral energy to the maximum of the corresponding Pierson-Moskowitz spectrum”, (γ) (DNV GL, 2016a; Hasselmann et al., 1973). Users can switch between a JONSWAP and a Pierson-Moskowitz spectrum by setting γ to 1. In Tidal Bladed the wave particle kinematics are also modelled to allow for pressure forces on submerged bodies to be calculated. The inclusion of a constrained wave of a specified height is also possible within the software.

OrcaFlex is a, “3D non-linear time domain finite element programme”, (Orcina, 2014) used by Orbital Marine Power to model O2 hydrodynamics. The software is capable of modelling the mooring configuration of the O2 as well as its trim response to thrust loads from tidal stream-rotor interaction. OrcaFlex can model a wide range of wave fields. Five frequency spectra are pre-programmed into the software and can be selected with the user defining wave height, period, and direction. OrcaFlex has the ability for multiple user defined wave directions. Breaking waves are notoriously difficult to model due to their complex physics. OrcaFlex implements a catching equation that alerts the user to unrealistic wave steepness (Orcina, 2014). Wave-current interactions are attempted by OrcaFlex in that the fluid velocity is corrected for current, however, this has no effect on wave period included (Orcina, 2014).

4.1. Wave statistics introduction

4.1.4 The wave climate in the Fall of Warness

The Fall of Warness tidal test site is situated with the island of Eday to the North-East and a number of other islands marginally further away to the South-West (see Figure 4.4).

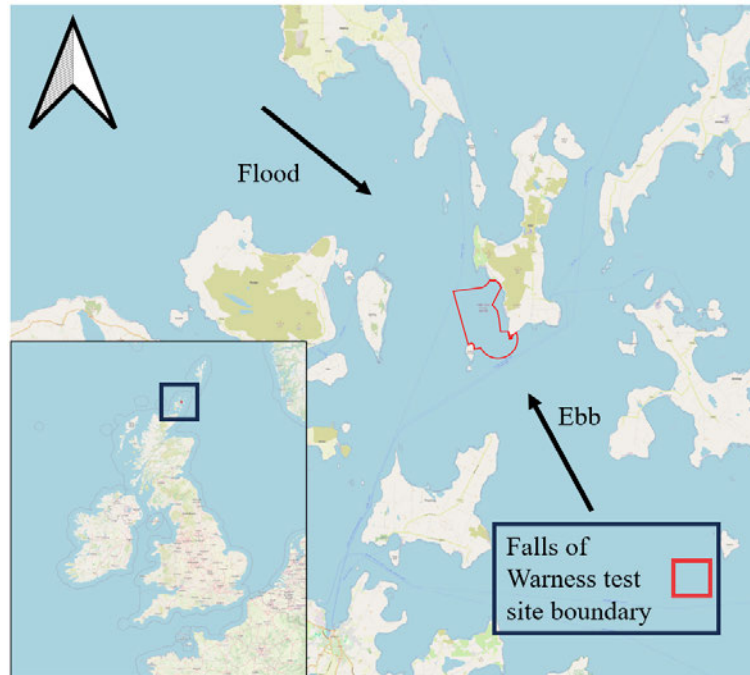


Figure 4.4: Map of the Fall of Warness tidal test site showing its location relative to neighbouring islands. Map courtesy of OpenStreetMap.org, test site boundary courtesy of EMEC.

The tide flows from the North-West on the flood tide and from the South-East on the ebb tide along the channels visible in Figure 4.4. Swell waves are generated over a large fetch as was discussed earlier. As a result, the swell waves in the Fall of Warness are constrained to follow the direction of either the flood or ebb tide. The much smaller fetch to the South-West of the tidal site (see Figure 4.4) is only capable of generating smaller locally generated wind waves.

The main hull of the O2 is orientated inline with the flood or ebb direction depending on tidal state. Waves along these directions are referred to here as inline waves. The locally generated wind waves from the South-West approach the turbine perpendicularly to the main hull, these are referred to as beam-on waves.

4.1. Wave statistics introduction

The Fall of Warness has seen a number of studies on the wave climate present dating back as far as 2006 (Norris & Droniou, 2007; Osalusi, 2010). The ReDAPT project was a key study in which the Fall of Warness and a fixed seabed mounted tidal turbine were heavily instrumented generating a number of environmental datasets including on the wave climate (Sellar & Sutherland, 2016). It is standard for the wave climate at a tidal site to be recorded using an ADCP owing to the high current environment as discussed earlier. A legacy recording of a wave climate is limited in usefulness for Orbital. This is because hydrodynamic responses can not be inferred as the turbine was not in situ during wave recording. Instead, Orbital deploy their own ADCPs near the turbine while at site in order to collect data that can be compared to other data streams.

4.1.5 Chapter aims

This chapter tackles Aim 2 from Section 1.4. The objectives are met by generating two solutions to in-situ wave Hs and Tp measurement for a floating tidal energy device that are simple to implement and with a transferable methodology for future iterations of the Orbital Marine Power tidal turbine technology. The solutions presented represent a range of complexity. The accuracy of each Hs and Tp measurement method is assessed against an ADCP recording of wave height and period. The accuracy of recorded parameters required is set out on a case by case basis. This allows for the limitations of the approaches to be outlined and to present avenues for improvement.

The two methods for Hs and Tp calculation are both based on hull pitch time series data but are named the Dispersion Relation Method and REDACTED in order to differentiate them from one another. The two methods are presented with their results separately, followed by a joint discussion.

4.2 Materials used

4.2.1 Wave related time series data available from the O2

The O2 is a large rigid structure floating on the surface of the ocean. As such, there are limited sensors onboard that are indirectly measuring the effects of waves. The main data recorded, relating to waves, come from the physical motion of the turbine as it responds to incoming waves. The IMU records a time series of both pitch and heave of the O2 which is logged to the onboard computer.

4.2. Materials used

4.2.2 REDACTED

4.2.3 On-site wave statistics dataset

The accuracy of any model created can only be validated by comparison to the true value. This true value must be the product of an external recording process in order to maintain separation for comparison. In this study, an ADCP deployment was used as a comparison dataset.

An ADCP dataset of wave height was recorded using a 5-beam ADCP placed at (59.144, -2.816) and recorded from 28/11/2021 until 27/12/2021. The data from the ADCP were processed into wave variables using the RDI software ‘WavesMon’.

In this dataset, 60% of the data recorded was below $H_s=1$ m, however, the dataset also represents a large range of wave heights with the maximum H_s recorded at 4.12 m (see Figure 4.5). Despite large waves being of interest for Orbital Marine Power, the O2 has an operational wave height limit of $H_s=2$ m and so heights around this value are more pertinent for Orbital Marine Power to record robustly.

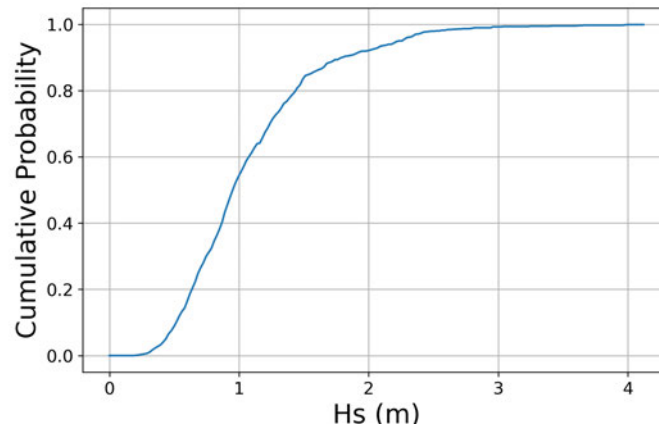


Figure 4.5: ADCP dataset cumulative percentage with respect to wave height showing the range of wave heights recorded in the set.

4.2. Materials used

4.2.4 Statistical tests

Throughout this chapter, the performance of wave recording methods is assessed by comparison with field data. This performance is quantified and visualised using statistical tests and comparison plots. The two key tools used are the Kolmogorov-Smirnov (KS) test and the Bland-Altman (BA) plot.

Kolmogorov-Smirnov test

The KS test is a non-parametric test used to test if two samples from a continuous or non-continuous dataset came from the same probability distribution. Parametric test often assume the underlying probability distribution is normal, while non-parametric tests make no assumption of the underlying probability distribution of a sample (Hollander, A. Wolfe, & Chicken, 2015). A non-parametric test is, therefore, useful for the analysis of waves as waves tend to not be normally distributed, as was discussed earlier.

The KS test outputs a test statistic as well as a P-value. The P-value indicates the probability the two datasets being tested are from the same distribution. The test statistic gives the maximum vertical difference between the cumulative probability distribution of both datasets. A plot of cumulative probability is a means of visualising the distributions that forms each of the datasets. Differences can be identified when two distributions are plotted together. The test statistic can therefore give an indication of how different the two distributions are.

Bland-Altman plot

A BA plot is a method for visualising the similarity or difference in two different methods of measuring the same thing. The plot was first presented by Altman and Bland (1983). The plot sees the mean value between the two measurement techniques for a time instance plotted on the x-axis and the difference between the two values on the y-axis. This allows for a measure of agreement that is not possible with a simple correlation value (Altman & Bland, 1983).

A number of statistics can be drawn out of a BA plot. It is assumed that the difference between the two measurement techniques is normally distributed (this can be forced if it is not the case (Giavarina, 2015)) and so standard normal distribution analysis can apply i.e., a mean value ± 1.96 represents a 95% probability bound for the data (Bland & Altman, 1999).

4.3 Methodology 1: The Dispersion Relation Method for the calculating of Hs and Tp

The first method for calculating wave statistics uses regular wave theory and the geometry of the O2. This method assumes that the waves are large enough that the O2 remains tangential to the water surface. In this case the O2 would appear as shown in Figure 4.6 with the pitch angle of the O2 determined by the tangential angle to the wave at the O2 location.

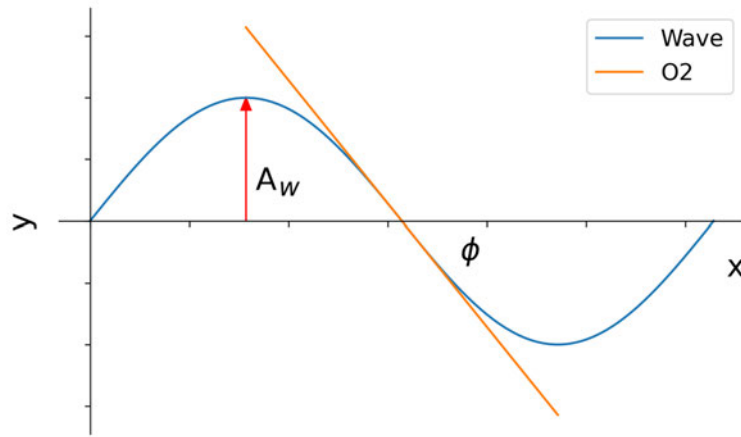


Figure 4.6: Simple schematic of the O2 following the surface of a perfect sinusoidal wave.

For this method, the shape of the wave is considered a perfect sinusoid by assuming deep water waves (this is a limitation of the method discussed later). The wave surface for the single wave seen in Figure 4.6 can be given as Equation 4.5 where A_w is the amplitude of the wave and λ is the wave length.

$$y = A_w \sin\left(\frac{2\pi x}{\lambda}\right) \quad (4.5)$$

The tangential angle to the wave surface is given by Equation 4.6.

$$\frac{dy}{dx} = \tan(\phi) = \frac{2A_w\pi}{\lambda} \cos\left(\frac{2\pi x}{\lambda}\right) \quad (4.6)$$

At the maximum pitch angle the equation for amplitude can be written as Equation 4.7.

4.3. Methodology 1: The Dispersion Relation Method for the calculating of Hs and Tp

$$A_w = \frac{\lambda}{2\pi} \tan(\phi_{max}) \quad (4.7)$$

From the deep water assumption (see Equation 4.3), wave length can be written as Equation 4.8 where g is acceleration due to gravity and T is the wave period.

$$\lambda = \frac{gT^2}{2\pi} \quad (4.8)$$

This leads to the instantaneous wave height given by Equation 4.9 where $H = 2A_w$.

$$H = 2 \frac{gT^2}{(2\pi)^2} \tan(\phi_{max}) \quad (4.9)$$

Equation 4.9 represents a method to hand calculate the instantaneous wave height for a given maximum pitch angle and period. This value is useful for calculating the height of a particularly large wave of interest but it does not allow for the calculation of the more commonly used statistical value of significant wave height.

In order to calculate meaningful wave statistics, Equation 4.9 was applied across a time series of pitch data from the O2 recorded at 10 Hz. The time series of pitch data was processed to identify local maxima and minima. The difference between these maxima and the preceding minima were taken as the maximum pitch angle as a result of each passing wave. Using this difference avoided affects of pitch as a result of trim due to O2 power generation. The time between each maximum was taken as the period of each individual wave.

Equation 4.9 was then used in conjunction with the maximum pitch angle and period of each wave as inputs. This allowed for the continual calculation of the wave field around the O2. The time series was then divided into 20-minute intervals. The significant wave height as well as peak wave period were calculated for each 20-minute period. The mean of the 1/3 largest waves was used to calculate Hs, while the peak period from a fast Fourier transform was used to find the peak period.

Using a single equation along with the numerous assumptions resulted in the need to calibrate this approach. This calibration was done by comparison to the ADCP dataset. The mean difference between the ADCP recorded data and the dispersion based method presented in this section, for the same time period, was plotted on a BA plot. Calibration consisted of forcing the line of best fit in the BA plot along $y=0$ to generate calibration constants that were then applied to each recorded value.

4.4 Results 1: The Dispersion Relation Method for the calculating of Hs and Tp

4.4.1 Wave Height

The Dispersion Relation Method and the seabed ADCP were measuring the same phenomenon and so a BA plot is appropriate to compare the two differing methods (see Section 4.2.4). Figure 4.7 shows that the comparison data are all grouped around zero difference, this is the effect of calibration to this ADCP dataset. Figure 4.7 also shows that there is a greater spread from the zero difference line with increasing mean with an average standard deviation of 0.397 m. This follows that 95% of the data falls within $\pm 1.96 * std$, or 0.778 m, from the $y = 0$ line in Figure 4.7.

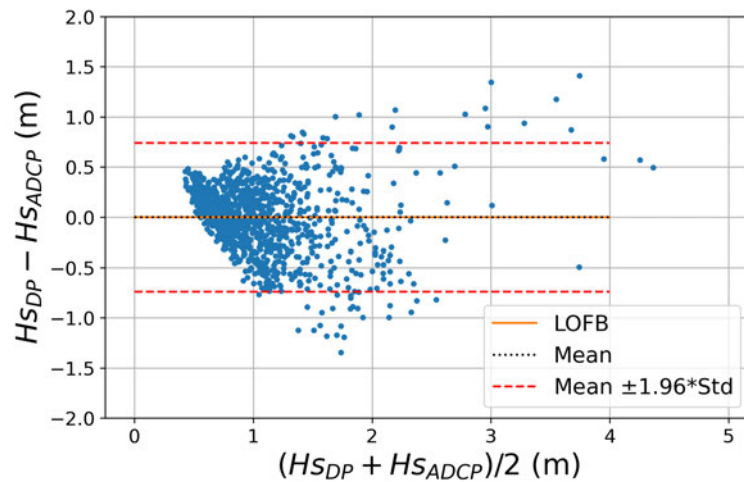


Figure 4.7: BA plot showing the difference between the seabed ADCP dataset wave height and the Dispersion Relation Method wave height against the mean of the two variables: where H_{SDP} is the significant wave height calculated from the dispersion relation and H_{sADCP} is the ADCP measure of significant wave height. A line of best fit, the mean difference, as well as the $\pm 1.96 * \text{difference standard deviation}$ limits are shown.

The KS test statistics (see Section 4.2.4) comparing the dispersion relation dataset and the ADCP field measurement dataset can be seen in Table 4.2 with the cumulative probability distribution function shown in Figure 4.8.

4.4. Results 1: The Dispersion Relation Method for the calculating of H_s and T_p

Table 4.2: KS test results for comparison of dispersion derived wave height and seabed ADCP measured wave height.

KS Test Results	
Test Statistic	0.2144
P-value	8.67×10^{-39}

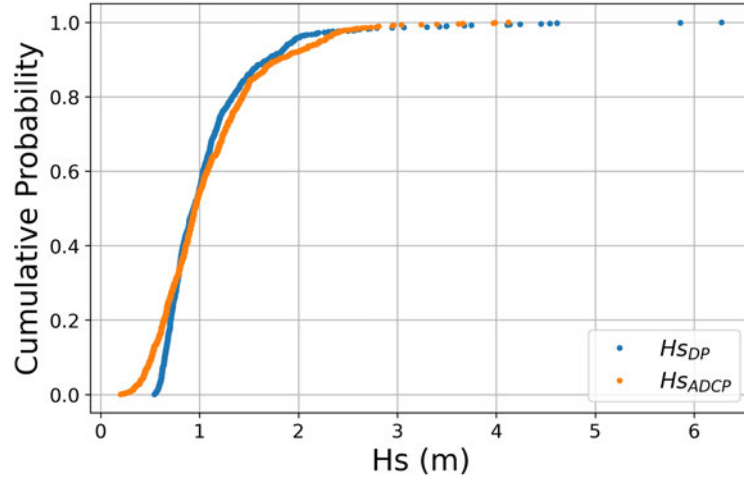


Figure 4.8: Cumulative probability distribution function of dispersion calculated significant wave height (H_{SDP}) and sea bed ADCP recorded significant wave height (H_{SADCP}).

4.4.2 Peak Wave Period

Peak wave period is the second variable of interest for calculation from the Dispersion Method outlined in this section. Figure 4.9 shows that 95% of the period values being calculated by this method are within ± 5.39 s of the values recorded by the seabed ADCP. The discrete nature of the ADCP period values is a result of early post processing using the software package WavesMon (Teledyne RD Instruments, 2011b).

The KS test statistics comparing the ADCP peak period dataset and the Dispersion Method calculated peak period can be seen in Table 4.3 with the cumulative probability distribution function shown in Figure 4.10.

Table 4.3: KS test results for comparison of dispersion derived wave Period and seabed measured wave Period.

KS Test Results	
Test Statistic	0.1399
P-value	1.925×10^{-9}

4.4. Results 1: The Dispersion Relation Method for the calculating of H_s and T_p

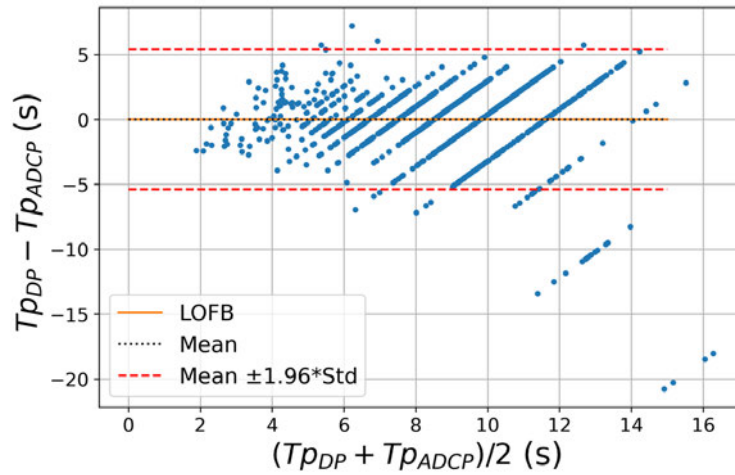


Figure 4.9: BA plot showing the difference between the seabed ADCP measured peak period ($T_{p_{ADCP}}$) and the Dispersion Relation Method peak period ($T_{p_{DP}}$) against the mean of the two variables. A line of best fit, the mean difference, as well as the ± 1.96 *mean difference limits are shown.

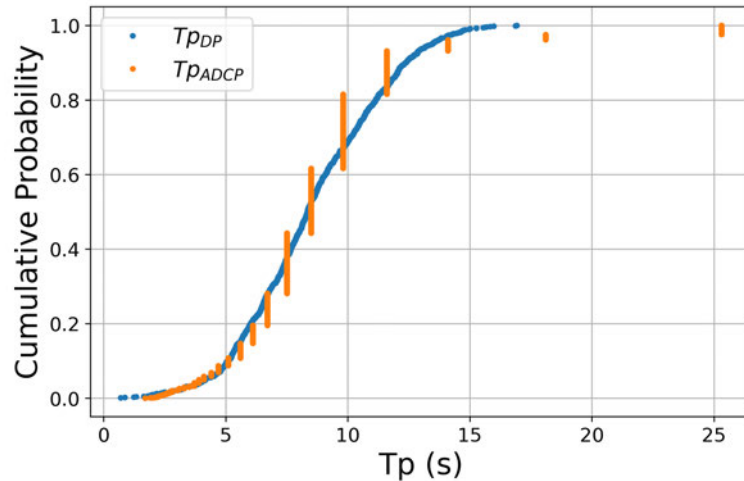


Figure 4.10: Cumulative probability distribution function of dispersion relation calculated peak wave period ($T_{p_{DP}}$) and sea bed ADCP recorded peak wave period ($T_{p_{ADCP}}$).

4.5 Methodology 2: REDACTED

4.6 Discussion

The accuracy needed from any wave height calculator is determined by the use case. In this particular instance, Orbital Marine Power have a range of use cases whereby wave height would need to be calculated. This ranges from safety for operations and maintenance access all the way to separating loads by wave height in order to gain more understanding of how the environment impacts the turbine.

Using this Dispersion Relation Method, the accuracy of the wave height was shown to be ± 0.778 m across the recording domain i.e. from $H_s=0$ to 4 m. This is low accuracy with 1 m waves being calculated as anything from 0.2 m to 1.8 m. These smaller waves are of more importance to Orbital Marine Power as the turbine can only operate in sea states less than around $H_s=2$ m and so this model can only be considered of limited usefulness for calculating H_s . Overall, Table 4.2 and 4.3 show that, with a statistical boundary of $P < 0.05$, it can be said that the Dispersion Relation Method is unable to map the wave height or period with any statistical significance.

REDACTED

The accuracy of wave height calculation from the various methods tracks with complexity. The assumption-laden Dispersion Relation Method is able to record the same mean as the seabed ADCP after being forced, however, the distribution recorded is not statistically similar (see Table 4.2). This compares to the REDACTED Method where it too is able to track the same mean after being forced, but also records the same distribution as the seabed ADCP (see Table REDACTED). Overall, however, the better of the two methods (the REDACTED Method) is still only able to record height to within 0.507 m with 95% confidence. This makes the method limited in its applicability.

Period recording is challenging in an energetic tidal environment even for a seabed ADCP. Using the period between pitch time series peaks followed by an FFT of periods (as described in the Dispersion Method, see Section 4.3) or the peak period using the REDACTED Method see their difficulties. Although both methods were calibrated to obtain the same mean as the seabed ADCP, statistically the methods failed to record the same distribution of period over the whole dataset (see Tables 4.3 and REDACTED). That said, between the two methods the Dispersion Method was able to record a distribution closer to the seabed ADCP than the REDACTED Method (Dispersion Relation Method KS test statistic : 0.1399, REDACTED Method KS test statistic : 0.2023).

4.6. Discussion

4.6.1 Methodology 1 Limitations

The Dispersion Relation Method has a number of limitations owing mainly to the simplification assumptions made during its formation. One limitation is the assumption that the O2 follows the surface of the waves perfectly and so the maximum hull pitch angle represents the maximum slope of the wave. This is not always a valid assumption as a result of the length of the O2. The incident wave length must be at least double the length of the O2 in order for only half a wave to be in contact at any one time. This would result in a wave length of 144 m. Assuming deep water for ease of calculation, the period of a 144 m wave is given by rearranging Equations 4.8 into Equation 4.10,

$$T = \sqrt{\lambda \frac{2\pi}{g}} \quad (4.10)$$

$$\lambda = 144 \text{ m}, \therefore T = 9.6 \text{ s} \quad (4.11)$$

A 9.6 s period wave is therefore needed for the turbine to only experience half a wave at a time. Larger waves on site are usually characterised by swell waves (see Figure 4.4). Generally, swell waves fall into the frequency band of between 8 and 15 s which coincides with the 9.6 s waves needed to avoid the affect of this limitation. That said, the assumption falls apart when the turbine is exposed to shorter period waves, wave that are not uncommon in a tidal site when the current can shorten the wave length of incident waves. Despite the period needed for half wave interaction with the O2 falling within the realms of the swell waves expected at site, the inertia of the 680 T O2 device will still cause the turbine to not follow the surface of the waves exactly.

Another inertia based limitation of the Dispersion Relation Method is that the wave recorded by the IMU will not be all of the waves present. This is mostly due to smaller waves being unable to alter the pitch of the device. As a result, the wave statistics for Hs, using the average of the 1/3 of the largest waves, may not work in this method the same way it might for a, low inertia, point recording wave buoy as not all the waves are recorded.

4.6. Discussion

4.6.2 Methodology 2 Limitations

REDACTED

4.6.3 Extending wave statistics to 3 dimensions

Wave direction is an important parameter to record as the transverse asymmetry of the O2 gives rise to different loading conditions based on wave direction. This asymmetric loading phenomenon makes a wave direction parameter important for classifying loads, enhancing understanding of loads, as well as informing dynamic de-rating as a turbine safety feature. For the O2, the direction of the waves is also important as the local tide speed will act to alter the wave climate between tides. Dividing wave direction into beam-on and in-line wave is also a useful separation. The O2 and its long slender main hull reacts very differently depending on wave direction. Despite the fetch for beam-on waves being very small in comparison to the in-line case due to the narrow nature of the Fall of Warness (see Figure 4.4), the beam-on wave generated locally can be a significant loading case for a number of load-of-interests. For this reason, the importance of wave direction is not squarely on the absolute direction, but rather, on the direction split in to forward, aft, and beam-on.

Estimating wave direction from a floating platform in a tidal environment using wave period, tide speed, and the corresponding Doppler shift

The method presented here for in-line wave direction calculation from onboard sensor data uses the Doppler shift. This method works on the principal that, if the tide is moving in the same direction as the waves, the addition of a tidal flow will act to increase the wave period. Tide and wave directions that oppose each other will cause a reduction in the wave period. This is summarised in Equation 4.12 where ω_R is the resultant wave frequency, ω_I is the incident wave frequency, κ is the wave number, and u is the tidal stream velocity (Hashemi & Lewis, 2017).

$$\omega_R = \omega_I + \kappa u \tag{4.12}$$

Using a number of assumptions listed below, Equation 4.12 is left with only one unknown that can be solved to find wave direction of the external wave field.

4.6. Discussion

1. The external wave field direction changes slower than the on-site wave field due to wave-current interactions at site that are not present beyond the site.
2. There is an accurate recording of the wave period and tide speed.
3. The external wave direction is constant for the duration over which it is being calculated.

This is explained more simply by saying, if the external wave field direction remains constant and the tide speed increases then the wave direction will be denoted by the corresponding change in wave period. This theory can be seen in Figure 4.11 where the period increases when the tide speed is negative. The deduction can therefore be made, in this example, that the waves are coming from the ebb direction.

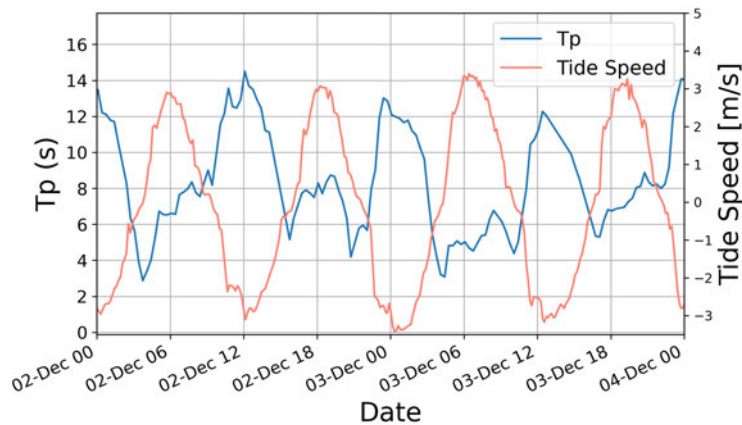


Figure 4.11: Pitching period and tide speed against time.

This theory could be applied to every two consecutive period readings along with their corresponding flow speeds. For each pair it could be deduced if the external wave field is coming from the same or opposite direction as the incident flow. This method requires at least two period readings for every directional reading and so represents an average across twice the duration of the period calculation. This relies on Assumption 3 above, that wave direction is static for at least this time duration.

Wave Direction Limitations

In order to obtain wave direction using the method outlined above, period must be recorded along with tide speed. In this chapter, two methods for calculating wave period were discussed. The technique outlined in the Dispersion Relation Method offered the most accurate recording of T_p when compared to the seabed ADCP T_p measurement. Of arguably equal importance as accuracy, in the period measurement for the Doppler Wave

4.6. Discussion

Direction Method, is consistency. The Doppler Method is only concerned with relative change in period compared to the neighbouring data point, and so, provided the error in period measurement is consistent, this method will still hold. Between the two approaches to T_p measurement outlined in this chapter, neither were able to replicate ADCP T_p measurements to a statistically significant level (see Table 4.10 and REDACTED).

The lack of accuracy in T_p calculations from the two methods presented inhibits the application of this method for wave direction calculations. While the Doppler Methods works in principal to give wave direction, further efforts are needed in the development of an accurate T_p measurement using onboard sensors before this method for wave direction can be implemented.

4.7 Application and impact

The applications of an accurate measure of wave height, wave period, and wave direction are wide ranging for Orbital Marine Power as well as for the wider sector. The ability to record these metrics without the need for additional instrumentation offers a chance to save costs and have an uninterrupted log of wave statistics. This chapter successfully fulfilled Aim 2 from Section 1.4 by creating a method for wave height measurement that only relies on sensors placed internally within the O2. The REDACTED method for wave height measurement has been used to allow for the classification of maximum loads by wave height as well as fatigue loads. The wave height measurements have also been used by the operations and maintenance team to help determine the wave height envelope for safe access.

The code developed from the REDACTED method was also implemented into the cloud based data storage system (described in Section 2.2.3) within a key performance indicator table. This table is currently updated every day with the expectation of direct logging in the future. Constant logging of the data and calculation of wave height will result in the continuous and semi-live stream of wave height and period measurement. This can then be used to make operational safe limit decisions in order to avoid high load events due to extreme waves. This in turn, would aid in increasing the life expectancy of the turbine by reducing the overall number of high cycle stresses.

4.7. Application and impact

The methods presented are fundamentally based on the geometry and hydrodynamic response of the O2. As a result, the methods are not site specific and can, therefore, be applied on O2 turbines in other tidal location. Orbital Marine Power is an ambitious company with a number of turbines in the pipeline aided by success in government backed auction rounds for CfDs. A number of different sites are also being prospected. These measures of wave statistics will serve to remove the need for expensive instrumentation at these sites further reducing the cost of the installations.

From a wider sector perspective, this study serves to validate and quantify the efficacy of the methods presented. The REDACTED Method methodology could be applied to other technology, naturally with the need to adapt the REDACTED for the particular turbine.

4.8 Conclusion

The ability to record wave height, period, and direction is important for the tidal sector as these values represent another loading regime that can effect both fatigue and ultimate load states. The wave environment is particularly important for floating tidal energy as these devices are located in the most energetic region of the waves. While short term recording of wave conditions can give some useful insights into loading regimes, the continuous recording of wave statistics sees many more benefits.

Two different methods for the continuous recording of wave height and period were presented using the main hull pitch of the O2 as the input data source. The Dispersion Relation Method used a number of large assumptions including that the O2 tracked the sea surface. The Dispersion Relation method was only able to measure wave height to within ± 0.78 m and peak period to within ± 5.4 s with 95% confidence when compared to a seabed ADCP. The REDACTED Method used REDACTED. The REDACTED Method was only able to measure wave height to within ± 0.51 m and peak period to within ± 4.5 s with 95% confidence when compared to a seabed ADCP. Of the four variables being measured (H_s and T_p from the Dispersion Relation Method and REDACTED Method) only H_s from the REDACTED Method was found to be statistically similar to the measure from the seabed ADCP.

A method for the derivation of wave direction from a peak period-flow speed relation was presented. The method, while potentially feasible, required a better recording of peak period and so was left as further work.

4.8. Conclusion

Continuous and reliable recording of wave height and period ensures a large spread of wave statistics and operational states are captured. This enables analysis of power, loads, and motion all relative to wave height with more data than would be available from a finite wave recording campaign.

Validation of a Numerical Simulation Tool Used to Model O2 Drive-Train Loads

5.1 Introduction

The use of numerical simulation tools is commonplace in any engineering application as well as other industries as a means of rapid scenario testing (Wang, Yu, Berto, Cai, & Bao, 2019; Yoro, Daramola, Sekoai, Wilson, & Eterigho-Ikelegbe, 2021). The incorporation of these tools enables fast modeling of design loads and the non-destructive testing of ultimate and fatigue loads. Numerical modelling, therefore, brings with it a large cost and time saving compared to physical modeling. While the benefits of numerical modelling and testing are vast, their application requires an in-depth understanding of the system being modelled as well as field trials for validation before the simulation can be fully trusted.

For tidal energy developers, the application of numerical modeling enables cost savings, however, another advantage is seen through continuity. Often, a number of software packages are used in the design and operation of a tidal turbine, the validation of these software allows confidence in their use for future designs. A single validation process for a software package rather than the validation of a single design sees cost saving for present devices as well as into the future.

5.1. Introduction

5.1.1 Tidal Bladed

Tidal Bladed is the industry standard drive-train load numerical modelling software as described in Section 4.1.3. A key aspect of Tidal Bladed is the inclusion of the ability to model controller dynamics. Four different controller types are catered for to align with developers preferences (DNV GL, 2016a). The modelling of waves is also included in Tidal Bladed (see Section 4.1.3).

Tidal Bladed validation

Tidal Bladed has been validated in a limited number of studies. An early study to validate Tidal Bladed, before it was acquired by DNV GL, saw comparisons to an 800 mm turbine in a flume tank. Bahaj, Batten, and McCann (2007) recorded blade efficiencies as well as lift and drag forces of the scale model turbine at four discrete blade angles. The study found the largest disagreement between Tidal Bladed and the scale model in conditions away from the design case. Overall, the study found predictions from Tidal Bladed to be “Satisfactory” (Bahaj et al., 2007). This small scale comparison represents an initial stage in the validation of Tidal Bladed but falls short of containing enough data to enable the extrapolation of the software validation to a full scale tidal device in a real energetic tidal environment.

A study by Parkinson and Collier (2016) looked to fill this research gap by comparing Tidal Bladed predictions to the full scale Alstom Ocean Energy’s DEEP-Gen IV 1 MW tidal turbine installed and tested in the Fall of Warness as part of the Reliable Data Acquisition Platform for Tidal energy (ReDAPT) project. This study looked at, “electrical power, pitch angle and blade near-root bending moment”, (Parkinson & Collier, 2016). This study looked at 10-minute statistics including mean, min, max, and DEL and found negligible affect of blockage on the DEL of the near-root blade bending as well as good agreement of flood and ebb blade min, mean, and max blade bending loads. The study by Parkinson and Collier (2016), while going beyond the previous study by Bahaj et al. (2007), only pertains to a single rotor tidal turbine. They also do not consider wave-current interactions when defining the model environmental conditions.

As yet, the literature does not contain the validation of Tidal Bladed deployed to predict the drive-train loads of a full scale, twin horizontal rotor, floating tidal turbine. This study looks to fill this gap by comparing predicted loads from a model of the O2 in Tidal Bladed to real data recorded in-situ during operation in the Fall of Warness. This study covers comparison between Tidal Bladed and the O2 at two different power set-points. The main

5.1. Introduction

focus is the drive-train loads of the O2 including blade loads, rotor thrust and torques, and hub bending, but, also covers an assessment of the controller implementation in Tidal Bladed. This is the first systematic Tidal Bladed validation conducted by Orbital for the O2.

5.1.2 Tidal terminology

The tidal sector uses language derived from the wind sector to describe different sections of a power curve for a horizontal axis, pitch controlled, turbine (Pao & Johnson, 2009). This terminology is used in this chapter to aid discussion of turbine dynamics at different flow speeds.

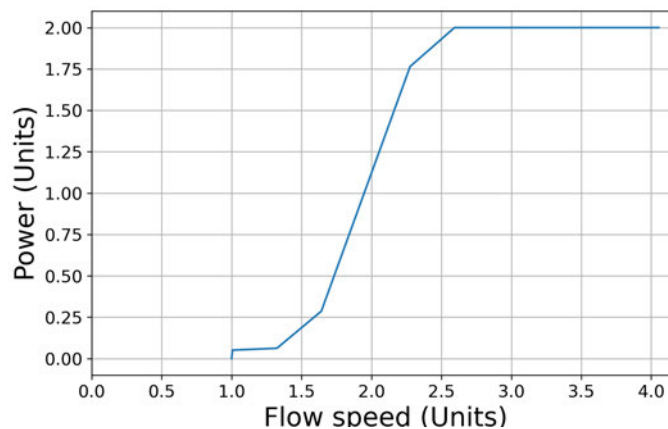


Figure 5.1: Example of a typical power curve for a pitch regulated horizontal axis turbine for wind or tidal. This is not the power curve from any particular device and only serves as an example to enable discussion of flow speed region terminology.

Figure 5.1 shows a typical power curve for a pitch regulated horizontal axis turbine. As such there are a number of distinct areas of interest. Initially, between $0 < FlowSpeed < 1$, the incident resource is not enough to generate hub rotation or power. When $FlowSpeed = 1$, the turbine has reached the ‘cut-in’ speed, at which enough speed is present to generate electricity. Above the cut-in speed, the turbine blades maintain a constant pitch. At about $FlowSpeed = 2.5$ the turbine reaches the ‘rated speed’ (see Figure 5.1). Above rated speed the turbine blades pitch to shed power and maintain a constant power. The point around the rated speed where the turbine changes from fixed pitch to pitch regulated is called the transition zone.

5.1. Introduction

5.1.3 Aims and Objectives

This body of work fulfils Aim 3 from Section 1.4 by systematically validating each drive-train load parameter of interest measured from the O2 against Tidal Bladed. The model setup is discussed demonstrating the validity of a like-for-like comparison. A model run matrix along with pre- and post-processing requirements are outlined to ensure repeatability. This is followed by a direct comparison between Tidal Bladed outputs and field data with the identification and description of good and poor correlation. Reasons for disparities are discussed before the impacts of this study are highlighted and conclusions drawn.

5.2 Materials and Methods

5.2.1 Tidal Bladed model

Orbital Marine Power have spent a large effort and person-hours to create and refine a full model of the O2 within Tidal Bladed (not for or by this thesis). The Tidal Bladed model covers the entire turbine and is used by Orbital Marine Power for a range of load studies. The creation and deployment of the model is outside the scope of this thesis. The modelling team at Orbital Marine Power were given the run matrix described in Section 5.2.2 and returned variables of interest.

Tidal Bladed, like most modelling software uses a number of assumptions to aid efficient computing. Tidal Bladed uses BEM theory to calculate blade loads on the turbine rotor to avoid the expensive computation of a Computational Fluid Dynamics (CFD) flow field (DNV GL, 2016a). The flow field is modelled as drag on the non lift faces of the O2 including the legs and superstructure. Wave forces are modelled using Morison's equation within Tidal Bladed (DNV GL, 2016a; Morison, et al., 1950). The model simplifications include the omission of any increase in turbine weight and or drag as a result of marine growth. It is expected that initial years of marine growth will not impact the dynamics of the O2, however, after 20-25 years of operations during the turbine lifetime, it is possible that a non-trivial quantity of growth will materialise. It is important that a further Tidal Bladed be conducted with marine growth accounted for or for the growth to be removed at regular intervals to ensure a validation remains relevant.

5.2. Materials and Methods

Controller

Tidal Bladed allows the implementation of a turbine controller within the model. This allows for incident protocols and shutdown command chains to be trialed and analysed. The implementation of the turbine controller also enables a realistic response to the incident environmental conditions to be realised.

The real O2 controller was included in the model used for this study. O2 data at the 1.7 MW set point were artificially truncated by a 1.5 m/s cut-in speed. This was not included in the 2 MW set point O2 controller or the 2 MW and 1.7 MW set point controller in the Tidal Bladed model to give a more complete data set. The controller was designed in-house by Orbital Marine Power. This thesis had no part in the design and implementation of the controller and is only concerned with the drive-train load implications of its inclusion in both the real datasets and the Tidal Bladed model. Using the real controller ensures a like for like comparison between the turbine and the model.

5.2.2 Model run matrix

The validation of the O2 loads was done by direct comparison of 10-minute averaged data. This was done at two different operational set points labeled *Phase 1* and *Phase 2*. *Phase 1* pertains to a 19-day dataset of 1.7 MW maximum power output between 22/12/2021 and 9/1/2022 while *Phase 2* uses the same process at a higher maximum power output of 2 MW for 30 days between 1/9/2022 and 30/9/2022.

The 10-minute average tide speed, wave period, and wave height were extracted from O2 recorded time series data for both *Phase 1* and *2* datasets. The wave parameters were calculated using the method outlined in Section 4.5, while the tide speed was recorded from the forward and aft downward facing ADCP onboard the O2. For each unique tide speed, wave height, and wave period recorded in either *Phase 1* or *Phase 2*, a 10-minute Tidal Bladed simulation of the O2 was run using the same environment parameters giving a data base for direct comparison.

5.2. Materials and Methods

5.2.3 Data preprocessing

Tide Speed

The tide speed recorded for this analysis came from the forward and aft ADCPs onboard the O2. This tide speed data tag is logged at 10 Hz and is used as the standard recording of tide speed for other analysis as well as for the controller.

This tide speed tag uses a 0.5 m bin at hub height below the forward and aft ADCP. The recording works by switching between ADCPs depending on the flow direction. This enables the recording to be as uninfluenced as possible from the structure of the O2 as well as thrust affects from operation while recording from onboard the O2. The choice of using one ADCP bin at hub height enabled for continuous and integrated logging with the other data streams as the processing required was minimal. The mean difference between selecting this single bin and a Power Weighted Rotor Average (PWRA) performed in accordance with IEC (2013) is shown in Table 5.1. Where the PWRA is given by Equation 5.1 where $\hat{U}_{i,j,n}$ is the power weighted current velocity, A_{rot} is the rotor area, $U_{i,j,k,n}$ is the instantaneous tidal current velocity at time j, location bin k, and speed bin i for data point n, and A_k is the area of location bin (IEC, 2013). It can be seen that the difference is minimal and within an allowable accuracy for graphical representation.

$$\hat{U}_{i,j,n} = \left[\frac{1}{A_{rot}} \cdot \sum_{k=1}^S (U_{i,j,k,n}^3 \cdot A_k) \right]^{\frac{1}{3}} \quad (5.1)$$

Table 5.1: Mean and standard deviation of difference between Power Weighted Rotor Average (PWRA) and single hub height bin for forward and aft downward facing ADCPs on board the O2 over a 30 day period covering speeds from -4 to 4 m/s.

	ADCP Location	mean (m/s)	std (m/s)
PWRA-single bin	Forward	-0.016	0.136
	Aft	-0.013	0.150

5.2. Materials and Methods

Blade loads and blade derived loads

The blades are a key component of the O2 as they are the point of contact with the tidal resource. As a result, the blades are well instrumented. Each blade contain strain gauges that can record bending in the X and Y plane. These strain gauges were calibrated using weights hung on the end of the blades before deployment of the turbine.

With the recording of X and Y bending forces, a number of other loads can be derived. When combined with pitch angle, the bending forces can be resolved to give thrust, torque, and hub bending. The turbine has a secondary measurement of torque using strain gauges on the Low Speed Shaft (LSS). As a result, in an attempt to differentiate between these torque measurements, the torque resolved from blade pitch angle and bending forces will be labelled as ‘torque from blades’, while the torque from the low speed shaft strain gauges will be labeled LSS torque.

Resolving these bending moments onto a new plane works on the assumption that the centre of pressure on the blades remains constant as the blades pitch. This is not necessarily true and so the bending forces in Tidal Bladed were also resolved in a similar way to ensure any error was consistent between the O2 data and the model data.

Torque temperature correction

Strain gauges were deployed on the LSS of each drive-train by Orbital Marine Power in order to directly measure torque. These strain gauges contained two pairs of 45° and -45° gauges placed 180° apart on the drive shaft. The two pairs of gauges should experience the same temperature dependency and so the affect of temperature on the torque measurement should be negated. In reality, however, the sensor setup has very small tolerances and so some temperature dependency was inevitable.

To remove and re-zero the LSS torque measurement with respect to temperature the relationship between temperature and torque reading was established as part of this thesis. This was done while not generating in order to isolate the direct temperature affect on the torque measurement. Figure 5.2 shows the turbine cooling down after a period generation and the corresponding torque measured from the LSS strain gauge sensors while no torque is applied from the blades.

The torque-temperature dependency was removed by correlating temperature and torque, during no power generation, to obtain a linear relation. The temperature corrected torque for the corresponding temperature at each time step was then subtracted from the raw torque value. This was done on both sides.

5.2. Materials and Methods

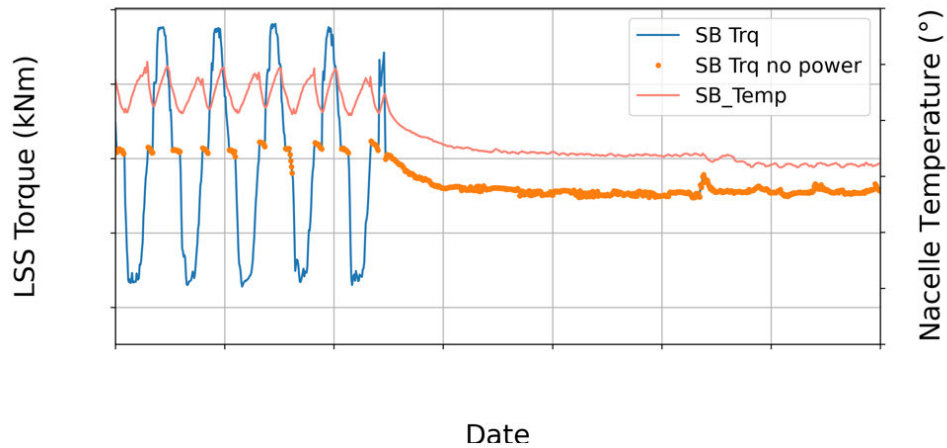


Figure 5.2: Torque from LSS strain gauge measurement and nacelle temperature for starboard nacelle against time showing a temperature dependency of the sensor.

The temperature correction developed as part of this thesis (described above) was applied to the live LSS torque data and is now logged as a data stream. This corrected torque value is now used for other analysis showing direct impact from this thesis.

5.2.4 Blade coordinate system

This Chapter looks at blade bending moments in both the x and y directions. The coordinate reference system for both the model and field datasets are the same and is shown in Figure 5.3. Bending in the y direction is denoted as ‘My’ and bending in the x direction is denoted as ‘Mx’.

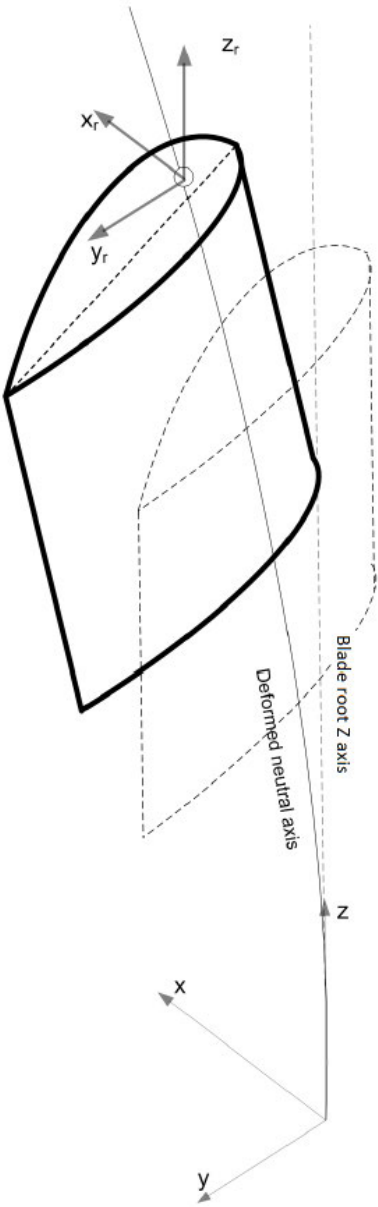


Figure 5.3: Blade root coordinate system used for both the numerical model of the O2 and the O2 itself (DNV GL, 2016b).

5.2. Materials and Methods

5.2.5 Data post-processing

The feature extraction was identical for *Phase 1* 1.7 MW set point and *Phase 2* 2 MW set point datasets. The datasets were divided into 10-minute windows from which the statistics were extracted. A full list of statistics extracted is shown in Table 5.2. The mean, maximum, standard deviation, DEL, and Root Mean Squared (RMS) were extracted depending on the tag. A number of absolute values were also recorded for the blade pitch angle including travel and range. Tags that were common on the Port Side (PS) and Starboard (SB) side saw the extraction of both sides for comparison.

Table 5.2: Loads related data tags and the associated calculated statistics for the validation of Tidal Bladed including whether a tag was duplicated for PS and SB symmetry. The results sections for each of the metrics are also shown for ease of navigation through this document.

Data tag	PS&SB	Calculated metrics						Section No.
		Mean	Max	std	DEL	RMS	Abs	
Hs		X						
Tp		X						
Tide Speed		X						
Blade 1 root My	X	X	X		X			5.3.1
Blade 2 root My	X	X	X		X			5.3.1
Blade 1 root Mx	X	X	X					5.3.2
Blade 2 root Mx	X	X	X					5.3.2
Rotor thrust	X	X	X		X			5.3.3
LSS rotor torque - Blades	X	X	X		X			5.3.4
LSS rotor torque - Sensor	X	X	X		X			5.3.5
Generator Speed	X	X	X	X	X			5.3.6
Blade 1 pitch travel	X						X	5.3.7
Blade 1 pitch rate	X					X		5.3.7
Blade 1 pitch range	X						X	5.3.7
Blade 1 pitch angle	X	X						5.3.7
Blade 2 pitch angle	X	X						5.3.7
Blade 1 pitch motor torque	X	X	X		X			5.3.8
Blade 2 pitch motor torque	X	X	X		X			5.3.8

5.2. Materials and Methods

Each 10-minute Tidal Bladed simulation had the same values extracted as shown in Table 5.2. A function was translated from MATLAB to Python that allowed data to be extracted from Tidal Bladed in to a Python environment. This function was a direct translation of work done by S Parkinson.

Calculated metric: Mean, Max, std, and RMS

The mean, maximum, standard deviation, and root-mean-squared of each 10-minute window were all calculated using standard Python calls.

Calculated metric: Damage Equivalent Loads

A DEL function was created to enable the calculation of 10-minute DEL values for data tags of interest. The DEL value represents a single load at a prescribed frequency that would generate the same damage as the accumulation of all cycles at all amplitudes and frequencies over the time window.

The DEL function followed the DEL calculation set out by Hayman (2012). Equation 5.2 shows how the Miner's rule damage, D_j , is set equal to the equivalent cycles, n_j^{eq} , over the number of allowable cycles at the damage equivalent load, N_j^{eq} .

$$D_j = \sum_i \frac{n_{ji}}{N_{ji}} = \frac{n_j^{eq}}{N_j^{eq}} \quad (5.2)$$

The number of cycles at the damage equivalent load, n_j^{eq} , is simply the product of the frequency selected for the DEL, f^{eq} , and the time period over which the DEL is being calculated, T_j , as can be seen in Equation 5.3.

$$n_j^{eq} = f^{eq} T_j \quad (5.3)$$

The number of allowable cycles at a load range, N_i , is given by Equation 5.4 where L^{ult} is the ultimate load, L^{MF} is the mean load, L_i^R is the load range for cycle i , and m is the S-N curve exponent.

$$N_i = \left(\frac{L^{ult} - |L^{MF}|}{\frac{1}{2} L_i^R} \right)^m \quad (5.4)$$

5.2. Materials and Methods

Equation 5.4 can be used to calculate the number of allowable cycles at the damage equivalent load, N_j^{eq} , where the damage equivalent load is DEL_j (see Equation 5.5).

$$N_j^{eq} = \left(\frac{L^{ult} - |L^{MF}|}{\frac{1}{2}DEL_j} \right)^m \quad (5.5)$$

Substituting Equations 5.4 and 5.5 into Equation 5.2 gives the equation for DEL_j (see Equation 5.6).

$$DEL_j = \left(\frac{\sum_i (n_{ji} (L_{ji}^R)^m)}{n_j^{eq}} \right)^{\frac{1}{m}} \quad (5.6)$$

This method for calculating DEL as set out by Hayman (2012) is identical to the method used by Tidal Bladed (DNV GL, 2016a). The Python function created to calculate DELs uses ‘*rainflow.extract_cycles*’ from the ‘*rainflow*’ Python package to rainflow count the cycles in the time window (Janiszewski, 2023). The DEL can then be calculated in accordance with Equation 5.6.

Calculated metric: Absolute

Two absolute 10-minute values were calculated as can be seen in Table 5.2. These were blade pitch travel (see Equation 5.7) and range (see Equation 5.8) for each blade where ψ is the blade pitch angle and N is the number of values inside the 10-minute time window. Travel was calculated as the sum of all absolute differences between each pitch angle step for the duration over the time window. Range was calculated as the difference between the largest and smallest blade pitch angle recorded in each time window.

$$10 \text{ min Pitch Travel} = \left(\sum_{i=1}^N |\Delta\psi(i)| \right)_{10 \text{ mins}} / 600 \quad (5.7)$$

$$10 \text{ min Pitch Range} = \max_{t=0}^{10 \text{ min}} \psi(t) - \min_{t=0}^{10 \text{ min}} \psi(t) \quad (5.8)$$

5.3 Results

The comparison results of the O2 recorded data and the numerical model data are presented in this section. The data for the O2 at 2 MW maximum power output (2 MW set point) and 1.7 MW maximum power output (1.7 MW set point) are presented together for each variable to aid comparison. Blade root bending data are presented first, followed by rotor torques, generator metrics, and finally controller metrics. The discussion of results comes in the subsequent section after the presentation of the results themselves.

5.3.1 Blade root My metrics

Blade mean My

REDACTED

Blade max My

REDACTED

Blade DEL My

REDACTED

5.3.2 Blade root Mx metrics

Blade mean Mx

REDACTED

Blade max Mx

REDACTED

5.3.3 Rotor thrust metrics

Rotor mean thrust

REDACTED

5.3. Results

Rotor max thrust

REDACTED

Rotor DEL thrust

REDACTED

5.3.4 Rotor torque derived from blades loads metrics

Rotor mean torque derived from blade loads

REDACTED

Rotor max torque derived from blade loads

REDACTED

Rotor DEL torque derived from blade loads

REDACTED

5.3.5 Rotor torque from low speed shaft (LSS) sensor metrics

Rotor mean torque from LSS sensor

REDACTED

Rotor max torque from LSS sensor

REDACTED

Rotor DEL torque from LSS sensor

REDACTED

5.3. Results

5.3.6 Generator speed metrics

Generator mean speed

REDACTED

Generator max speed

REDACTED

Generator speed standard deviation

REDACTED

5.3.7 Blade pitch angle metrics

Blade pitch angle travel and mean pitch rate

REDACTED

Blade pitch angle range

REDACTED

Blade pitch angle mean

REDACTED

5.3.8 Blade pitch motor metrics

Blade pitch motor mean torque

REDACTED

Blade pitch motor max torque

REDACTED

5.3. Results

Blade pitch motor DEL torque

REDACTED

5.4 Discussion

Points raised by the results are discussed. Physical explanations are presented for discrepancies as well as an example of the commercial applications of this study.

5.4.1 Tidal site horizontal flow shear

REDACTED

5.4.2 Leg shadow

REDACTED

5.4.3 Controller

REDACTED

5.4.4 Blade derived values

Multiple independent measurements of the same system allows for confidence in recording as well as redundancy. The O2 has two measurements of LSS torque: one from direct strain gauge sensors on the LSS, and one from blade loads resolved (see Section 5.2.3).

Comparing LSS sensor and blade derived logging of the LSS torque, an obvious difference is observable above rated in the Tidal Bladed predictions (see Figures REDACTED). While the LSS sensor measurement of torque remains constant for flow speeds above $|U| > 2.5$ m/s, the blade derived torque sees a reduction in torque with speed. This region of rated power is such that the controller is maintaining a constant torque. The reduction in torque seen by the blade derived torques above rated speed is due to the physics of the calculation for resolving blade forces into shaft torque. The calculation works on the premise that the M_x and M_y bending forces on the blades work on the same 3-D axis system as the blade pitch. However, as the blade pitches, the center of pressure on the blade moves away from it's original position and so the bending moments move away from

5.4. Discussion

their original axis system. When the torque is calculated with the invalid assumption of constant location of center of pressure the system appears to decrease in torque above rated. Despite this known limitation, it is still of note that Tidal Bladed is able to record very similar torques when the calculation method is kept constant between modeled and recorded data.

5.4.5 Outliers

Figure 5.4: REDACTED

REDACTED

5.4.6 Yield implications of load limit

REDACTED

5.4.7 Limitations

This study comes with a number of limitations inherent in a discrete time period study. One limitation is in the maximum values presented. The maxima recorded are over a short period of time (close to 30 days for each dataset) to be statistically representative of the turbine lifetime. As such, the presentation of maxima values may be misleading if compared to lifetime load limits.

The Tidal Bladed run matrix is determined by 10-minute average tide speed, wave height, and wave period. The wave statistics represent a limitation to this study due to their accuracy. While the wave height measurement was shown to be accurate to within 0.5 m, the measure of peak wave period is shown to lack accuracy (see Chapter 4). Errors in the model run matrix could lead to errors in the comparison outputs, however, the run matrix is large and encompasses many combinations of tide speed, significant wave height, and peak wave period. The assumption is, therefore, that this limitation in the run matrix is only influential for combinations of environmental parameters that fall outside the ‘norm’ as the majority of combinations are already accounted for in the O2 and Tidal Bladed datasets.

5.5 Application and Impact

The ability to reliably model drive-train loads using a numerical simulation tool creates the basis for rapid design testing under a range of loading scenarios. For the designers of the O2, the successful completion of Aim 3 from Section 1.4 through this validation of Tidal Bladed acts as an enabler in carrying Tidal Bladed forward to future designs of turbines where in-situ data collection is not yet an option.

More broadly, this validation of Tidal Bladed benefits other tidal developers hoping also to use the software. While this validation process encompasses intellectual property belonging to Orbital Marine Power, the study gives Orbital Marine Power more confidence to invest time and resources into the software. This in turn gives the providers of Tidal Bladed, DNV GL, a business case to ensure the future of the software with updates and technical support that can then be utilised by the rest of the tidal industry.

5.6 Conclusion

A validation of Tidal Bladed was performed by comparison to in-situ data from the O2, a 2 MW floating tidal turbine. The study looked predominantly at drive-train loads including blade loads, torque loads, thrust loads, and rotational speed metrics but also touches on model controller accuracy. The study was repeated at two different power set points to understand, not only how the software compares to measured data for one case, but how the modeling approach by Orbital Marine Power enables scaling of turbine design. This is imperative for the future use of the software as a key design tool for Orbital Marine Power as well as other turbine developers.

The study showed that a number of O2 loads were slightly lower than predicted, demonstrating the marginal conservative nature of Tidal Bladed under this particular setup. The damage equivalent loads were particularly well captured by the modelling software at lower wave heights while some controller dynamics struggled.

A number of unmodeled physical features were shown to increase disparity between modeled and recorded loads especially on the ebb tide. These included horizontal flow shear across the real tidal site that was not included in the model. This phenomenon caused differences in blade and hub loads between the port and starboard side rotors on the O2. Differences were also noted for drive-train loads between ebb and flood tides. These disparities were largely due to the flow meeting the leg structure before the rotor in the ebb case and not the flood case.

5.6. Conclusion

The implementation of the controller was shown to be influential for loads particularly around the transition flow speed. Higher torque and thrust DELs as well as the largest blade forces show that this region is of high importance to both fatigue and ultimate load states. The accuracy of Tidal Bladed in implementing a controller was shown to be good for a number of key performance indicators while it struggled in certain regions of the power curve.

The ability for Tidal Bladed to mirror loads based on location of sensors was also explored. The rotor LSS torque in the model was calculated using blade bending loads in the same way as it was for the O2: using given locations of load sensors. Tidal Bladed was able to follow the mean, maximum, and DEL of the LSS torque derived from blade loads very closely to that recorded by the O2. The model was also able to follow interesting physical blade phenomena including the change in radial position of the centre of pressure as the blade pitch.

A number of variables saw a decrease in similarity between Tidal Bladed and O2 data with increased wave height. The extent of this disagreement was explored and potential reasons are suggested. This lack of similarity is only a concern for larger wave heights which are either uncommon or would normally result in the shutdown of the turbine for survival purposes. The accuracy of the wave height recording was a major factor for consideration.

The affect on yield of blade load limiting alarms based on Tidal Bladed was also explored. It was shown that the slightly non-conservative nature of Tidal Bladed in recording blade My maximums led to unrealistic yield reductions for a given blade load limit.

Overall, this study has shown the accuracy of Tidal Bladed in modelling a highly dynamic floating utility scale tidal turbine as well as where a number of limitations lie. Demonstrating the accuracy of Tidal Bladed enables Orbital Marine Power, and other turbine developers, to ascertain, and have confidence in, appropriate safety factors based on loads outputted by the modelling software.

PART II

Floating Tidal Turbine Incident Velocimetry
and Increasing Knowledge-Return from Data
through Novel Sensor Applications

Application of ADCPs for Floating Tidal Turbine Incident Resource Measurement

6.1 Introduction

Velocimetry is the study of velocity in a liquid. Measurement of flow velocity is key to the tidal sector as it is recording a parameter of the resource. Velocimetry is important at all scales and phases in the development of a tidal device, from small scale tank testing to flow measurements in a full scale commercial site. Measuring a highly turbulent, energetic, 3-dimensional environment, however, has its difficulties at all scales.

The choice of sensor for velocimetry is determined by use case with a large number of sensor technologies aimed at different levels of accuracy, sensing volume, complexity, and cost. As well as these hardware choices, the location and ancillary structure for the sensor are also key variables.

One of the most prolific sensors used for velocimetry in the tidal industry is the ADCP. These sensors are manufactured by a number of different companies and have a range of configurations for varied applications.

6.1.1 ADCP principal of operation

An ADCP emits a pulse of sound with a specified frequency. The instrument then records the frequency shift of the reflected sound wave as it returns from moving water particles. The frequency shift of the returning wave, as a result of the Doppler shift, allows the instrument to calculate the speed of the particles that created the reflection along the beam axis. Analysing this Doppler shift at different times, and therefore different particle distances away from the sensor head, enables the speed of a profile of points along the direction of the beam to be determined (Nortek AS, 2018). This profile is divided into

6.1. Introduction

'bins' which act as discrete steps of averaged flow along the profile (see Figure 6.1). ADCPs often deploy numerous transducers at different angles allowing for the vector resolution of flow along the beam into an Earth or sensor x, y, z frame of reference. An assumption of homogeneity of flow speed is made for equal distances from each transducer in the resolutions of 3-Dimensional speeds.

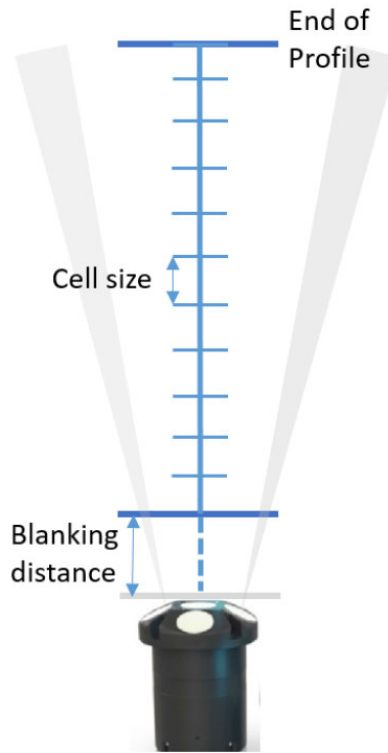


Figure 6.1: ADCP profiling range divided into bins with a cell size. The blanking distance and end of profile are also shown (Nortek AS, 2018).

ADCPs have a blanking distance before which the sensor is unable to record speeds accurately. The blanking distance is a result of the transducer and/or surrounding structures continuing to ring for a short period after the emission of a sound wave. The transducer vibrates as a result of transmission, during which time it is unable to accurately perform as a receiver of the reflected sound wave. Ringing occurs at the emission frequency and so recordings taken during ringing are not Doppler shifted. This biases the velocity reading to zero (Teledyne RD Instruments, 2011a). This time delay between transmission and readiness to receive corresponds to a distance where accurate recording is not possible i.e., the blanking distance (Nortek AS, 2018) (see Figure 6.1).

6.1. Introduction

Blanking distance for an ADCP is a function of transmission frequency and energy as frequencies attenuate at different speeds. Higher frequency ADCPs will have a shorter blanking distance while lower frequency ADCPs will have a greater blanking distance (see Table 6.1). Often test tanks are only a number of meters deep (FloWave, 2018; MARIN, n.d.; THEoREM, 2018) and so low frequency ADCPs with a large blanking distance are not practical for recording in this setting. As a result, these sensors are best suited to oceanic deployments.

Table 6.1: Typical blanking distances for ADCPs using different transmission frequencies. Adapted from Teledyne RD Instruments (2011a).

Frequency (kHz)	Blanking Distance (m)
75	6
150	4
300	2
600	1
1200	0.5

For an ADCP, noise, or the recording of erroneous data, is a key performance limiter. An ADCP removes the effect of white noise by averaging numerous recordings (Nortek AS, 2018). Signal to noise ratio is used to quantify the effect of noise within a signal. Noise proliferation within the recorded beam increases with distance from the sensor head leading to a lower signal to noise ratio at the end of the profile. This increase in noise with distance creates a range limit for the profile (see Figure 6.1). This range is influenced by emitted frequency and power, as well as environmental parameters like turbulence and suspended sediment volume.

ADCPs are used for tidal velocimetry because of a number of coinciding traits. ADCPs are able to,

- Record speeds non-intrusively along a profile.
- Record velocities in three dimensions.
- Be self contained for long deployments or be connected to an external power source.
- Record at different discrete bin sizes depending on sensor type.

As such, they have a range of commercial and research use cases.

6.1. Introduction

6.1.2 The application of ADCPs in the full scale tidal sector

ADCPs are commonplace throughout the tidal sector owing to their versatility and desirable traits as described in Section 6.1.1. Their main application within the full scale tidal sector can be divided into resource assessments, the recording of additional site features other than mean flow, technology progression and cutting edge research applications, and in following guidance of highly specific technical specification documentation.

Resource assessment

A resource assessment is used to gain an accurate understanding of the flow at a site. This is important for site selection, tidal forecasting, and revenue forecasting. The IEC generated a technical specification outlining a method for performing a resource assessment (IEC, 2015b). The technical specification outlines how a single ADCP can be used to determine the resource at one location or be used to validate a computational model for a site-wide resource assessment.

ADCPs are used commonly as a means to validate computational models of tidal sites either directly following the technical specification document, for example, Cornett, Baker, Piche, Toupin, and Nistor (2014); Marsh et al. (2021); Ramos and Ringwood (2016), or using the document as a guide (Yang et al., 2021). The technical specification was created to align resource assessment model validation practices and so the use of ADCPs for model validation also out dates the technical specification (Cornett, Durand, & Serrer, 2010; Lawrence et al., 2009)

Recording additional site features

An ADCP has three methods available for measuring wave height. When a beam from an ADCP reaches a boundary before the end of the beam range a very obvious amplitude spike from the returning signal is recorded. This phenomenon can be used to measure wave height by surface tracking (Nortek AS, 2018). ADCPs are also able to record the wave orbital velocities in order to determine wave height. As standard within an ADCP is a pressure sensor. This pressure sensor can also be used to calculate wave parameters.

The ability to measure wave height as well as tidal speed from a single sensor is valuable and allows for studies into field measured wave-current interactions (Colucci, Johanning, Hardwick, & Strong, 2014). Identifying waves using an ADCP can also be used to filter datasets based on wave conditions of interest (Sellar et al., 2018).

6.1. Introduction

Along with wave and mean velocity measurements, ADCPs are frequently used to study shear and turbulence within a tidal site (Osalusi, Side, & Harris, 2009; Sellar et al., 2018). These studies are important as shear and turbulence can increase cycles on a tidal turbine (Ahmed et al., 2017).

Technology progression and cutting edge ADCP research applications

ADCPs continue to be developed from both the ADCP OEM and the research community. The development of 5-beam ADCPs enable surface tracking wave measurement as well as a direct measure of flow towards the ADCP. This gives benefits to wave height recording as well as the 3-D flow being recorded by the ADCP. 5-Beam ADCPs are now a standard product line from major ADCP manufacturers (Nortek AS, n.d.-b; SonTek, 2023; Teledyne RD Instruments, 2016).

ADCPs have been used in a range of novel configurations other than the traditional seabed or vessel mounted setup. Drifters utilising a simple Global Positioning Systems (GPS) can be used to track sea surface velocities and house other sensors (Benjamins, Dale, Van Geel, & Wilson, 2016). Downward facing ADCPs have been incorporated into drifters to track the velocity of the entire water column (Guerra, Hay, Karsten, Trowse, & Cheel, 2021). The use of ADCPs on drifters removes any effect on the flow from deployment on a large vessel but does increase the movement expected from a small wave climate.

Another advancement in ADCP design was the development of a Convergent-beam Acoustic Doppler Current Profiler (C-ADCP). Developed by The University of Edinburgh, the C-ADCP allows for a point measurement of flow speed in the water column (Sellar, Harding, & Richmond, 2015). Traditional divergent-beam ADCPs assume homogeneity at each bin height, an assumption that reduces in validity with divergent distance (Teledyne RD Instruments, 2011a). The C-ADCP is not hampered by this assumption and so increases the breadth of ADCP deployment scenarios to include highly turbulent flow like that of wake behind an operating tidal turbine (Sellar et al., 2015).

6.1. Introduction

IEC/TS 62600-200 Power performance assessment (PPA)

A Power Performance Assessment (PPA) is a specific use-case for ADCPs. PPAs culminate in the creation of a power curve comprising of the power produced for a given incident flow. Power curves are important for inter- and intra-company turbine design comparisons as well as forecasting revenue to aid investor confidence. The importance of correctly derived power curves necessitated the creation of a power performance assessment standard. However, a non-converged industry like tidal energy poses difficulties for the creation of a turbine-agnostic standard.

Across all standard developers, one of the principal guidance documents for conducting a PPA for a tidal turbine was published by the IEC. At this stage, the document is a Technical Specification (TS). Published in 2013, TS 62600-200 outlines the process for a PPA for tidal energy (IEC, 2013). So far, the document has only been used once to produce a third-party verified PPA from an accredited test center for a tidal developer (EMEC, 2021). However, TS 62600-200 has been used on other projects as a means of creating a robust power curve (McNaughton et al., 2015). This lack of uptake, one official use since 2013, could be due to a number of factors including cost, technology readiness level of turbine designs, and barriers to application of the document itself created by site and machine specific frictions.

The measure of incident flow in a complex energetic tidal environment is non-trivial, but efforts are made in TS 62600-200 to outline a measurement technique. TS 62600-200, in its current form, prescribes the recording of incident flow using one or more ADCPs. TS 62600-200 places a number of constraints on the measurement of incident flow using these ADCPs (IEC, 2013). On a high level, these include:

1. Profiled bin location. The ADCP must profile the water column across the entire rotor height.
2. Bin height. The ADCP must record bins with a maximum height of 1 m.
3. Location. The ADCP must be placed in an area that represents the free-stream flow incident on the turbine without being so close that the turbine itself affects the flow recorded.
4. Duration of measurement. The ADCP must measure the flow for a period of 30 days in order to obtain a full spring-neap tidal cycle.
5. Sampling rate. An appropriate amount of data is needed during the study.
6. Velocity resolution. The accuracy of velocity measurement is important for uncertainty calculations.

6.1. Introduction

The TS 62600-200 document works with ‘Equivalent diameters’ for rotor diameter in order to accommodate different shape and setup of rotors which is at the discretion of the turbine designer. For a twin rotor device like the O2, with rotors on the same plane, the capture area over which the flow is averaged within TS 62600-200 is given by Equation 6.1 (Section 3.10 of TS 62600-200 (IEC, 2013)).

$$D_E = (D_1^2 + D_2^2)^{1/2} \quad (6.1)$$

Where D_E is the equivalent diameter and D_1 and D_2 are the diameters of the two separate rotors. For the O2, D_1 and D_2 are both 20 m, D_E is therefore 28.3 m.

The power curve created following TS 62600-200 compares incident flow with power produced. In order to be compliant with TS 62600-200, ADCPs for incident flow measurement must be located within prescribed areas relative to the tidal energy converters. These prescribed areas can be subdivided into two orientations: Orientation A or Orientation B. Length scales for ADCP locations are given in equivalent diameters (D_E) specific to each turbine. For Orientation A the ADCP must be placed in a region $2 D_E$ upstream of the rotor with a width of D_E and a length of $3 D_E$ (see Figure 6.2a). This must be repeated for both tidal directions experienced by the turbine: ebb and flood. Orientation B requires two ADCPs, each placed either side of the rotor. In Orientation B, the deployable area is a square of length D_E at a distance of D_E to the rotor (see Figure 6.2b). These locations represent regions of flow close to the turbine while remaining in the undisturbed free-stream. The options of Orientation A or B both require the deployment of two ADCPs: either upstream flood and ebb for Orientation A, or port and starboard for Orientation B (see Figure 6.2a and 6.2b).

The placement of the ADCP prescribed areas are relative to the extraction plane of the tidal energy converter. This remains the case for a floating turbine, however, given the movement of the floating platform (and its attached rotors) these prescribed areas move correspondingly.

Vertically profiling ADCPs (either on the surface facing downwards or the seabed facing upwards) are the only method for incident flow measurement set out in TS 62600-200 (IEC, 2013). While the application of seabed-mounted ADCPs for seabed-mounted tidal turbines has been demonstrated (EMEC, 2021; McNaughton et al., 2015), the suitability of the technique, as currently set out in TS 62600-200, for floating tidal turbines has not been assessed.

6.1. Introduction

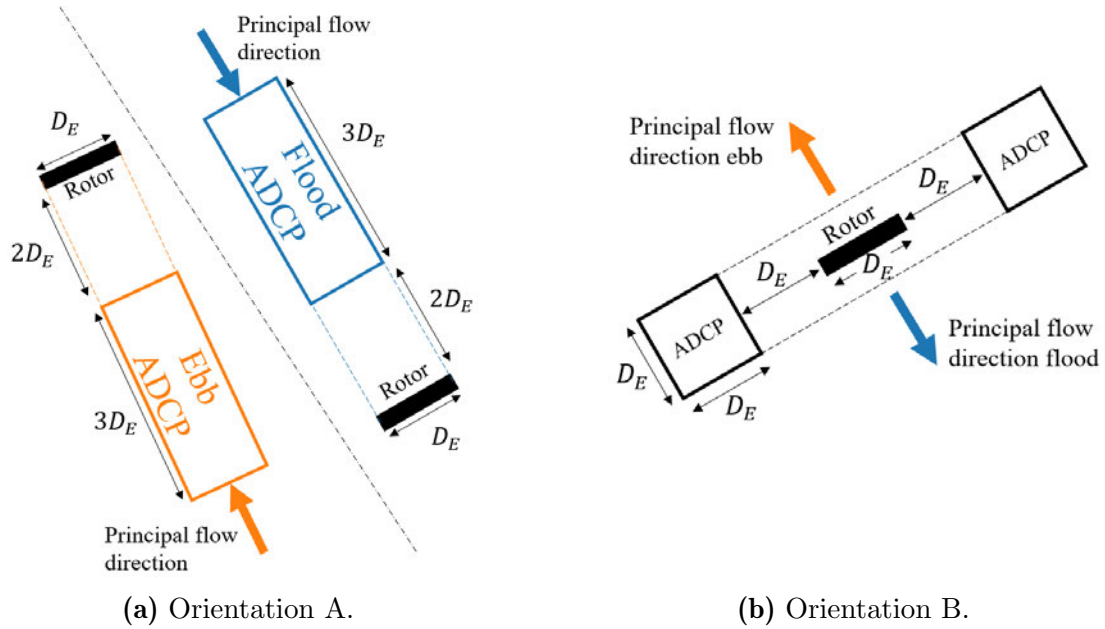


Figure 6.2: ADCP deployment regions following IEC/TS 62600-200 guidance for a power performance assessment. Both possible orientations are shown with lengths defined in equivalent rotor diameters (D_E). Image adapted from IEC (2013).

In the tidal sector, power performance assessment standards are important from a funding perspective as it relates directly to the revenue an asset can generate. Investor confidence is increased by demonstrating adherence to a standard or technical specification.

6.1.3 Research gaps

Tidal energy, as a sector, has seen many developments since the publication of the IEC/TS62600-200 Power Performance Assessment standards in 2013 (IEC, 2013). One key change is the increase in ‘floating’ tidal as a sector. This has been seen in the first two rounds of CfD to contain a ring-fence for tidal energy (2022-2023) in which 50% of parent companies awarded CfDs were floating tidal developers (GOV.UK, 2022, 2023). As a result of this increase from the floating tidal sector, unforeseen limitations in the prescribed method for incident resource measurement when applied to floating tidal energy have materialised. The key turbine and ADCP specific limitations when applying the TS 62600-200 to floating tidal devices are outlined by TIGER (2022) and include:

1. Beam spread in upper water column for seabed mounted ADCP.
2. ADCP side lobe contamination.
3. Interference between ADCPs.
4. Seabed ADCP placement.

6.1. Introduction

5. Obstructions due to floating design including cables and anchor arrays.
6. Floating turbine motion.
7. Onboard ADCP placement and orientation.

Data from a real utility scale floating tidal turbine deployment have never been analysed to corroborate and quantify the extent of these limitations. This is the focus of this chapter.

6.2 The application of ADCPs for incident flow measurement of a floating tidal turbine in accordance with the PPA technical specification

How, and if, the ADCP location constraint can be adhered to by a floating tidal turbine has ramifications for floating tidal developers generating a power performance assessment (as outlined in TIGER (2022)). This study quantifies to what extent the technical specification can be adhered to and if adherence incurs an added financial burden not realised for fixed bottom tidal turbines.

6.2.1 Methodology

The turbine geo-location dataset for this study came from a Differential Global Positioning Systems (D-GPS) tracker mounted inside the O2 tidal turbine (see Section 2.2). The dataset comes from 30 days of power production in September 2022 while the turbine was rating at 2 MW. The turbine was moored at Berth 5 in the Fall of Warness tidal test site for the duration of the study (see Figure 1.2). This 30-day period represents the typical performance of the O2 over a spring-neap cycle. During the period of data collection, the O2 saw a mean 10-minute significant wave height of 0.69 m with a standard deviation of 0.40 m (see Figure 6.3). The maximum significant wave height experienced was 2.88 m. These are typical environmental conditions experienced by the O2 on site.

6.2. Incident flow measurement in accordance with TS 62600-200

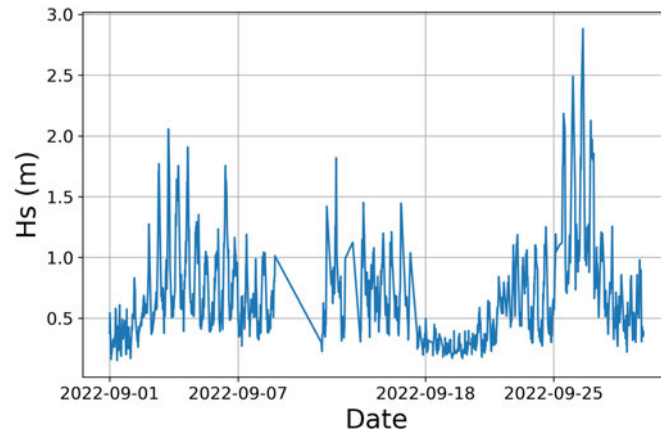


Figure 6.3: Significant wave height on site for the duration of the September 2022 dataset.

Moving ADCP area

As discussed, for floating turbine deployments, the prescribed ADCP measurement areas will change in time (relative to the seabed), as the tidal turbine moves (see Figure 6.2). This work uses the turbine position, as measured on the operational O2 device, to quantify area in which a seabed ADCP can be deployed and maintain TS 62600-200 compliance irrespective of turbine movement. Key to this analysis is the calculation of how this movement reduces the deployable area for a seabed ADCP compared to a static turbine of the same equivalent rotor diameter.

In order to compute this reduction in area, the time variant (relative to the seabed) ADCP prescribed deployment areas were recorded. The area of common overlap between these moving ADCP areas, dubbed the coincident area or ‘ A_C ’, was calculated. This overlap area is smaller than the original size of the permissible ADCP box outlined by the IEC (2013) by definition. This coincident area was then compared to the constant ADCP box dimensions, ‘ A ’, (which varies by ADCP orientation type and D_E only, set out in Figure 6.2) using Equation 6.2. A percentage area remaining, ‘ A_R ’, is calculated using Equation 6.2,

$$A_R = \frac{(A - A_C)}{A} * 100 \quad (6.2)$$

6.2. Incident flow measurement in accordance with TS 62600-200

where A is the original ADCP location box size: $3D_E^2$ for Orientation A and D_E^2 for Orientation B (see Figure 6.2a and 6.2b). The value A_C is the coincident area of overlap for time and space varying ADCP box locations for a floating turbine, and A_R is the percentage area remaining of the original ADCP boxes given the movement of the turbine.

6.2.2 Results

Assessment of Seabed ADCP Deployable Area Reduction due to Turbine Motion

The time-variant ADCP prescribed area locations relative to the seabed (referred to as boxes) for Orientation A and B, for flood and ebb tide, can be seen in Figures 6.4a and 6.4b for 10-minute average turbine locations over the 30-day dataset. Figure 6.4a shows that, despite the movement of the O2, an area where the 10-minute boxes overlap is present for this 30-day dataset in both ebb and flood. The overlapping area approaches triangular in shape with a wider area closer to the turbine, narrowing with distance away for Orientation A. Figure 6.4b shows that the adjacent ADCP location boxes for Orientation B do not overlap between flood and ebb. There is, however, distinct area of overlap within flood and ebb separately. The general shape of overlapping regions are squares for Orientation B.

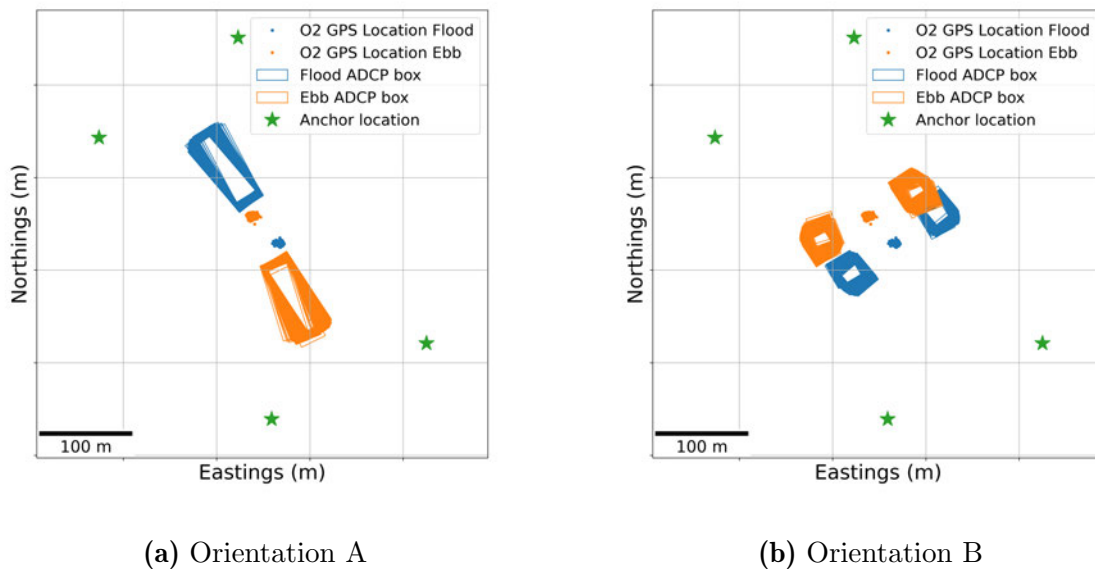


Figure 6.4: O2 10-minute average operational location for 30 days with respective location of TS 62600-200 defined ADCP permissible deployment areas.

6.2. Incident flow measurement in accordance with TS 62600-200

The value of A_C was calculated for the dataset for both Orientation A and B across flood and ebb tides by calculating polygon intersections using the ‘shapely.Geometry’ Python library together with Equation 6.2 to generate summary statistics. Table 6.2 shows that the movement of the O2 has reduced the permissible area for ADCP deployment by as much as 68% for Orientation A and as much as 87% for Orientation B over the entire 30-day dataset. It can be seen that A_R is less on the ebb for both Orientation A and B with Orientation A seeing a difference between tides of 17 percentage points. Orientation B sees a similar A_R on port and starboard side during the ebb tide, whereas, there is a difference of 4 percentage points between sides on the flood tide.

Table 6.2: A_R for dataset divided into ebb and flood for Orientation A and B and into port and starboard for Orientation B.

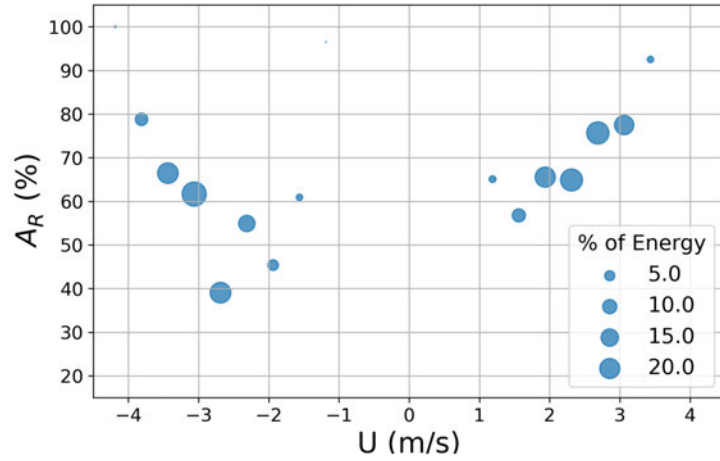
Orientation		A_R	
		Flood	Ebb
A		49%	32%
B	PS	23%	14%
	SB	27%	13%

Figures 6.5a and 6.5b show how A_R changes with flow speed for both ADCP orientations. The flood tide speed range from 1 m/s to 4 m/s was divided into 9 tide speed brackets, and similarly, the ebb tide from -1 m/s to -4 m/s was divided into 9 speed brackets. The value for A_R was calculated for all time instances where flow speed was within the same flow speed bracket in the 30-day dataset. This was repeated for each flow speed bracket. A_R as well as the energy generated in that flow speed bracket were recorded. Energy generated in each speed bracket was divided by total energy generated over the 30-day dataset for the same tide state giving a non-dimensional percentage of energy generation at that flow speed that is dependent on the power curve and resource.

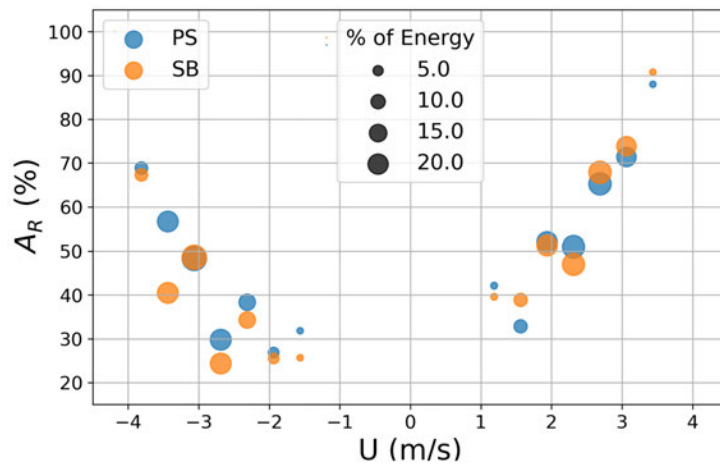
It can be seen that flow speeds of close to 2 m/s and -2 m/s represent the lowest values of A_R and therefore the largest turbine movement for Orientation A (see Figure 6.5a). For Orientation B, the maximum movement denoted by the smallest A_R also occurs at a slower speed (see Figure 6.5b). It can also be seen that the ebb tide experiences the greatest disparity between PS and SB values of A_R for Orientation B.

Figures 6.5a and 6.5b show that a large proportion of energy generation occurs in conjunction with large movements (see large marker size below $A_R = 70\%$ for both orientations). Higher flows for Orientation A and B see the largest values of A_R , but also a small proportion of energy generation.

6.2. Incident flow measurement in accordance with TS 62600-200



(a) Orientation A



(b) Orientation B

Figure 6.5: A_R against tide speed. Each tide speed value represents the middle of a 0.625 m/s speed bracket. Marker size represents the percentage of energy generated for ebb or flood in that tide speed bracket for this dataset.

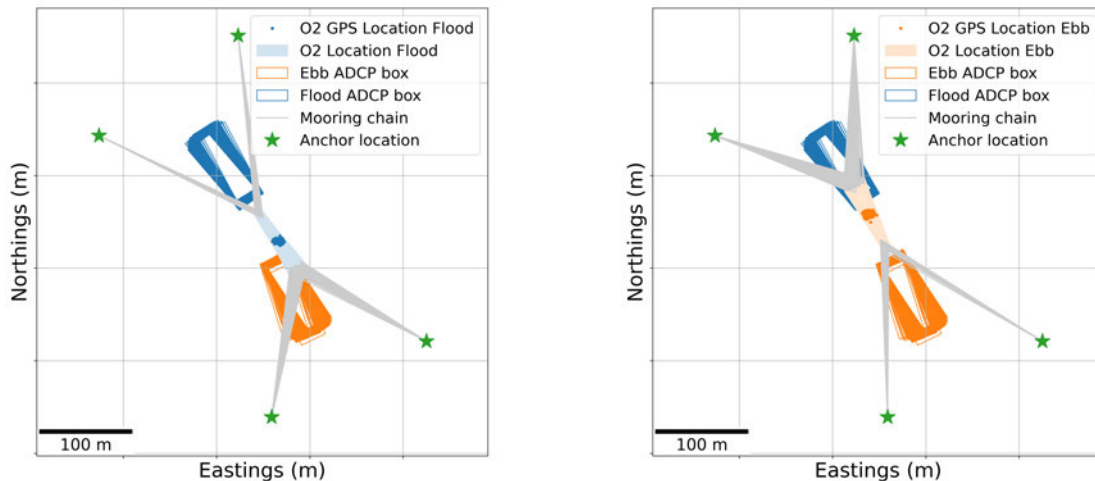
Assessment of Seabed ADCP Deployable Area Reduction due to Riser Interference

The water column around a floating tidal turbine sees equipment that would not be present for a seabed-mounted tidal turbine. Mooring chains and dynamic electrical cables can impede acoustic signals relied upon by ADCPs or even strike the sensors themselves. Acoustic signals emitted by an ADCP that impinge on a mooring chain will see a large spike in amplitude as the signal is reflected. The signal is unable to travel through these objects and so can limit the range of affected beams.

6.2. Incident flow measurement in accordance with TS 62600-200

Figure 6.6a shows Orientation A during flood and ebb tide and how the mooring chains impinge on the ADCP box locations. This effect does not exist for Orientation B. The mooring chains rise from the seabed and so could affect the ADCP measurement at different water column heights depending on where the ADCP is placed and the instantaneous positioning of the mooring chains. A standard four-beam ADCP with 25° beam angle placed in 35 m water would see a beam cone at the surface with a diameter of 30 m. This beam cone is increased further should a seabed-mounted ADCP experience small, tidal flow induced, oscillations during operation. Ensuring the chain does not enter this acoustic cone leads to a further reduction in area the ADCP could be located.

In addition to beam striking, there is the possibility of physical chain striking of the seabed ADCP. Upstream mooring lines are highly loaded during O2 power generation which moves the chain-seabed touchdown point towards the anchors. The downstream mooring chains are less highly loaded moving the chain-seabed touchdown point towards the turbine. The orange boxes in Figure 6.6 represent the ADCP permissible area for measuring ebb tide incident flow (see Figures 6.2a and 6.4a). This sensor would be idle during flood tide. Figure 6.6 shows that the downstream mooring chains could strike the seabed mounted ADCP depending on mooring touchdown location. This is then repeated and reflected for the blue boxes representing the location of a seabed ADCP for flood incident flow recording.



(a) Orientation A Flood

(b) Orientation A Ebb

Figure 6.6: O2 operational location 10-minute average for a month with respective location of ADCP boxes.

6.2. Incident flow measurement in accordance with TS 62600-200

On the Vertical Separation of the ADCP to the Floating Rotor: Bottom-Mounted ADCPs

Standard practice for measurement with a 25° divergent seabed ADCP is the removal of the top 10% of data to account for side lobe interactions at the sea surface boundary (Teledyne RD Instruments, 2011a). Side lobe interaction occurs when the acoustic beam meets a boundary that is not perpendicular to the beam trajectory, often the sea surface, leading to reflection at different points across the beam. The abrupt nature of this boundary generates reflections from the weaker side lobe of the beam at amplitudes close to that expected by the main beam water column reflections, thus contaminating the signal (Lentz, Kirincich, & Plueddemann, 2022). While 10% is used as a nominal value for discarded data, the extent of side lobe contamination is dependent on bin size, frequency, and sensor geometry (Lentz et al., 2022). For beam angles of 30° the contamination can be as much as 15% of the water column (Teledyne RD Instruments, 2011a).

The O2 rotor has a clearance of 3 m to the sea surface and so water depth greater than 30 m would see a 25° divergent seabed ADCP incapable of measuring the top of the rotor area (demonstrated in Figure 6.7). 71% of the Fall of Warness tidal test site exceeds 30 m water depth (see Figure 6.8). Therefore, the deployment of a 25° divergent ADCP could record across the entire rotor diameter of the O2 in 29% of the site. This value is for lowest astronomical tide, therefore will increase depending on tidal state.

The 30 m limit is also exceeded by other tidal sites targeted by developers for utility tidal energy including the Minas Passage and Pentland Firth (Karsten, 2011; Waldman et al., 2017). Given the boundary nature of side lobe contamination, extrapolation is needed to calculate the power weighted rotor average flow speed. However, extrapolation is not permissible within the TS 62600-200 (IEC, 2013).

6.2. Incident flow measurement in accordance with TS 62600-200

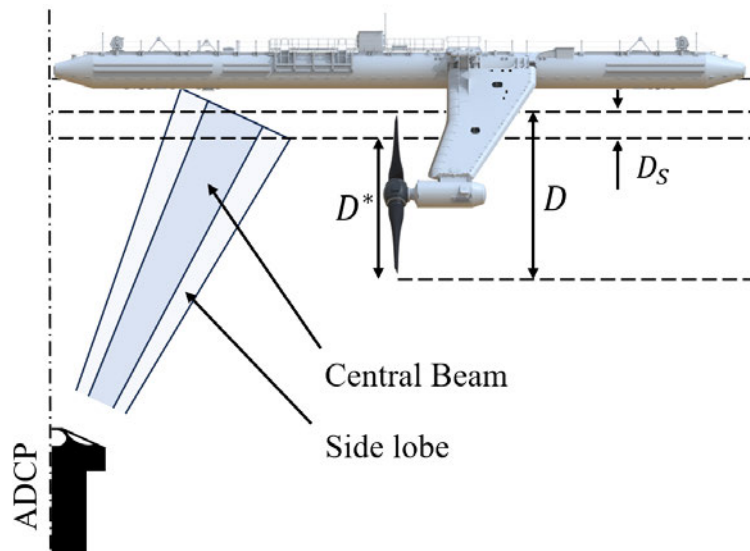


Figure 6.7: Representation of side lobe contamination limiting measurable water column in front of rotor to D^* , where $D^* = D - D_S$, with D being the rotor diameter and D_S being the region of rotor measurement distorted by side lobe contamination. ADCP not to scale.

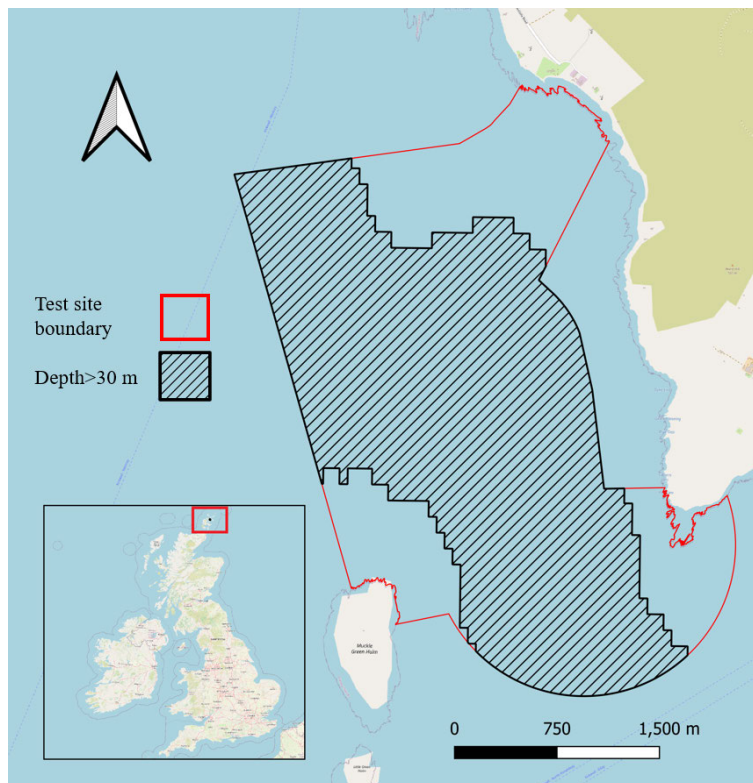


Figure 6.8: Area of the Fall of Warness tidal test site where 30 m depth is exceeded. Map courtesy of openstreetmap.org, test site boundary courtesy of EMEC, and bathymetry courtesy of Orbital Marine Power.

6.2. Incident flow measurement in accordance with TS 62600-200

On the Vertical Separation of the ADCP to the Floating Rotor: Surface-Mounted ADCPs

A downward ADCP sees a similar boundary issue to the seabed ADCP as discussed earlier. In this case it is the initial boundary created by the blanking distance that results in the top portion of the rotor area potentially not being recorded (depicted in Figure 6.9).

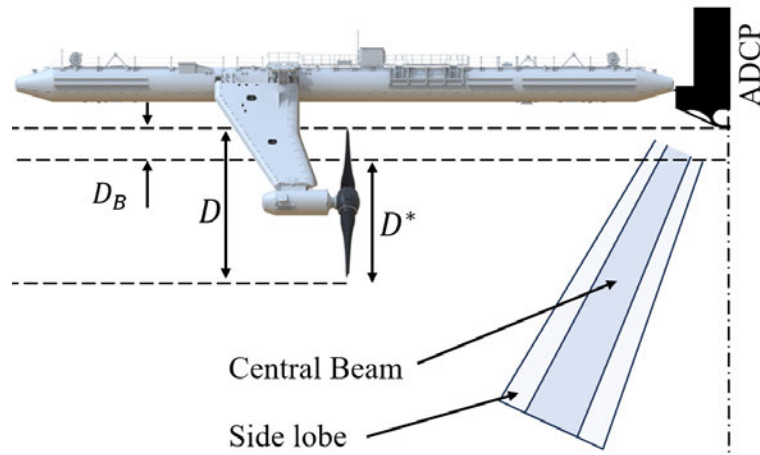


Figure 6.9: Representation of blanking distance limiting measurable water column in front of rotor to D^* . Where $D^* = D - D_B$, with D being the rotor diameter and D_B being the region of rotor measurement omitted due to blanking distance. ADCP not to scale.

The transducer on an ADCP physically vibrates to generate a sound wave. This vibration must be allowed to attenuate sufficiently before a returning sound wave can be accurately recorded by the same transducer. The time delay associated with the vibration attenuation, or ‘ringing’, manifests as a distance over which recordings would be contaminated. This initial distance in front of the ADCP is therefore omitted from recording and is named the blanking distance (Nortek AS, 2018).

Typically, the blanking distance of an ADCP is less than the 3 m for the O2 between the sea surface and the rotor top-dead-center. However, the inclusion of a frame to mount the ADCP as well as positioning the instrument beyond the boundary layer from the main hull can reduce the distance between the end of the blanking distance and the beginning of the rotor. In some cases, it is possible that the additional depth the ADCP must be placed due to mounting requirement can lead to the blanking distance encroaching on the rotor. In this case, flow velocities can not be recorded across the entire rotor diameter using a downward facing ADCP.

6.2. Incident flow measurement in accordance with TS 62600-200

Levels of Compliance with Orientation B Constraints at Varying Tidal Channel Locations.

Energetic tidal sites experience shear on both the horizontal and vertical planes. Vertical shear sees a change in flow speed through the water column and is well studied using seabed-mounted ADCPs (Greenwood et al., 2019; Osalusi et al., 2009). ADCP Orientation B in TS 62600-200 is open to effects from horizontal shear, or a difference in flow speeds along a transect perpendicular to the main flow speed, as two ADCPs are needed on the same plane to calculate the rotor flow velocity (see Figure 6.2b). As a result, TS 62600-200 imposes a limit to the allowable difference in flow speed between the port and starboard ADCP flow measurements for each time instance of below 10% (IEC, 2013). This 10% threshold ensures linear interpolation between the two ADCPs remains valid for the calculation of the flow at the turbine location. The distance between the center of the port and starboard ADCP permissible locations is $4 * D_E$ (see Figure 6.2b). For the O2, this is a distance of 113.2 m.

The Fall of Warness is a highly energetic tidal site with flow features varying in time and space throughout a tidal cycle. How these features affect the TS 62600-200 threshold of less than 10% difference across 113.2 m for the O2 has an impact on ADCP orientations selection for a power performance assessment.

Data from a 3D regional-scale hydrodynamic model (TELEMAC 3D) created by The University of Edinburgh was used to conduct a preliminary study on how this 10% threshold limits the use of ADCP Orientation B for the O2 within the Fall of Warness. The TELEMAC 3D model of the Fall of Warness covered a period of one day (7/7/2023) and featured 10 layers. For this work, the 3D flow field of the site over a typical day was used. Waves were ignored for this study. The setup and execution of the model was done by the research team at The University of Edinburgh and only the analysis of the output data was the work of this thesis.

Four transect lines perpendicular to the dominant flow direction were extracted from the TELEMAC 3D model (see Figure 6.10). For each point along a transect, representing a potential O2 location, the flow speed recorded by a port and starboard ADCP in Orientation B were calculated. This was repeated for each time step in the day-long dataset. From this, the duration of time the port and starboard velocity reading remained within 10% of each other for each location was calculated.

6.2. Incident flow measurement in accordance with TS 62600-200

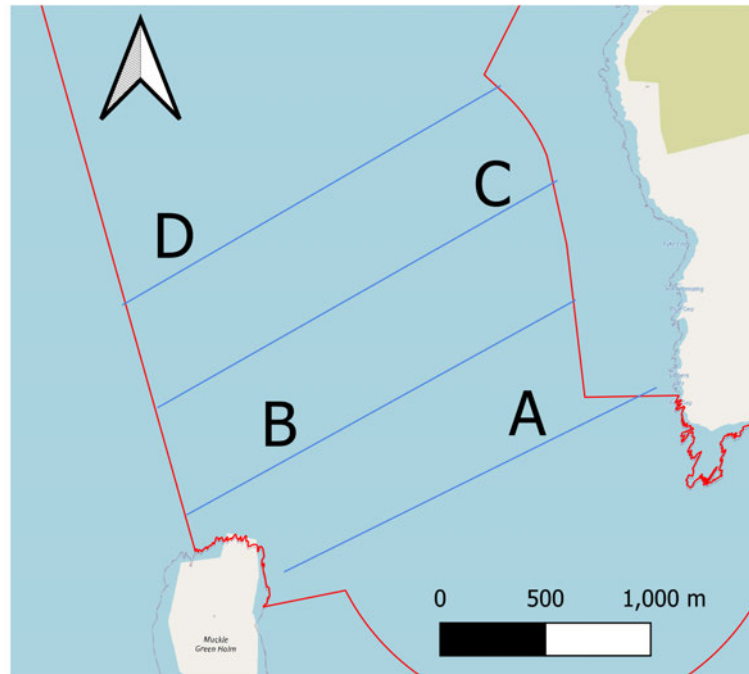


Figure 6.10: Map of the Fall of Warness showing the location of transect lines across which data were extracted from the TELEMAC 3D model. Map courtesy of openstreetmap.org, test site boundary courtesy of EMEC.

Figure 6.11 shows the percentage of time each point along each transect spent below the 10% difference threshold. The values were divided into ebb ($U < -1.5$ m/s) and flood ($U > 1.5$ m/s) tide for comparison. The data were then further divided into high and low resource with high resource indicating locations where the absolute flow speed reached over 2.5 m/s. It can be seen that each transect has a very clear central region where the 10% threshold is met for the entire ebb and flood tide. The right side of each transect sees a region of low compliance with the 10% threshold. The beginning of this region is transect and tide specific.

Table 6.3 shows the percentage of each transect where Orientation B meets the 10% threshold for the entire dataset i.e., the proportion of each transect in Figure 6.11 where the 100% of the dataset meets the TS 62600-200 10% threshold. It can be seen that the ebb tide consistently experiences a smaller span where the 10% threshold is met. It can also be seen that, when only considering the areas of high resource, a higher percentage of the transect is compliant with the threshold.

6.2. Incident flow measurement in accordance with TS 62600-200

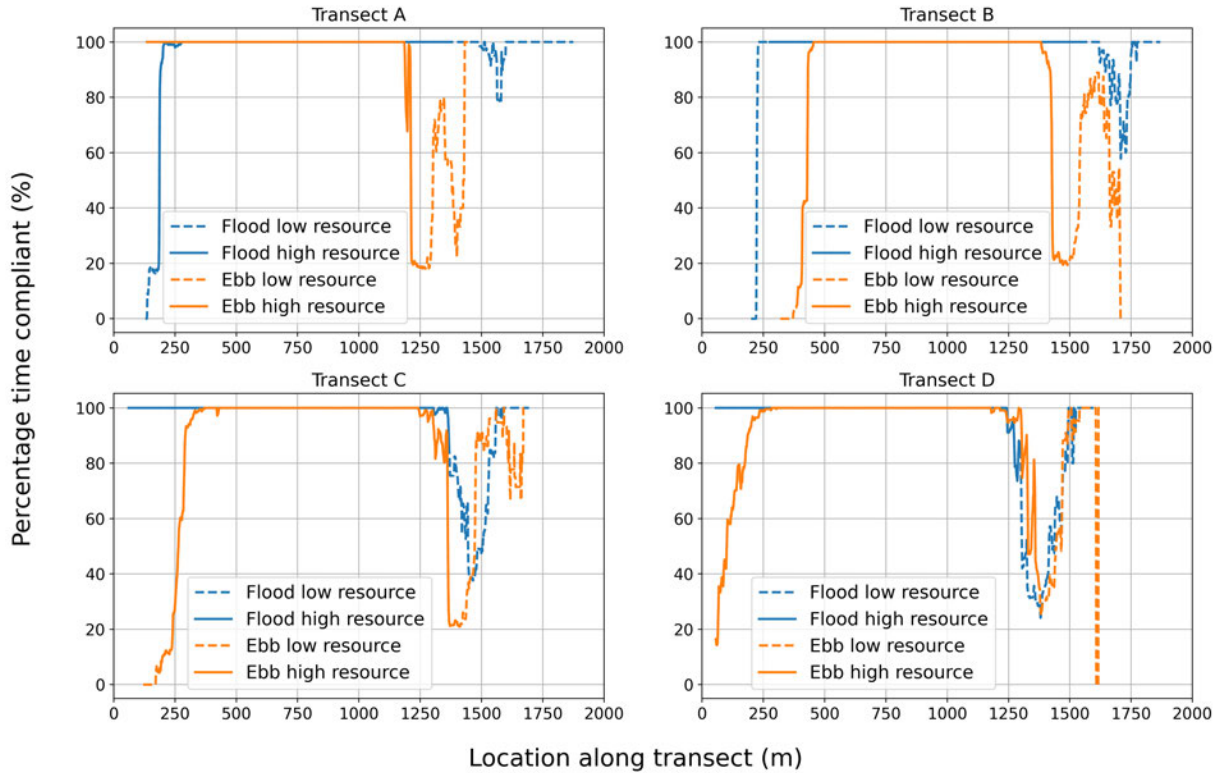


Figure 6.11: Four transects of the Fall of Warness showing the percentage of time, over a day, each location along the transect meets the IEC 10% threshold for horizontal shear between ADCPs in Orientation B. Data is shown for absolute speeds over 1.5 m/s with high resource indicating locations where absolute flow speed reaches above 2.5 m/s.

Table 6.3: Percentage of transect span whereby 10% horizontal flow shear limit is met for the entire dataset. This is the percentage of Figure 6.11 where percentage time compliant across the transect is at 100%.

Transect	Percentage of realistic* transect span shear-limit compliant**			
	Flood entire transect	Flood high resource	Ebb entire transect	Ebb high resource
A	86%	91%	81%	93%
B	91%	100%	69%	84%
C	85%	97%	58%	70%
D	83%	95%	64%	69%

*Where realistic transect span refers to positions a turbine could be placed given depth constraints.

**Where compliant refers to meeting the 10% horizontal flow shear limit as discussed earlier.

6.2. Incident flow measurement in accordance with TS 62600-200

Limitations in horizontal flow shear study

The extraction of a transect from the TELEMAC 3D model required a flow direction datum against which a perpendicular line could be drawn. For this study, the perpendicular transect lines were approximated by comparison to the average flow direction from the fastest section of the flow. The assumption then follows that the rotor and ADCP plane remain on this line throughout the tidal cycle. This assumption defines one direction, however, the meandering nature of the tidal flow creates a change in direction. Any change in direction will not be recorded by this method as the perpendicular flow to the transect line is only considered.

This assumption is further limited by the compliant nature of the O2 mooring lines, as discussed earlier. In reality, the plane along which the rotor and ADCP prescribed locations are located changes throughout the tide. Figure 6.4b shows that this movement is only slight for the O2 deployed location and that the port and starboard ADCPs can remain in a single position for ebb or flood. This might not be the case for other locations.

As with any study, data quantity impacts on error margins. The TELEMAC 3D model was run for 1 day leading to a representative dataset from which, representative values were extracted. This study was designed to inform decision making not to cover all eventualities.

6.2.3 Discussion

The area in which an ADCP can be placed on the seabed for incident flow measurement compliant with TS 62600-200 is smaller for a floating tidal turbine when compared to a fixed bottom tidal turbine of the same equivalent rotor diameter. This is due to a range of factors that affect deployment of ADCPs for a TS 62600-200 compliant PPA in different ways.

Turbine Movement

The moderate movement, attributed to compliant moorings, of a floating tidal turbine can reduce the size of the permissible ADCP deployment area for incident flow measurement for a PPA as defined in TS 62600-200 (IEC, 2013). The O2 has a 4-chain catenary mooring spread allowing for an excursion of ± 25 m. Figure 6.4 and Table 6.2 shows that A_R , the percentage of technical specification described ADCP deployment area remaining after turbine movement is accounted for (defined in Equation 6.2), is reduced to less than a half

6.2. Incident flow measurement in accordance with TS 62600-200

for all seabed ADCP orientations available to developers in TS 62600-200. This incurs the need for increased accuracy from marine operators when deploying the ADCPs. This will increase costs when compared to the area available for deployment for a seabed-mounted, stationary, tidal turbine of the same equivalent rotor diameter.

Orientation A is possible with two ADCPs for the floating tidal turbine considered in this work as well as a stationary seabed-mounted turbine. However, due to movement alone, Orientation B sees the need for twice the number of sensors that are needed for a seabed-mounted tidal turbine (see Figure 6.4b). An increase in number of ADCPs in close proximity can cause crosstalk between ADCPs and have consequences for data quality that will require attention in the post-processing of velocity data (Greenwood et al., 2019).

The issue of movement and a reduction in A_R is common throughout the power curve and so can not be remedied by ignoring certain flow speeds (see Figure 6.5). Reductions in A_R could see the need for longer data collection campaigns to allow for the collection of a complete ‘technical specification compliant’ dataset. An increase in data collection period brings with it a protracted risk period as well as a the need for equipment over a longer period of time, both of which bring additional cost to the data collection.

Riser Interference

The avoidance of mooring lines by ADCP acoustic beams can reduce the permissible sensor deployment area. The 4-chain catenary mooring configuration of the O2 creates a marginal impingement of mooring chains into the area in which an ADCP can be deployed for a PPA within TS 62600-200 (see Figure 6.6). The mooring systems of other floating tidal turbines can be significantly different in design. The predecessor to the O2, the SR2000, used a single forward and single aft mooring line which would guarantee ‘mooring line-acoustic beam’ clashing using ADCP Orientation A. It is important, therefore, to analyse the potential for riser interference on a case by case basis. This study is only to demonstrate the importance of accounting for this limitation.

More importantly, the location of the downstream mooring lines pose a threat to striking a seabed mounted ADCP. Mooring chain striking of a sensor would likely destroy the unit.

6.2. Incident flow measurement in accordance with TS 62600-200

Sea Surface Boundary

Limits on ADCP vertical profile range can result in gaps in velocity recording for rotor areas in the upper water column that can not be filled while remaining within TS 62600-200. Range limitations brought about by side lobe contamination can be reduced by using an ADCP with a narrow beam divergence (Teledyne RD Instruments, 2011a). In some cases, the water column depth may be too great to be overcome by ‘off the shelf’ sensors. Additional costs are incurred by developers constrained to choose between a select few instruments or the need to design a bespoke instrument.

ADCP Initial Sensing Constraint

While downward facing ADCPs are permissible within the TS 62600-200, care is necessary in understanding profiling limits. ADCP blanking distance has the potential to inhibit the ability for a profile across the entire rotor to be recorded if it is not accounted for in the design of the sensor mounting. Should the developer be constrained by mounting choice, ADCP setup and selection can be used to remove the blanking distance issue. This, however, limits the ADCP selection available to the developer, potentially increasing costs.

The resolution of beam data into a 3-D coordinate system requires the assumption of homogeneity of flow at the same recording distance for each ADCP beam. The turbine mounted, downward facing, ADCP recording benefits from using early cells along the profiling area in the calculation. This means the assumption of homogeneity across the beam profiles is more valid than if the cells further away were used in the calculations (Teledyne RD Instruments, 2011a). The use of early cells in the profile does, however, result in early bins not having diverged to the width of the rotor plane area. This could throw doubt on whether the calculated value is a true reflection of the spatially averaged flow at that particular rotor segment height as required by TS 62600-200.

Horizontal Flow Shear

While options on ADCP orientation are provided by the IEC, the presence of horizontal shear across an energetic tidal site has been shown to restrict deployable orientations for some locations in reality.

6.2. Incident flow measurement in accordance with TS 62600-200

Where Orientation B meets the 10% threshold, set by TS 62600-200, is highly influenced by local flow features. Transect A in Figure 6.11 shows how the presence of a large eddy line in the ebb tide causes a high degree of horizontal shear around 1200 m along the transect line. The presence of this flow feature results in the 10% threshold in velocity difference between port and starboard ADCPs no longer holding. This feature is replicated in Transect B, C, and D.

Another eddy line that is apparent is that generated by the small island on the southwest of the test area (Muckle Green Holm). Transect C and D remain in deeper water on their left-most extremity owing to the test site boundary limit rather than a land mass boundary. It can be seen that this leads to compliance with the 10% shear threshold at this boundary on the flood tide. On the ebb tide, Transect C and D right-most extremity is situated in the wake of Muckle Green Holm with this turbulent eddy causing a breakdown in the 10% threshold in this region (see Figure 6.11).

The data contained within Figure 6.11 must be held in context with the resource available at each point along the transect. In reality, the large eddy lines causing a high degree of horizontal flow shear on either side of the transect lines, depending on the tide, represent a boundary between high and low resource. Given the slow flow, and therefore low resource, after these eddy lines, it is unlikely a tidal turbine would be located here (see Figure 6.11). The locations in which the TS 62600-200 power performance constraints are met can be used to present an area of the Fall of Warness in which Orientation B can be used. In reality, it is for TS 62600-200 to be implementable where the turbines are placed. In this case, the 10% threshold in horizontal shear is not surpassed in the central tidal channel that represents the greatest resource. However, it is possible that edge cases exist whereby the turbine is placed in a region the 10% limitation is not met and therefore Orientation B is ruled out as a deployment option on these grounds in the Fall of Warness.

Similarly to the affect from turbine motion, a value of below 100% compliance with the 10% threshold for a location does not remove the ability to place an ADCP here. Instead, these locations represent positions that would require an increased duration of ADCP deployment in order to obtain data for the duration required by TS 62600-200. While these positions are still feasible on the basis of horizontal flow shear, the increased deployment time represents additional costs.

6.2. Incident flow measurement in accordance with TS 62600-200

O2 Specific Considerations

Downward looking ADCPs were shown to be a credible option for incident flow measurement under specific conditions, provided blanking distance is accounted for. TS 62600-200 does not prescribe the vertical orientation of the ADCPs used in the measurement of incident flow. Therefore, provided the floating structure enables the placement of downward ADCPs in the prescribed locations (see Figure 6.2), this option could save operational costs associated with deploying seabed ADCPs. The reality for the O2 is, however, that the structure is not large enough given the rotor diameter to place downward ADCPs in the TS 62600-200 prescribed locations. In the case of the O2, this ADCP orientation is also limited by the blanking distance phenomenon seen by ADCPs owing to the small distance between rotor top-dead-center and the sea surface.

6.3 Application and impact

The sector impact of a truly technology-agnostic power performance assessment manifests itself as an even playing field for developers. In its current format, the IEC/TS 62600-200 (IEC, 2013) is vulnerable to advancements in tidal technology that render it impractical and therefore unused (McNaughton et al., 2015). The application of standards builds investor confidence in the technology but also in the standards. The standards process is symbiotic, with industry needing to play an active role in development of standards that it is applying.

This work has fulfilled Aim 4 from Section 1.4 by quantifying shortcomings of TS 62600-200 in its current format when applied to floating tidal turbines and made the case for new thinking around incident resource measurement. Alternatives to measurement techniques outlined by IEC (2013) have the potential to greatly reduce costs for power performance assessments of floating tidal turbines bringing them inline with the cost for seabed turbines.

6.4 Conclusion

Learning from industry shows that measurement of the incident flow in a way that complies with existing standards is a challenge for floating tidal turbine developers wishing to complete an accredited power performance assessment. To quantify this problem, a critical analysis of ADCP deployment for incident resource measurement compliant with ‘IEC TS 62600-200: Electricity producing tidal energy converters – Power performance assessment’ for floating tidal energy was presented.

It has been shown that the permissible seabed area in which an ADCP can be deployed is significantly smaller for a floating tidal turbine than for a fixed turbine of the same equivalent rotor diameter. The primary reason for this is movement of the floating platform, however, the addition of chain and electrical cable in the water column further reduces the seabed area in which an ADCP can be deployed. Reduction in permissible area means an increase in accuracy needed by the marine operations teams in the deployment of ADCPs, which results in an increase in cost and complexity. For the specific case of the O2 tackled here, it was shown that the inline ADCP deployment set out in TS 62600-200 (Orientation A) is not possible (see Figure 6.6). The adjacent ADCP deployment set out in TS 62600-200, while technically feasible for the O2, is practically not realistic given the tight deployment margins (see Figure 6.4b and Table 6.2).

The profiling range of an ADCP and the effect of both the initial and final boundary conditions results in a restriction on ADCP configurations in some scenarios. Large seabed depths combined with shallow rotor heights were shown to restrict allowable ADCP beam divergence angles, while blanking distance affected downward facing ADCP configurations. A reduction in the applicable types of ADCP restricts sensor choice and can increase costs for a developer.

It is clear that measurement of the incident flow in a way that complies with existing standards remains a challenge for floating tidal turbine developers. In order to remain technology-agnostic irrespective of sector advancements, TS 62600-200 should be updated to include additional options for ADCP orientations that allow the incident resource to be measured in a way that is more practical for floating tidal turbines. Continued close collaboration is required between technology developers and standards bodies to ensure the requirements in the standards are practical to comply with, and reflect learning from, operating turbines in the field.

6.4. Conclusion

Additional methods for incident resource measurement have already been suggested to the IEC for the second edition of TS 62600-200. One progressive suggestion is the application of a hub height, horizontally profiling, ADCP mounted on the floating turbine itself (TIGER, 2022). A feasibility assessment of this solution is tackled in the next chapter.

Application of a Horizontal Turbine Mounted Hub Height ADCP for Incident Resource Measurement

7.1 Introduction

Incident flow velocity is a key parameter for a tidal turbine from both a control and performance perspective. Standard practice for the deployment of ADCPs for incident flow measurement of a seabed mounted tidal turbine is to place the ADCP on the sea bed profiling the vertical water column (Harrold et al., 2020; McNaughton et al., 2015). Isolated ADCPs rely on battery power and therefore have a defined deployment period after which they require collection for data extraction. Placing an ADCP onboard a tidal turbine, however, enables continuous sensor power and, therefore, a continuous measurement campaign. A number of studies have seen the deployment of ADCPs onboard a tidal turbine (RealTide Consortium, 2021; Sellar et al., 2018).

The IEC stipulates that true incident flow data must be obtained from beyond the influence of the turbine on the flow (IEC, 2013) (as discussed in Chapter 6). In order to record incident flow from onboard a tidal turbine, the turbine structure must be large enough for the ADCP to be placed far from the rotor or the ADCP must be placed horizontally profiling into the flow. Vertically profiling turbine-mounted ADCPs for incident flow measurement for the O2 are inhibited by an inability to be situated beyond the influence of the turbine on the flow given the rotor size relative to the size of the super structure. As a result, a horizontal ADCP deployment is the only means of incident flow measurement using a turbine mounted ADCP. The ADCP must, however, exhibit an ‘adequate profiling range’ to reach the free-stream. The deployment of a horizontal ADCP has already been suggested as an addition to the next iteration of the IEC guidance on incident resource measurement for power performance assessment (TIGER, 2022).

7.1. Introduction

Previous horizontal ADCP deployments on tidal turbines for inflow analysis include the DeepGen-IV (Sellar et al., 2018), the Sabella D10 (RealTide Consortium, 2021), and the DeltaStream 400 kW turbine (Harrold et al., 2020). The DeepGen-IV saw a horizontal single beam Nortek Continental profiling behind the rotor, and a single beam Nortek AD2CP placed on the rotating hub profiling forward of the rotor. The Sabella D10 saw the deployment of a 5-beam Nortek Signature 500 on the aft of the turbine profiling rearward: due to the fixed nature of the turbine, this constituted incident profiling on the ebb tide. The DeltaStream turbine saw a single beam 1 MHz Nortek Aquadopp sensor placed in the rotating nose cone of the turbine profiling into the incident flow.

7.1.1 Research gaps

The deployment of ADCPs from onboard a tidal turbine enables a further reduction of seabed operations for a floating tidal turbine. However, the deployment of a horizontal ADCP at hub height on a floating, utility scale, tidal turbine remains a research gap. While theoretical advantages include continuous sensor power and data collection, the envelope of application has not been tested. This chapter quantifies the range of a horizontal ADCP placed at hub height on a floating tidal turbine as a function of sensor manufacturer stated range, while also exploring advantages and shortcomings of sensor configurations.

7.1.2 Aims and objectives

This body of work fulfills Aim 5 from Section 1.4 by critically analysing the appropriateness of deploying a 5-beam ADCP horizontally at hub height on a floating tidal turbine in order to measure incident flow. This is done by assessing the performance envelope of 5-beam ADCP deployed in the field on the O2. The range of a single horizontal beam under varying flow conditions is assessed and non-dimensionalised by comparison to the turbine diameter. The effect of beam combinations on range and incident flow velocity accuracy is also explored. Finally the suitability of the method as a means of incident flow measurement is assessed and situational specific barriers to deployment are explored. The results are then discussed before impacts are outlined and conclusions drawn.

7.2 Method

This work outlines the operational envelope of a horizontally mounted 5-beam ADCP when placed at hub height on a utility scale floating tidal turbine. Firstly, the study identifies the range of a single horizontal beam under a number of incident flow speeds in order to inform technology developers of expected range for the instrument used. Secondly, an assessment of horizontal flow measurement accuracy and range from divergent beams of a horizontally mounted ADCP is presented. The results are then discussed and conclusions drawn.

7.2.1 The ADCP

A 500 kHz Nortek Signature 500 5-beam ADCP was placed on the port side leg of the O2. The instrument was placed near the rotor centre, however, was offset as seen in Figures 7.1 and 7.2. The instrument was positioned horizontally pointing aft using a mounting bracket. The leg position of the ADCP avoids rotation that would be seen from a hub mounted ADCP.

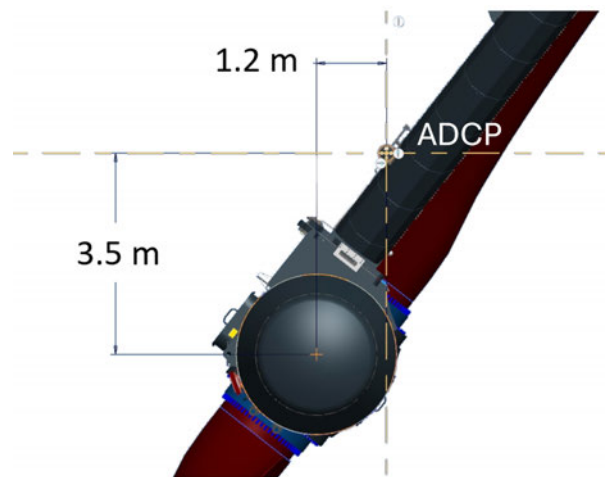


Figure 7.1: Leg ADCP location as viewed from aft of the O2 with distances to the hub center shown.

The 5-beam ADCP was orientated with the central beam pointing horizontally aft with the other two pairs of diverging beams placed along the vertical and horizontal plane. This resulted in a ‘+’ shape when viewed from in front of the sensor head. All five of the transducers were activated, recording continuously at 4 Hz for the duration of the dataset.

7.2. Method

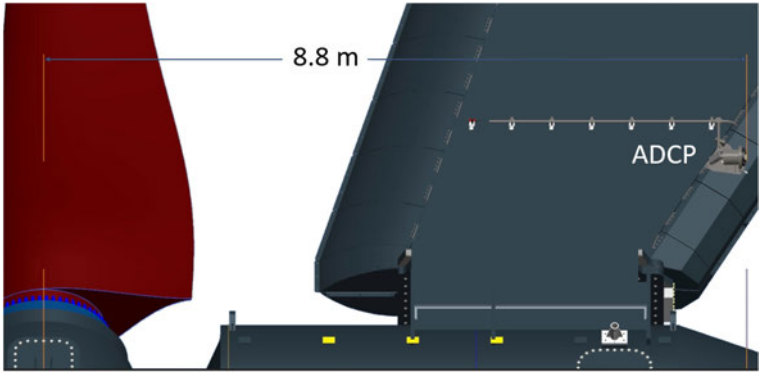


Figure 7.2: Leg ADCP location as viewed from the port side of the O2 with distance to the hub center shown.

The coordinate system used in the analysis of horizontal ADCP data remained that of the instrument itself (see Figure 7.3). This results in the flow towards the sensors being on the *Z* axis, i.e., the turbine inline flow.

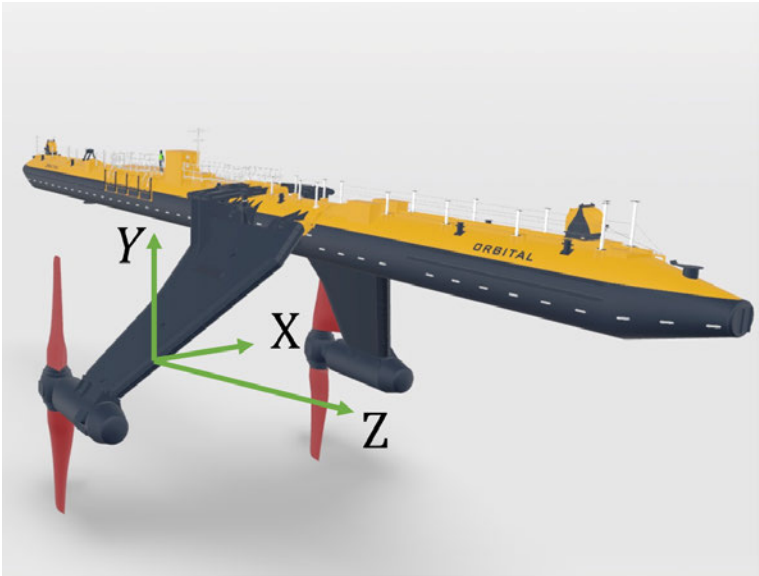


Figure 7.3: Leg ADCP coordinate system used in this chapter

7.2. Method

7.2.2 Introduction to dataset recorded by the horizontal ADCP and the corresponding operating and environmental conditions

Data were recorded using the horizontal ADCP from the 1/3/2023 until the 14/3/2023 representing seven tidal cycles. The horizontal ADCP logged 5 beams continuously in 1-meter bins for 68 bins at 4 Hz. This time period represents a 14-day dataset and covers the continuous logging of close to a full springs tidal cycle. Only flow towards the sensor was considered for this study as this represents incident resource. Flow away from the sensor was contaminated by turbine rotor and instrument setup wake.

Figure 7.4 shows the environmental conditions during the data acquisition campaign. The wave height was recorded using the REDACTED Method described in Section 4.5 where it was shown that wave height could be recorded to ± 0.51 m with 95% confidence. It can be seen that the wave height remained below $H_s = 1.3 \pm 0.51$ m for the duration of the data acquisition period.

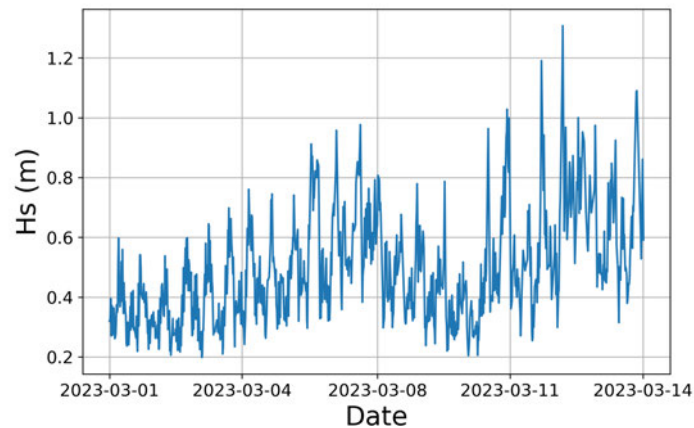


Figure 7.4: Significant wave height for duration of non-generation dataset.

7.2.3 Data quality control procedure

Quality Assurance / Quality Control of Real-Time Oceanographic Data (QARTOD) is a framework of quality control manuals for a range of oceanic measurement variables. The framework was created to ensure consistency of data processing when data is shared between national data centres in the United States (U.S. Integrated Ocean Observing

7.2. Method

System, 2020). Within QARTOD exists a framework for quality control for in-situ current measurement using an ADCP (U.S. Integrated Ocean Observing System, 2019). Quality control of ADCP data is used to ensure erroneous data is not included in processes performed post data collection.

The QARTOD process begins with the raw collection of data using an ADCP. Each datum in the recording is then evaluated with respect to tests and flagged as either passed, not evaluated, suspect, failed, or missing. Suspect data points are then investigated to determine their validity. Nonconformists within the dataset to the QARTOD tests are removed or assigned a NaN value.

The data from the horizontal ADCP were filtered using a number of QARTOD filters (see Tables 7.1 and 7.2). Only points that passed all filters were used in the results section of this work.

Beam Quality Control-Application of QARTOD

Beam data recorded by the horizontal ADCP were filtered using QARTOD tests with constraints outlined in Table 7.1 with the addition of a bespoke filter for horizontal ADCP deployment. Filters were applied to each bin and each beam for the duration of the dataset. Failure to meet filter criteria resulted in a flagged data point.

Table 7.1: Beam filters applied to horizontal ADCP dataset

Test ID	Test function
T6	Flag bin if amplitude is less than 30 dB
T8	Flag bin if correlation is less than 80%
T15	Flag all bins if pitch, heading, or roll rate is more than 2.5 °/s
T18	Flag if amplitude is not within 0.1 dB of previous bin
JDK1	Flag if velocity in bin is not within ± 0.5 m/s of the median of beam for that time

Filter JDK1 was applied only to the central beam of the horizontal ADCP to remove spikes from the dataset. Under uniform flow conditions with streamlines parallel to a horizontal seabed, it is expected that the horizontal beam would record the same velocity at each bin distance from the sensor. This is because there are no shear profiles across the study domain as would be the case for an upward facing, seabed mounted, ADCP. These conditions are not realised in the field, however, spikes away from the median value along the beam are considered suspect and are flagged by this filter.

7.2. Method

Demonstration of successful data collection with stringent filters can act as a clear baseline of quality control for future studies.

Coordinate transform

To convert beam velocity measurements to instrument coordinates the beams were coordinate transformed. The output of this stage was instrument coordinate velocities from the sensor to the end of the measurement domain. The physical orientation of the beams used in the coordinate transformation determines the plane being recorded. Each opposite pair of divergent transducers can record in one plane while beam 5 can only record directly in front of the ADCP.

One of the underpinning assumptions in the transformation of beam velocities to instrument coordinates is homogeneous flow at each bin distance from the sensor (Nortek AS, 2018). It is assumed that every beam is measuring the same velocity at each bin distance away from the sensor head.

Transformed Quality Control

The coordinate transformed flow speeds were further quality controlled with a second level of QARTOD filters (see Table 7.2). Each of these filters (T10 and T20) were used to de-spike the resolved data. Including a limit to velocity maximum and bin by bin velocity difference ensured that errors introduced by the transformation process were removed.

Table 7.2: Transformed Filters

Test ID	Test function
T10	Flag bin if velocity is greater than 8 m/s
T20	Flag bin if magnitude of velocity is more than ± 0.8 m/s of the previous bin

7.2.4 Single beam maximum range

The maximum range achievable by a horizontal ADCP in an energetic tidal environment is an important variable as it sets the domain limit for future studies with the sensor. This includes any studies using a horizontal turbine mounted ADCP for a power performance assessment to measure the free-stream tidal velocity. Developing an understanding of the ability for a horizontal ADCP to range to the free-stream is important in this context.

7.2. Method

The maximum distance data can be recorded to is defined, in this case, as the quantity of data remaining post quality control filters. The aim of this study was not to define a maximum range but rather to demonstrate the effect of range on the volume of data remaining post quality control. It is then for the ADCP user to determine a suitable level of data rejection for their study and, therefore, the range they can expect.

7.2.5 Incident flow from divergent beams

For a horizontal ADCP the Z-axis represents the inline flow to the turbine (see Figure 7.3). To record velocities along the Z-axis using a 4-beam ADCP a number of beams are combined as there is no beam directly in line with the Z-axis and therefore no direct measurement (Nortek AS, 2018). Traditional 4-beam ADCP deployments use opposite beams to record two separate values for the Z-axis velocity. The difference in these two values of Z-axis velocity is then used as a quality control parameter often called the ‘error velocity’. The issue with this method is that these derived values for Z-axis velocity could be subject to the same error disguising them from a comparison filter.

Beam 5 of a 5-beam ADCP, like that used in this study, represents a direct measurement of the Z-axis velocity (see Figure 7.3). As such, this study compares the direct measurement of the Z-axis velocity (Beam 5) to the Z-axis velocities from transformed divergent beams in a bid to quantify the true error in Z-axis velocity from transformed beams when the ADCP is placed horizontally.

Due to the deployment characteristics as well as the orientation of the horizontal ADCP, Beam 4 is located closest to a boundary (the sea surface). As a result, the range of this beam is limited by surface strike. Given the depth of deployment as well as the angle of the beam to the horizontal, this beam can only reach 17 m. This can be seen in Figure 7.5 where the amplitude of Beam 4 increases as it strikes the sea surface. For this study, any data recorded by Beam 4 after 17 m from the sensor head were omitted.

7.3 Results

7.3.1 Single beam range

The data from Beam 5 were quality controlled using the filters outlined in Section 7.2.3. The percentage of data removed after the application of each filter can be seen in Figure 7.6 with negative flow speeds representing flow approaching the sensor. Positive flow speeds recorded were omitted in this study as discussed earlier.

7.3. Results

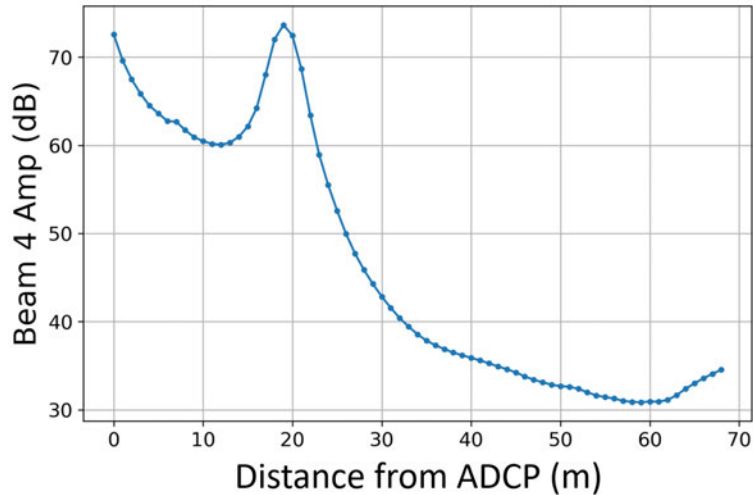


Figure 7.5: Mean amplitude of Beam 4 against distance in front of the horizontal ADCP showing sea surface strike around 17 m.

Figure 7.6 shows that most of the data were able to pass through the amplitude filter (T6) in the initial 40 m of the study area. The T6 filter shows a sharp increase in data removed from 40 m to the end of the domain. This increase is seen most dramatically in the lower absolute flow speeds with less than 20% of data remaining when tide speed is between -1.5 m/s and 0 m/s beyond 50 m from the ADCP. The correlation based filter represented by T8 in Figure 7.6 shows a similar high pass rate for the initial study area. The decline in passing data for T8 begins at 30 m and accelerates at 40 m. Again, it can be seen that the filter is removing more data at lower flow speeds. Filter T15 removed data as a result of high rates of pitch, roll, or yaw. Figure 7.6 shows that no data reached this threshold and so this filter had no effect on the dataset. Filter T18 was designed as a method to remove spikes in amplitude due to suspended bodies in the water column. Figure 7.6 shows that very little data was removed by this filter. Filter JDK1 removed a large proportion of data from higher flow speeds in close proximity to the horizontal ADCP as can be seen in Figure 7.6. JDK1 had a further small effect throughout the study domain with a noticeable removal of data from the mid range region of around 25 m, but a small amount when compared to T6 and T8.

Figure 7.6 also shows the combined result of all filters used for the quality control of the beam data in this study. It is clear that between 5 m and 25 m over 90% of data meet the requirements set out by the QARTOD filters for all flow speeds. Beyond 25 m, -2.5 m/s to -4.5 m/s sees a large removal of data. Lower speeds see a larger volume of data removal, over 90% removed, while higher absolute speeds see only around 60% of data removed by the end of the study domain.

7.3. Results

Table 7.3 shows the range from the horizontal ADCP for a given acceptable data loss and flow speed. The value for acceptable data loss is to the discretion of the user and will have an impact on the uncertainty of the flow measurements. It can be seen that the full range of the sensor configuration (68 m) is reached if 60% data loss is accepted at -3.75 m/s. It can also be seen, as was shown in Figure 7.6, that slower flows inhibit the range of the horizontal ADCP.

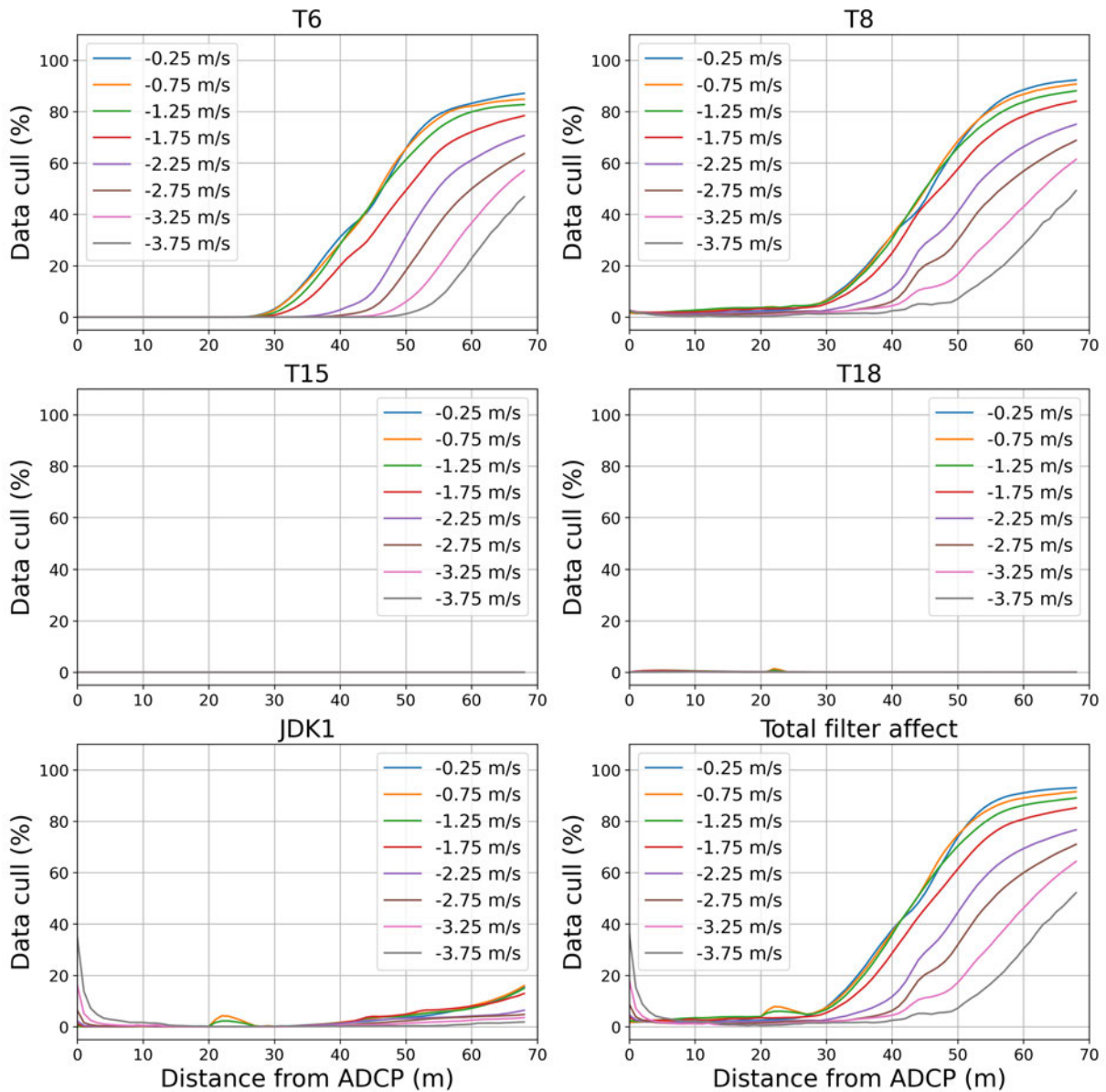


Figure 7.6: Percentage of data removed in Beam 5 after filters applied, as a function of distance in front of the horizontal ADCP for a range of flow speed brackets. Each sub-figure represents a different filter with each line representing a 0.5 m/s speed bracket with the bracket centre indicated. The total filter affect is shown in the bottom right sub-figure.

7.3. Results

Table 7.3: Horizontal ADCP range in meters for a given acceptable data loss percentage and flow speed.

U (m/s)	Data loss				
	90%	80%	70%	60%	50%
-0.25	57.9	51.9	49.1	46.8	44.5
-0.75	62.6	52.2	48.5	46.0	43.7
-1.25	68.0	54.3	49.9	46.5	43.7
-1.75	68.0	58.9	52.9	49.5	46.3
-2.25	68.0	68.0	60.6	54.8	51.5
-2.75	68.0	68.0	67.2	60.0	55.4
-3.25	68.0	68.0	68.0	65.7	61.4
-3.75	68.0	68.0	68.0	68.0	67.2

7.3.2 Incident flow from divergent beams

Z-axis velocities recorded by Beam 5 were compared to a number of Z-axis velocities derived from diverging beams. For simplicity of notation Z-axis velocities from Beam 5 will be written as Z_5 while Z-axis velocities from diverging beams will have the beam numbers used as the subscript (e.g. Z-axis velocity derived from Beams 1, 2, 3, and 4 will be written as $Z_{1,2,3,4}$).

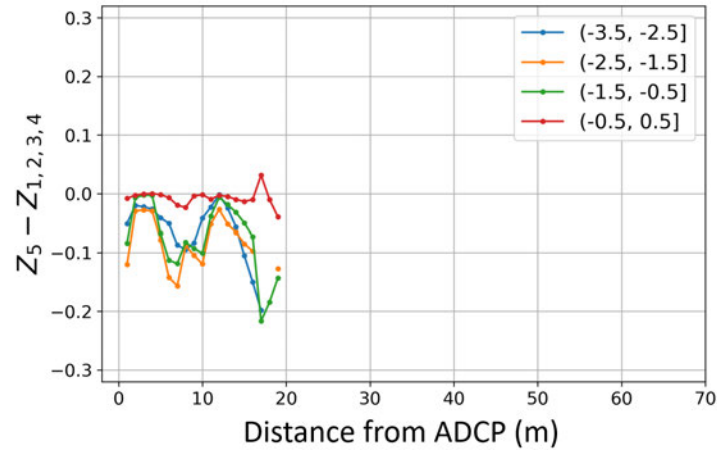
Two different measurements of Z-axis velocity were made using combinations of diverging beams: $Z_{1,3}$ and $Z_{1,2,3,4}$. The flow speed bin averages are displayed in Figure 7.7. These graphs represent the average velocity error compared to Z_5 for each distance bin. Quality control filters were applied as per Tables 7.1 and 7.2. Distance bins where more than 70% of data were removed by filters were considered beyond the range of the horizontal ADCP for this study.

Figure 7.7a shows the difference between Z_5 and $Z_{1,2,3,4}$. The absolute difference in velocity never goes beyond 0.1 m/s at low flow speeds, while higher flow speeds are responsible for more variation with distance as well as greater errors. This figure only extends to 17 m as Beam 4 strikes the sea surface after this distance as discussed in Section 7.2.5.

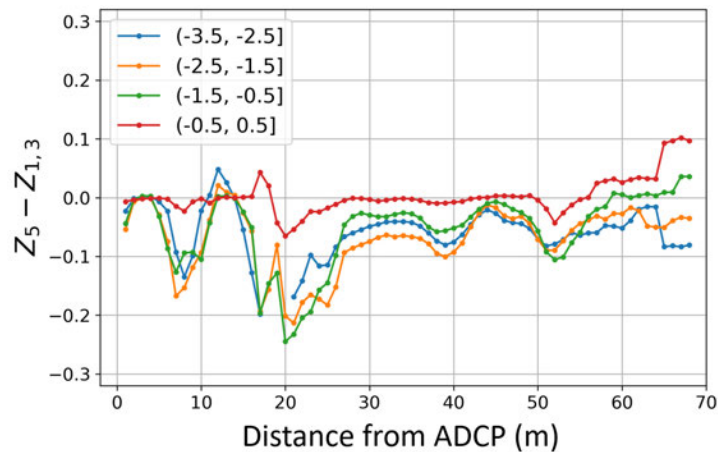
Figure 7.7b shows the error in recording for $Z_{1,3}$. Using only Beams 1 and 3, $Z_{1,3}$ is able to record velocities to 68 m for slower flow speeds as well as higher speeds. The absolute error in measurement across all tide speeds is only momentarily greater than 0.2 m/s.

The majority of the span shown in the sub-figures of Figure 7.7 sees a negative value of Z velocity error. This suggests that the Z velocity recorded using beam transformations is higher than Z velocities recorded by Beam 5 directly, irrespective of the choice of beams.

7.4. Discussion



(a) $Z_5 - Z_{1,2,3,4}$ against distance.



(b) $Z_5 - Z_{1,3}$ against distance.

Figure 7.7: Z velocity from beam combinations compared to Beam 5 against distance from horizontal ADCP binned by flow speed.

7.4 Discussion

The Nortek Signature 500 data sheet indicates a maximum range of 70 m in average mode (Nortek AS, n.d.-b). This study demonstrated that a horizontally mounted Nortek Signature 500 ADCP is not capable of profiling to the maximum range indicated by the manufacturer under every flow condition due to the high energy nature of the environment. The range was, in fact, shown to be flow speed dependant for a Nortek Signature 500. Despite this dependency, 50 m represents the distance at which the horizontal ADCP could measure while maintaining over 50% of all data post rigorous quality control for all speeds for this sturdy setup. The purpose of this study was to demonstrate a ‘percentage data

7.4. Discussion

rejection - range' dependency for a single instrument, and so the percentage data rejection that correlates with 'end of range' is not explicitly identified. Rather, it is for the operator to determine the percentage rejection that is deemed appropriate given sensitivity and uncertainty requirements for a study on a case by case basis.

It is important to note that the choice of sensor frequency and power are also deciding factors in the range of an ADCP. Previous horizontal deployments of 1 MHz single beam sensors have seen ranges much less than this study. The 1 MHz Nortek Aquadopp single beam ADCP placed in the nose cone of a seabed mounted tidal turbine in Harrold et al. (2020) ranged approximately 21 m, while a Nortek AD2CP 1 MHz single beam sensor in McNaughton et al. (2015) ranged 13 m upstream.

7.4.1 Horizontal ADCP for power performance assessment

A power performance assessment is one major use-case of incident flow measurement using a horizontal ADCP. IEC/TS 62600-200 is a major guidance document in the creation of a turbine power curve (IEC, 2013). The document, in its current form, mandates incident flow measurement from a vertically profiling ADCP placed in the free-stream flow. The document is very specific in the identification of incident free-stream measurement locations as was discussed in Chapter 6. For the recording of incident flow from in front of the turbine, an ADCP must be placed 2 to 5 rotor diameters upstream of, and inline with, the rotor (IEC, 2013). The power performance assessment also requires flow measurement over the entire rotor capture area of the turbine.

Current best practices for generating a power curve for the O2 is to apply a pragmatic interpretation of TS 62600-200 and attach provisos in the presentation of the results. Downward facing ADCPs placed at the forward and aft extremities of the main turbine superstructure represent the furthest upstream measurement of the turbine incident flow. An O2 power curve is created by plotting power values against the power weighted rotor average inflow as calculated by these downward facing ADCP with forward and aft ADCPs used for flood and ebb respectively. Power curves are then presented with the limitations of the approach outlined. The application of a horizontal ADCP at hub height, with an appropriate range, would enable Orbital to measure the incident flow from the free stream, as prescribed in the TS. This would increase the level of compliance with TS 62600-200 in the formulation of the turbine power curve

7.4. Discussion

Single beam range

Given the required non-dimensional upstream distance for free stream flow recording according to TS 62600-200 (IEC, 2013), the range requirement for the use of a horizontal ADCP for incident flow recording is turbine specific. That said, the ADCP range found in Harrold et al. (2020) using a 1 MHz Nortek Aquadopp and in McNaughton et al. (2015) using a 1 MHz Nortek AD2CP represented $1.75D_E$ and $0.72D_E$ of respective turbines, where D_E is the equivalent turbine rotor diameter. This is much shorter than the TS 62600-200 prescribed distance of $2-5D_E$.

The acoustic frequency of an ADCP has a bearing on the manufacturer stated range. There is therefore an effect on the total range when deployed horizontally as can be seen in Table 7.4. The values contained in Table 7.4 are not directly comparable, in part as the sensors were at different water column heights, but give an indication of the range achievable.

Table 7.4: Range of three horizontal ADCPs deployed on full scale tidal turbines along with manufacturer stated range including the Nortek Signature 500 studied in this paper (Harrold et al., 2020; McNaughton et al., 2015; Nortek AS, n.d.-a).

Sensor	Manufacturer Stated range (m)	Horizontal range in an energetic tidal environment (m)
1 MHz Nortek Aquadopp	25	20.4
1 MHz Nortek AD2CP	-	13
Nortek Signature 500	70	31 (with 10% data loss see Figure 7.6).

This study has shown that the range of the single central beam on the Nortek Signature 500 is flow speed specific. In order for a horizontal Nortek Signature 500 to reach the free stream of an O2 turbine according to the TS 62600-200 (IEC, 2013), the ADCP would have to range 56.6 m (see Equation 6.1) under all flow conditions. This is only possible with the acceptance of 90% data loss for the Nortek Signature 500 used in this study, according to Table 7.3.

7.4. Discussion

Incident flow from divergent beams

It is important that, within TS 62600-200, the incident flow measured represents an average of the flow speed experienced by the entire rotor diameter (IEC, 2013). For a horizontal ADCP this manifests as a beam cone the diameter of the rotor at the measurement bin. In the instance that a single ADCP beam ranges into the free-stream for a specific tidal turbine, it is likely that the beam cone of a single beam will not diverge to the rotor diameter for larger turbines.

In these cases, in order to have a diverged acoustic cone the size of the rotor area, a multiple beam approach must be adopted. Figure 7.7 shows that beam combination is an important consideration when using a horizontally mounted ADCP in a multi-beam configuration. It is likely that one divergent beam will strike a boundary before the location of the free-stream: either the sea surface (as seen in Figure 7.5) or the sea floor for turbines placed lower in the water column.

The transverse flow homogeneity assumed in the combination of multiple beams for instrument coordinate flow speed transformation is inherently flawed for a horizontally mounted ADCP. This is because vertical shear profiles through the water column ensure that the flow speeds across the measurement area differ. At the limit of $Z_{1,2,3,4}$, 17 m from the sensor head, the beam cone of the 25° divergent beams is 15.8 m in diameter. The difference in flow speed at the top and bottom of this beam cone can be assessed by looking at the shear profile, U , given by Equation 7.1 where U_{ref} is a reference velocity, y is the height above the seabed on the y-axis (see Figure 7.3), y_{ref} is the height at which U_{ref} occurs, and α is the shear profile exponent. Assuming a $\frac{1}{5}^{th}$ shear profile exponent (Naberezhnykh, Ingram, Ashton, & Culina, 2023) and a water depth of 35 m for the site, the flow speed difference between the top and bottom of the beam cone on the y-axis (see Figure 7.3) is as much as 14% 17 m in front of the sensor head. The shear profile has less affect on $Z_{1,3}$ as beam 1 and 3 are on the horizontal plane and so only diverge at the beam width on the y-axis (see Figure 7.3). In this case, only a 2% difference in flow speed between the upper and lower cone limits would be expected at $2D_E$ (56.6 m) in front of the sensor head. That said, $Z_{1,2,3,4}$ has diverged to ± 8 m on the x-axis and ± 8 m on the y-axis (see Figure 7.3) by 17 m, while $Z_{1,3}$ has diverged ± 26 m on the x-axis and only ± 1.4 m on the y-axis by 56.6 m. In both cases, the beam cone is not the same size and shape at the measurement location as the turbine rotor.

$$U(y) = U_{ref} \left(\frac{y}{y_{ref}} \right)^\alpha \text{ for } y \geq 0 \quad (7.1)$$

7.4. Discussion

Figure 7.7 shows that the single beam, Beam 5, measure of Z velocity (Z_5) is consistently lower than the transformed divergent beam recording in both the 4 beam and 2 beam case ($Z_{1,2,3,4}$ and $Z_{1,3}$). A power curve created using Beam 5 would, therefore, be more optimistic than a power curve using either of the divergent beam combinations presented.

7.4.2 Additional applications of a horizontal hub height ADCP

Turbine wake

While a hub mounted ADCP has been shown to provide a practical solution to floating tidal energy inflow measurement, the sensors setup can be leveraged for advancements in understanding in other areas. The O2 does not vane between tides resulting in the horizontal ADCP measuring the inflow on one tide and the wake on the next. Profiling along the axis of wake propagation enables a time domain view from a single profile. How this profile changes with incident flow speed, and between operating states, can also be analysed for array configurations and downstream turbine interactions.

The live and uninterrupted recording of incident flow towards a turbine from a horizontal hub height ADCP presents the possibility for controller applications. Feed forward turbine control, like that already used in the wind industry (Miquelez-Madariaga, Lizarraga-Zubeldia, Diaz de Corcuera, & Elso, 2022; Russell et al., 2024), could reduce loads on a turbine enabling a further reduction in costs for the developer.

Direct measurement of turbine blockage using a horizontal ADCP

Blockage is the slowing of flow as it approaches the rotor and occurs as a result of the rotor applying thrust back to the flow. The distance to which blockage affects inflow upstream of the turbine is a key consideration in locating the incident free-stream and is a further application of a horizontal hub height ADCP. Beam 5 can be used to record the blockage profile as the flow slowed approaching the turbine. Beam 5 is perpendicular to the plane of energy extraction, and therefore is a direct measurement of the blockage affect at different distances in front of the turbine.

7.4. Discussion

7.4.3 Direct measurement of turbine blockage using a horizontal ADCP

The ability for a horizontal ADCP to directly measure turbine blockage was assessed by collecting data from the horizontal ADCP during generation. The generation dataset comprised of Beam 5 data from the horizontal ADCP between 12/8/2022 and 15/8/2022 representing five tidal cycles. The O2 was generating at a 2 MW set point for the duration of this data recording period. The wave conditions during data recording for the duration of the generation dataset, as calculated by the REDACTED Method (see Section 4.5), can be seen in Figure 7.8. Wave heights remained below $H_s=1.1$ m for this data set.

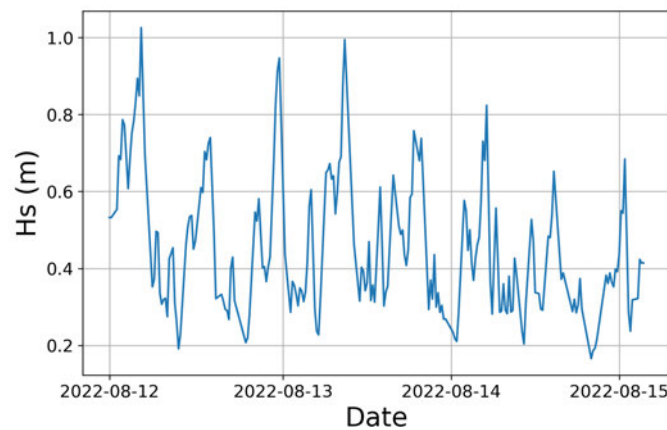


Figure 7.8: Significant wave height for duration of generation horizontal ADCP dataset.

Direct measurement of turbine blockage: Results

From the generation dataset, each profile recorded was grouped according to the flow speed at 20 m in front of the ADCP. Each profile was then separated into five flow speed brackets, each with a width of 0.4 m/s. The average profile within each speed bracket was then calculated and normalised by the speed at $z=20$ m from the ADCP (following the previously defined coordinate system in Figure 7.3). Figure 7.9 shows the five averaged inflow profiles. In each case, the flow is moving towards the ADCP, i.e. with time, the flow is moving from $z=70$ m towards $z=0$ m.

It can be seen that, as the flow approaches the ADCP at $z=0$ m, the flow decreases in speed (see Figure 7.9). The flow speed sees a drop to 85% of the normalised flow speed in the most extreme case (flow speeds of between -2.5 and -2.1 m/s). Beyond 30 m from the ADCP, the measurement experiences a large drop in velocity followed by a reduction in uniformity. This large drop at 35 m is most extreme for lower absolute flow speeds but is seen in all flow speed brackets in the generation dataset.

7.4. Discussion

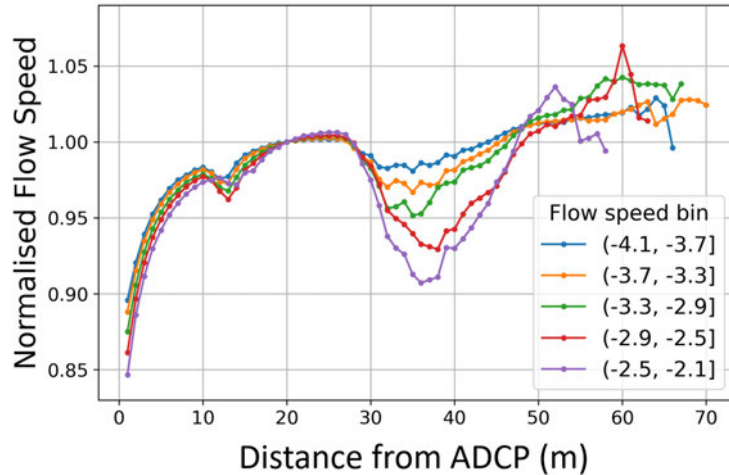


Figure 7.9: Flow speed binned by beam-wise average (between 20 m and 30 m for 4 days in August 2022 during 2 MW rated power. Each plot is normalised by flow speed at 20 m in front of the horizontal ADCP.

Direct measurement of turbine blockage: Discussion

Distances of $z=0$ to 25 m along Beam 5 clearly show the flow slowing down as it approaches the turbine. This is a direct result of the turbine thrust acting on the incident flow, i.e., blockage. Figure 7.9 shows the smooth curve expected from blockage between 0 m and 10 m that was also reported by Harrold et al. (2020).

Figure 7.9 also shows an unexpected slowing of the flow beyond 30 m. This phenomenon can be explained by looking at the turbine dynamics under thrust. As the turbine generates power, the blades see a thrust. This thrust is transmitted to the upstream mooring lines which move from a catenary configuration to a taught mode. As the mooring lines are connected to the super structure, there is also a moment generated that acts to pitch the nose of the turbine down, and into, the oncoming flow. Figure 7.10 shows that as the mooring lines become taught, they move in front of Beam 5 of the horizontal ADCP. The distance at which the mooring lines impinge on Beam 5 coincides with the drop in flow speed shown in Figure 7.9 suggesting the data in this region is not reliable. The mooring chains are a physical barrier to the acoustic signal from the ADCP causing data from after this impediment to be unreliable also.

7.4. Discussion

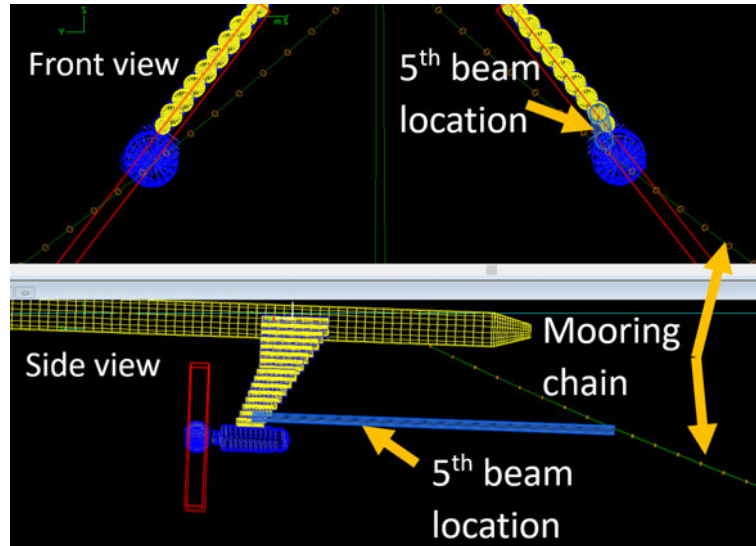


Figure 7.10: OrcaFlex Location of Beam 5 from the horizontal ADCP in relation to the mooring lines when the turbine is under generation thrust.

The affect of the chain impinging on the acoustic beam under thrust is demonstrated further in Figure 7.11 which show a similar plot to Figure 7.9. This plot was generated in the same way as Figure 7.9, however, using the non-generation dataset presented in Section 7.2.2. The lack of a dramatic slowing of flow between 30 m and 50 m in this figure demonstrates the phenomenon recorded in Figure 7.9 was a direct result of the movement of the mooring chain due to turbine generation.

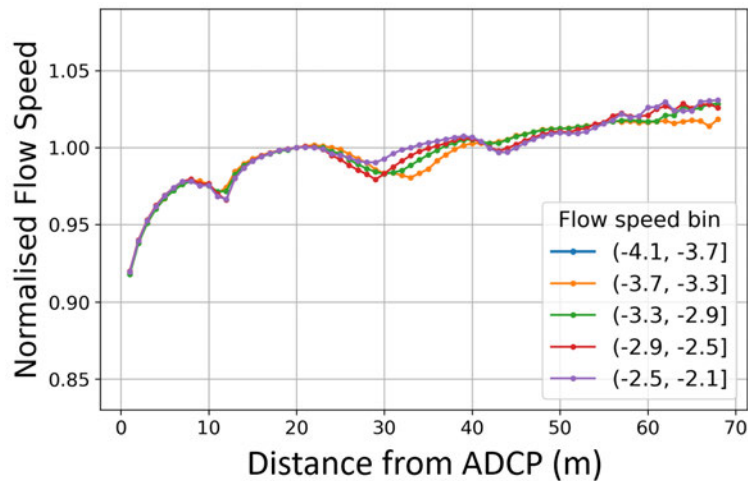


Figure 7.11: Flow speed binned by beam-wise average (between 20 m and 30 m for 4 days in August 2022 during no power generation). Each plot is normalised by flow speed at 20 m in front of the turbine.

7.5 Application and impact

The shortcomings of current ADCP practices for incident flow measurement were outlined in Chapter 6. This Chapter follows on and, by fulfilling Aim 5 from Section 1.4, shows a credible alternative to the incident flow measurement technique prescribed by the incumbent IEC technical specification for a PPA (IEC, 2013). Although the suggestion of horizontal ADCPs deployed on a tidal turbine for incident flow measurement has already been suggested (RealTide Consortium, 2019, 2020; TIGER, 2022), and applied on a seabed mounted turbine (Harrold et al., 2020; McNaughton et al., 2015; RealTide Consortium, 2021), this study was the first analysis of range from a deployment on a floating utility scale tidal turbine.

The work contained in this chapter has:

- Developed a methodology for the testing of range of a horizontally mounted ADCP placed hub height on a floating tidal turbine.
- Identified the range of a single horizontal beam from a horizontally mounted Nortek Signature 500 in a real world energetic tidal environment.
- Shown the implications of boundary proximity on divergent beams when an ADCP is placed horizontally.
- Demonstrated the impact of beam choice on range when using beam combinations to measure incident flow with a horizontal ADCP.
- Presented limitations, unique to floating tidal turbines, in the use of horizontal ADCPs for incident flow measurement under generation conditions.

The analysis presented has clear application and impact as it demonstrates the operational envelope of a horizontally mounted ADCP on a floating tidal turbine. It is shown that the choice and setup of a turbine mounted ADCP is important for sensor range. It has also shown that the turbine dynamics must be considered in the deployment of ADCPs to avoid interaction and interference from mooring chains.

7.6 Conclusion

The application of turbine-based sensors is key for floating tidal energy as it avoids the need for additional seabed operations. Incident flow measurement is, however, a difficult parameter to record from onboard a turbine due to the necessity for measurements to be outwith the influence of the turbine itself. Horizontal ADCPs represent a realistic means of incident flow measurement upstream of the turbine.

7.6. Conclusion

This study shows that compliance with free-stream range requirements for large tidal turbines is a challenge for horizontal ADCPs. Large turbines require a greater horizontal ADCP range as ‘free-stream’ location up-stream is a function of turbine diameter. As a result, more data is lost from an ADCP at the free-stream of a larger tidal turbine. This has implications for uncertainty calculations for a power performance assessment.

Standard compliant incident flow measurement for a tidal turbine power performance assessment requires flow averaged over the entire rotor diameter. This study shows that the use of divergent beams to obtain a ‘rotor area sized beam cone’ can have implications on accuracy on flow speed measurements. The choice of beams is also important for divergent beam cone range.

The study concluded with the demonstration of turbine-flow interactions during generation. It was shown that, while horizontal ADCPs present a credible solution to direct blockage recording, it is important to consider turbine and riser dynamics in order to avoid impaired measurement campaigns.

Overall, while the deployment of horizontal turbine mounted ADCPs offer a lower operational cost option for incident flow measurement as well as a number of additional potential use-cases, ADCP configuration and setup are important considerations prior to deployment.

Chapter 8

Conclusions

8.1 Thesis conclusion and novelty

Sensors are the only means of gaining data from a real system in order to further understanding and allow for technological advancements. The balance between value of learning and cost of data is highly important for sectors where there are financial constraints. For the tidal sector, how a turbine is instrumented is important for everyday operations, but is equally important for recording unknowns in a failure scenario. The work contained in this thesis reduces costs for the floating tidal energy developer Orbital Marine Power by using existing sensors and datasets, and in some cases suggests new sensors, in order to gain new and low cost advancements in understanding to allow for better decision making going forward. The overall methodology is applicable for all turbine developers demonstrating an advancement for the sector.

The work contained in this thesis consisted of five chapters of novel work preceded by two chapters of introductions. Chapter 3 acts as a bridge looking at a number of small case studies on process streamlining as a means of reducing the person hours associated with routine tasks. In executing this chapter, time was freed up for other activities. Chapter 3 also acted as a foundation for code used in the chapters that followed. The novelty in this chapter came predominantly from the use of Python on internal Orbital Marine Power processes. Leaning into a Python code approach for accelerating these processes enabled time savings of 10s of hours for a number of case studies.

Chapters 4 to 7 are specific work packages identified as having a large potential for learning using sensors and datasets that, either already existed on the turbine for other purposes, or suggesting sensors that would represent a good knowledge-return on cost. The work packages selected were: Estimating tidal site wave statistics for the design, operation, and maintenance of the O2 using the existing onboard sensor suite; The validation of a numerical simulation tool used to model O2 drive-train loads; The application of ADCPs

8.1. Thesis conclusion and novelty

for floating tidal turbine incident resource measurement; The application of a horizontal turbine mounted hub height ADCP for incident resource measurement. Each topic was introduced before the method and results were presented, a discussion and conclusion followed including the explicit evaluation of sector impacts from the work.

Works contained in this thesis were disseminated through a number of modes. A list of disseminated works can be found in Appendix A.

8.1.1 Estimating tidal site wave statistics for the design, operation, and maintenance of the O2 using the existing onboard sensor suite

The study of waves is very pertinent for any marine energy application as waves introduce fatigue loading as well as ultimate load states. For tidal energy applications, the role of waves is no less important, however, the fast flowing tidal current makes standard wave measurement techniques like wave buoys impractical. Instead, other measurement techniques are used that often require stand alone seabed operations using sensors that have a limited power source with data that can only be collected on retrieval of the device.

Chapter 4 covers two methods of converting onboard motion data into wave statistics. The key motivation behind developing a new wave measurement process was the uninterrupted, live nature of wave recording that was possible using onboard sensors.

Two methods, of differing complexity, for calculating wave height and period were presented. The first method used the wave dispersion relation and simple assumptions on the sea surface following nature of the O2 structure. Method 1, The Dispersion Relation, was shown to have merits in gauging the general trend in significant wave height but lacked accuracy across the whole wave height spectrum. A similar result was found for wave period using this Dispersion Relation method. The second method REDACTED. Method 2, The REDACTED Method, was able to record inline significant wave height to within ± 0.5 m across a range of heights compared to wave height recording from a seabed mounted ADCP. Recording of peak wave period from Method 2 proved less accurate, in part due to the accuracy of the ADCP values used for comparison. The accuracy of each method has a large bearing on the use case applicability.

While the use of onboard sensor data to determine wave statistics is not novel, the methods used and the tidal environment application were novel. The REDACTED in particular was a new and successful approach.

8.1. Thesis conclusion and novelty

8.1.2 Validation of a numerical simulation tool used to model O2 drive-train loads

The use of numerical models for load analysis is prolific in the tidal industry. A budget constrained industry like tidal energy sees huge advantages in rapid and cheap environmental load analysis brought about by testing in this way. For Orbital Marine Power, Tidal Bladed from DNV-GL is the numerical model software of choice for drive-train loads.

Chapter 5 is a systematic comparison of data recorded by the O2 at a 2 MW and 1.7 MW set point and the Tidal Bladed model used to predict loads. Overall, the Tidal Bladed model showed good correlation with the recorded data at both a 2 MW and 1.7 MW set point for mean and maximum 10-minute load values as well as fatigue loads and other metrics. A number of ebb-flood disparities were noted as well as above and below rated differences. The comparison study looked primarily at blade loads and rotor shaft loads but also looked at the pitch controller dynamics. Outliers for each comparison were identified and justifications presented.

A demonstration of the immediate use of this comparison study was presented as the yield implications of blade loads limits. This showed that powering down for 10 minutes during the highest loads had a smaller impact on overall power generation according to real data compared to Tidal Bladed model data. The application of this Tidal Bladed validation study goes far beyond yield implications of load limit de-rating. The validation of the Tidal Bladed model enables confidence in using the software for the design of future iteration of the Orbital Marine Power tidal technology. The confidence attributable to well validated load models allows for lower safety factors, therefore lowering costs.

The comparison of Tidal Bladed to a seabed mounted tidal turbine has been made in the literature. The novelty of this study came from the extensive nature of the loads investigated across a dual rotor floating tidal turbine. Another key source of novelty comes from the floating nature of the turbine being compared to Tidal Bladed. Validating Tidal Bladed for a floating turbine demonstrates the entire sector applicability of Tidal Bladed.

8.1.3 Application of ADCPs for floating tidal turbine incident resource measurement

Incident flow measurement is key to the creation of a power performance curve used to forecast yield for a tidal turbine. IEC/TS 62600-200 is a leading document outlining a step-by-step process in the creation of a power curve for tidal energy. The TS 62600-200 document, however, has limitations when applied to floating tidal energy. Chapter 6 reviews these floating tidal energy limitations using data from an operational O2 in order to provide quantification. Most notably, these limitations came from ADCP placement, side lobe contamination, blanking distance, and horizontal flow shear.

Chapter 6 quantifies limitations, specific to floating tidal energy, to the use of TS 62600-200 as a reduction in area in which ADCPs can be placed while remaining within the technical specification guidelines compared to a seabed mounted turbine of the same equivalent diameter. The reduction in ADCP deployable area of as much as 87% for a particular ADCP orientation shows the increase in accuracy needed to comply with the technical specification for floating tidal energy (see Figure 6.4 and Table 6.2). Limitations brought about by riser interference, side lobe contamination, blanking distance, as well as the horizontal shear across a real tidal site all culminate in a narrow band of operation for a floating tidal turbine that allows for the ADCP measurement campaign to comply with the technical specification in order to measure incident resource.

The quantification of limitation in the application of TS 62600-200 for floating tidal turbines serves as an explanation for the low sector uptake of the document. Standards and technical specifications are important in the progression of a technology and so presenting barriers to uptake allows for informed amendments to be made in subsequent editions.

8.1.4 The application of a horizontal turbine mounted hub height ADCP for incident resource measurement

Chapter 7 is one solution to the impediments experienced by floating tidal turbines in the deployment of TS 62600-200 (seen in Chapter 6). A horizontal ADCP was shown to provide a suitable alternative to the technical specification for incident resource measurement under certain circumstances. The range of a Nortek Signature 500 5-beam ADCP mounted on the leg of the O2 was presented. This study showed that range is flow speed dependent. It was also shown that the Nortek Signature 500 struggles to meet range requirements set out by TS 62600-200 for larger turbines and that divergent beam combinations can

8.1. Thesis conclusion and novelty

deviate from direct single beam measurement of inline velocity for a Nortek Signature 500 5-beam ADCP. This study shows that developers have to think carefully about the capabilities of their chosen ADCP when deployed horizontally and its ability to range in to the free-stream for the full speed range of the power curve of their turbine.

This chapter also explored the direct measurement of blockage using a horizontal hub mounted ADCP. The horizontal ADCP was able to record blockage in the immediate proximity of the sensor, however, mooring line interference limited the recording range. This study showed that, although a horizontal ADCP is promising for the recording of flow features, it is important to account for all turbine positions in the deployment of the sensors. Despite the limitations of this setup on the O2, this study demonstrated that a horizontal ADCP could be used for blockage recording and even feed forward control for a tidal turbine with a different mooring configuration. This could aid in load reductions and therefore reduce costs for a tidal turbine.

8.2 Research contributions

8.2.1 Key novelty

Estimating tidal site wave statistics for the design, operation, and maintenance of the O2 using the existing onboard sensor suite

- This is the first use of motion data to estimate wave statistics for a utility scale in service floating tidal turbine. This is the first time, to the author's knowledge, that a floating tidal turbine has had a live onboard means of recording wave height and period.
- REDACTED

Validation of a numerical simulation tool used to model O2 drive-train loads

- This is the most comprehensive validation of Tidal Bladed for a floating tidal turbine using a concurrent dataset. The comparison was performed across 17 variables, including a number of controller dynamics (see Table 5.2). Validation of Tidal Bladed for a whole system enables a reduction in the number of modelling software needed which, in turn, brings down costs.

8.2. Research contributions

- This is the first comparison of wave induced fatigue and the associated error between Tidal Bladed and recorded data from a floating tidal turbine for four concurrent blade data streams (see Figure 5.4). This study demonstrated the error in damage equivalent loads calculated from Tidal Bladed and recorded data and how it changed with significant wave height.
- This is the first comparison of recorded and Tidal Bladed blade load limit implications of yield for a floating tidal turbine (see Figure ??). This predominantly looked at the flow speeds at which extreme blade loads were seen in the recorded data and the Tidal Bladed modelled data.

Application of ADCPs for floating tidal turbine incident resource measurement

- This is the first quantification of the effect deploying tidal turbines from a floating platform has on the ADCP placement in line with IEC/TS 62600-200. Section 6.2.2 shows the percentage decrease in permissible area for seabed ADCP deployment as a direct result of placing the turbines on a floating platform. The section also demonstrates that this reduction in area is across all tide speeds and is not just a result of low speed fluctuations in direction.
- First collection of all ADCP related impediments to compliance with IEC/TS 62600-200 incident flow measurement for a floating tidal turbine based on recorded GPS field data (see Chapter 6).

Application of a horizontal turbine mounted hub height ADCP for incident resource measurement

- The first application of a horizontally mounted rotor height ADCP on a utility scale twin rotor floating tidal turbine used to profile into the incident flow. This study (Chapter 7) follows on from literature on horizontal hub height ADCP deployments on a number of seabed mounted turbines.
- This is the first quantification of range of a horizontally mounted Nortek Signature 500 kHz ADCP placed on a floating tidal turbine (see Section 7.2.4). This study demonstrates the applicability of horizontally mounted ADCPs in the incident flow measurement of floating tidal turbines.

8.2. Research contributions

- This is the first comparison of how transformed divergent beam selection effects the inline flow measurement for a horizontal ADCP on a floating tidal turbine. Transformed divergent multi-beam approach is needed, in some cases, to obtain a beam cone of appropriate diameter for larger turbines. This study showed that beam selection is highly important for both range and accuracy of flow recorded.

8.3 Further Work

8.3.1 Estimating tidal site wave statistics for the design, operation, and maintenance of the O2 using the existing onboard sensor suite

The accuracy of wave statistics recording limits their use case. The accuracy of wave height and period measurement methods presented in Chapter 4 provided the first semi-live data recording of wave parameters from onboard a floating utility scale tidal turbine and were shown to be useful for a number of applications. An increase in accuracy of wave statistics recording would enable more expansive use cases. This could include live controller inputs which could be important in an array case where neighbouring turbines effect the waves on the next turbine.

One approach that could see an increase in accuracy is REDACTED. While a change in method may increase accuracy, the ease of replication may be lost with an increase in complexity. This complexity-accuracy would be a trade off that could be considered in future work.

Wave direction is a parameter that was difficult to determine from recorded motion of the O2's long slender body. An accurate means of determining wave direction would allow for the directional variable to be analysed in respect to loading of the turbine. An important piece of future work would be to establish a sound method for wave direction estimation. This may involve the deployment of additional sensors, however, it remains important that cost is outweighed by the value of the data collected.

8.3. Further Work

8.3.2 Validation of a numerical simulation tool used to model O2 drive-train loads

The validation of Tidal Bladed for the O2 at two different set points represents a body of work that can be used to increase confidence for Orbital Marine Power in the use of the Tidal Bladed software going forwards. The study contained in Chapter 5 used two separate 1-month datasets. A future study could look at using a longer dataset as a means to obtain a more concrete comparison. Additionally, the data from a larger time period coupled with a more accurate wave height, period, and direction estimation could be used to analyse the impact of waves on loads further.

Another study could look at the sensitivity of simplifying the Tidal Bladed model. If similar results were obtainable with a simplified mode, the processing time and corresponding cost could be reduced. The limiting simplification would need to be clearly defined and would likely be based on use case. For example, design loads issued to a third party would likely need the highest fidelity model while a simplified model could be used for a study of wave direction effects on loads. These levels of simplified models exist within Orbital Marine Power, however, more confidence could be created by a comparison to real, recorded, O2 data.

8.3.3 Application of ADCPs for floating tidal turbine incident resource measurement

The publication of difficulties in compliance with a technical specification enables IEC document maintenance teams to adjust requirements in subsequent editions. The work in Chapter 6 could be furthered by looking at other tidal sites to see if the same impediments to the execution of TS 62600-200 for floating tidal developers are present.

Within the Fall of Warness, the study in Chapter 6 looking at where ADCP Orientation B is not valid (see Section 6.2.2) could be extended over more transect lines. This could culminate in a heat map of the entire site indicating where the flow is not conducive with Orientation B. This heat map could then be used by EMEC to inform developers when conducting their own power performance assessments.

8.3. Further Work

8.3.4 The application of a horizontal turbine mounted hub height ADCP for incident resource measurement

Incident flow measurement remains an important step in the creation of a power curve for tidal turbines. A key section of Chapter 7 looked at the range of a horizontal ADCP, in this case a Nortek Signature 500 (see Section 7.2.4). Further work is needed to estimate the range of other ADCPs at different frequencies and powers. This would allow a developer to choose the appropriate instrument for the distance needed given their rotor diameter. This step is needed as it was shown that the manufacturer specified maximum range is not transferable to a horizontal application in an energetic tidal environment.

fin

Appendix A

Dissemination of works

1. Poster presentations:
 - Poster presentation: EXPLOITING DATA TO LOWER RISK IN FLOATING TIDAL ENERGY Machine and environmental data tools for the improved operation of the Orbital O2, IDCORE Company day 2022
 - Poster presentation: Using Data to Reduce Costs in Floating Tidal Energy, IDCORE Company day 2023
 - Poster presentation and slide presentation: Using Data to Reduce Costs in Floating Tidal Energy, University of Edinburgh post-graduate research conference 2023
 - Poster presentation: Using Data to Reduce Costs in Floating Tidal Energy, INORE symposium 2023
 - Poster presentation: Using Data to Reduce Costs in Floating Tidal Energy, IDCORE Company day 2024
2. Conference paper and presentation:
 - Dillenburger-Keenan, J., Miller, C., Sellar, B. (2024). Practicalities of Standard-Compliant Incident Resource Measurement for Floating Tidal Energy. In *Proceedings of The Thirty-fourth (2024) International Ocean and Polar Engineering Conference (ISOPE)*
3. Journal paper:
 - Dillenburger-Keenan, J.; Miller, C.; Sellar, B. On the Performance of a Horizontally Mounted ADCP in an Energetic Tidal Environment for Floating Tidal Turbine Applications. *Sensors* 2024, 24, 4462. <https://doi.org/10.3390s24144462>

Bibliography

- Ahmad, M., Kumar, A., & Ranjan, R. (2022). Recent Developments of Tidal Energy as Renewable Energy: An Overview. In R. Jha, V. Singh, V. Singh, L. Roy, & R. Thendiyath (Eds.), *Recent developments of tidal energy as renewable energy: An overview* (Vol. 117, pp. 329–343). Springer. doi: 10.1007/978-3-031-05057-2{_}29
- Ahmed, U., Apsley, D. D., Afgan, I., Stallard, T., & Stansby, P. K. (2017). Fluctuating loads on a tidal turbine due to velocity shear and turbulence: Comparison of CFD with field data. *Renewable Energy*, 112, 235–246. doi: 10.1016/j.renene.2017.05.048
- Altman, D. G., & Bland, J. M. (1983, 9). Measurement in Medicine: The Analysis of Method Comparison Studies. *The Statistician*, 32(3), 307–317. doi: 10.2307/2987937
- Antolovich, S. D., Baietto-Duborg, M., Bathias, C., Baudry, G., Bletry, M., Cazes, R., . . . Remy, L. (2013, 2). Cumulative Damage. In C. Bathias & A. Pineau (Eds.), *Fatigue of materials and structures* (pp. 47–110). Wiley. doi: 10.1002/9781118616994.ch2
- Bahaj, A., Batten, W., & McCann, G. (2007, 12). Experimental verifications of numerical predictions for the hydrodynamic performance of horizontal axis marine current turbines. *Renewable Energy*, 32(15), 2479–2490. doi: 10.1016/j.renene.2007.10.001
- Benjamins, S., Dale, A., Van Geel, N., & Wilson, B. (2016, 5). Riding the tide: Use of a moving tidal-stream habitat by harbour porpoises. *Marine Ecology Progress Series*, 549, 275–288. doi: 10.3354/meps11677
- Bland, J. M., & Altman, D. G. (1999). Measuring agreement in method comparison studies. *Statistical Methods in Medical Research*, 8, 135–160.
- Bouqata, B. (2018). Big Data and Analytics for Wind Energy Operations and Maintenance: Opportunities, Trends, and Challenges in the Industrial Internet. In *Frontiers of engineering reports on leading-edge engineering from the 2017 symposium* (pp. 25–28). Washinton, DC: The National Academies Press.
- Brodtkorb, A. H., & Nielsen, U. D. (2023, 1). Automatic sea state estimation with online trust measure based on ship response measurements. *Control Engineering Practice*, 130. doi: 10.1016/j.conengprac.2022.105375

- Brodtkorb, A. H., Nielsen, U. D., & Sørensen, A. J. (2018a, 1). Online wave estimation using vessel motion measurements. In *International federation of automatic control* (Vol. 51, pp. 244–249). Elsevier B.V. doi: 10.1016/j.ifacol.2018.09.510
- Brodtkorb, A. H., Nielsen, U. D., & Sørensen, A. J. (2018b, 1). Sea state estimation using vessel response in dynamic positioning. *Applied Ocean Research*, 70, 76–86. doi: 10.1016/j.apor.2017.09.005
- Brown, W. S. (2016). Elements of Physical Oceanography. In M. R. Dhanak & N. I. Xiros (Eds.), *Springer handbook of ocean engineering* (pp. 15–46). Springer International Publishing. doi: 10.1007/978-3-319-16649-0{_}4
- Callaghan, J., & Boud, R. (2006). *Future Marine Energy: Results of the marine energy challenge: Cost competitiveness and growth of wave and tidal stream energy* (Tech. Rep.).
- Carbon Trust. (2006). *Future Marine Energy*.
- Cavazzi, S., & Dutton, A. G. (2016, 3). An Offshore Wind Energy Geographic Information System (OWE-GIS) for assessment of the UK’s offshore wind energy potential. *Renewable Energy*, 87, 212–228. doi: 10.1016/j.renene.2015.09.021
- Codiga, D. (2023). *UTide Unified Tidal Analysis and Prediction Functions*. Retrieved from <https://www.mathworks.com/matlabcentral/fileexchange/46523-utide-unified-tidal-analysis-and-prediction-functions>
- Coles, D., Angeloudis, A., Greaves, D., Hastie, G., Lewis, M., Mackie, L., . . . Williamson, B. (2021, 11). A review of the UK and British Channel Islands practical tidal stream energy resource. *Proceedings of the Royal Society A: Mathematical, Physical and Engineering Sciences*, 477(2255). doi: 10.1098/rspa.2021.0469
- Colucci, A. M., Johanning, L., Hardwick, J. P., & Strong, B. (2014). Investigating the interaction of waves and currents from adcp field data. In *2014 oceans - st.john’s*. St.John’s, NL, Canada.
- Congress.gov. (2022). *Text - H.R.5376 - 117th Congress (2021-2022): Inflation Reduction Act of 2022*. Retrieved from <https://www.congress.gov/bill/117th-congress/house-bill/5376/text>.
- Cornett, A., Baker, S., Piche, S., Toupin, M., & Nistor, I. (2014, 11). Appraisal of IEC Standards for Wave and Tidal Energy Resource Assessment. In *4th international conference on ocean energy*. Halifax, Canada.

- Cornett, A., Durand, N., & Serrer, M. (2010, 10). 3-D Modelling and Assessment of Tidal Current Resources in the Bay of Fundy, Canada. In *3rd international conference on ocean energy*. Bilbao, Spain.
- Cossu, R., Penesis, I., Nader, J. R., Marsh, P., Perez, L., Couzi, C., . . . Osman, P. (2021, 11). Tidal energy site characterisation in a large tidal channel in Banks Strait, Tasmania, Australia. *Renewable Energy*, *177*, 859–870. doi: 10.1016/j.renene.2021.05.111
- Dalphinnet, A., Aouf, L., Law-Chune, S., & Tressol, M. (2023). *Product User Manual For Global Ocean Wave Analysis and Forecasting Product* (Tech. Rep.). Toulouse, France: MERCATOR OCEAN.
- Department for Business energy & Industrial Strategy. (2020). *UK Energy Statistics, 2019 & Q4 2019* (Tech. Rep.). London, UK: Government of the United Kingdom. Retrieved from www.gov.uk/government/statistics/provisional-uk-greenhouse-gas-emissions-national-
- DNV GL. (2016a). *Tidal Bladed Theory Manual*.
- DNV GL. (2016b). *Tidal Bladed User Manual*.
- Draycott, S., Sellar, B., Davey, T., Noble, D. R., Venugopal, V., & Ingram, D. M. (2019, 4). Capture and simulation of the ocean environment for offshore renewable energy. *Renewable and Sustainable Energy Reviews*, *104*, 15–29. doi: 10.1016/j.rser.2019.01.011
- Du Bois, P., Dumas, F., Morillon, M., Furgerot, L., Voiseux, C., Poizot, E., . . . Bennis, A. C. (2020, 8). The Alderney Race: General hydrodynamic and particular features: Alderney Race hydrodynamic and features. *Philosophical Transactions of the Royal Society A: Mathematical, Physical and Engineering Sciences*, *378*(2178). doi: 10.1098/rsta.2019.0492
- EMEC. (n.d.). *Assessment of Wave Energy Resource* (Tech. Rep.).
- EMEC. (2021, 5). *Press release: EMEC delivers world’s first international power performance assessment to Verdant*. Retrieved from <https://www.emec.org.uk/press-release-emec-delivers-worlds-first-internationally-recognised-power-performance-assessment-to-verdant-power/>

- EMEC. (2023a). *Grid-Connected Tidal Test Site*. Retrieved from <https://www.emec.org.uk/facilities/tidal-test-site/>
- EMEC. (2023b). *Our History*. Retrieved from <https://www.emec.org.uk/about-us/emec-history/>
- EMEC. (2023c). *Tidal Clients*. Retrieved from <https://www.emec.org.uk/about-us/our-tidal-clients/>
- European Commission. (2019). *The European Green Deal*.
- FloWave. (2018). *FloWave Ocean Energy Research Facility - How it works*. Retrieved from <https://www.flowavett.co.uk/how-it-works>
- Freebury, G., & Musial, W. (2000). Determining Equivalent Damage Loading for Full-Scale Wind Turbine Blade Fatigue Tests. In *19th american society of mechanical engineers (asme) wind energy symposium*. Reno, Nevada.
- Giavarina, D. (2015). Understanding Bland Altman analysis. *Biochemia Medica*, 25(2), 141–151. doi: 10.11613/BM.2015.015
- GOV.UK. (2002). *The Renewables Obligation Order 2002*. London, UK.
- GOV.UK. (2008). *Climate Change Act 2008*. London, UK.
- GOV.UK. (2014). *Contract for Difference Final Allocation Framework for the October 2014 Allocation Round*. London.
- GOV.UK. (2020). *The Ten Point Plan for a Green Industrial Revolution*. London, UK.
- GOV.UK. (2022). *Contracts for Difference Allocation Round 4 results*. London, UK.
- GOV.UK. (2023). *Contracts for Difference Allocation Round 5 results*. London, UK.
- Greenwood, C., Vogler, A., & Venugopal, V. (2019, 2). On the Variation of Turbulence in a High-Velocity Tidal Channel. *Energies*, 12(4), 672. doi: 10.3390/en12040672
- Guerra, M., Hay, A. E., Karsten, R., Trowse, G., & Cheel, R. A. (2021, 11). Turbulent flow mapping in a high-flow tidal channel using mobile acoustic Doppler current profilers. *Renewable Energy*, 177, 759–772. doi: 10.1016/j.renene.2021.05.133
- Hagerman, G., Fader, G., Carlin, G., & Bedard, R. (2006). *Nova Scotia Tidal In-Stream Energy Conversion (TISEC): Survey and Characterization of Potential Project Sites* (Tech. Rep.).

- Harrold, M., Ouro, P., & O'Doherty, T. (2020, 6). Performance assessment of a tidal turbine using two flow references. *Renewable Energy*, 153, 624–633. doi: 10.1016/j.renene.2019.12.052
- Hashemi, M. R., & Lewis, M. (2017). Wave-Tide Interactions in Ocean Renewable Energy. In Z. Yang & A. Copping (Eds.), *Marine renewable energy* (pp. 137–158). Springer International Publishing. doi: 10.1007/978-3-319-53536-4{_}6
- Hasselmann, K., Barnett, T. P., Bouws, E., Carlson, H., Cartwright, D. E., Enke, K., . . . Walden, H. (1973). *Measurements of wind-wave growth and swell decay during the Joint North Sea Wave Project (JONSWAP)* (Tech. Rep.). Hamburg: Deutsches Hydrographisches Institut.
- Hayman, G. J. (2012, 10). *Mlife Theory Manual for Version 1.00* (Tech. Rep.). National Renewable Energy Laboratory. Retrieved from <https://www.nrel.gov/wind/nwtc/assets/pdfs/mlife-theory.pdf>
- Hollander, M., A. Wolfe, D., & Chicken, E. (2015). *Nonparametric Statistical Methods*. Wiley. doi: 10.1002/9781119196037
- Holthuijsen, L. H. (2010, 2). Description of ocean waves. In *Waves in oceanic and coastal waters* (pp. 24–55). Cambridge University Press. doi: 10.1017/cbo9780511618536.004
- Huckerby, J. A., & Johnson, D. (2008). New Zealand's Wave and Tidal Energy Resources and their Timetable for Development. In *2nd international conference on ocean energy (icoe 2008)*. Brest, France.
- IEC. (2013). *IEC/TS 62600-200. Marine energy - wave, tidal and other water current converters - Part 200: electricity producing tidal energy converters - power performance assessment*.
- IEC. (2015a). *IEC/TS 62600-101 Marine energy - Wave, tidal and other water current converters - Part 101: Wave energy resource assessment and characterization*.
- IEC. (2015b). *IEC/TS 62600-201 Marine energy - Wave, tidal and other water current converters - Part 201: Tidal energy resource assessment and characterization*.
- IRENA. (2020). *Wind Energy*. Retrieved from <https://www.irena.org/Energy-Transition/Technology/Wind-energy#:~:text=Global%20installed%20wind%20generation%20capacity%20%E2%80%93%20both%20onshore,733%20GW%20by%202018%20according%20to%20IRENA%E2%80%99s%20data>.

- IRENA. (2023). *IRENASTAT Online Data Query Tool*. Retrieved from <https://pxweb.irena.org/pxweb/en/IRENASTAT/>
- Iseki, T., & Ohtsu, K. (2000, 2). Bayesian estimation of directional wave spectra based on ship motions. *Control Engineering Practice*, 8(2), 215–219. doi: 10.1016/S0967-0661(99)00156-2
- Janiszewski, P. (2023). *rainflow 3.2.0*. Retrieved from <https://pypi.org/project/rainflow/>
- Kangaji, L., Orumwense, E., & Abo-Al-ez, K. (2022, 7). Modelling and simulation of tidal energy generation system: a systematic literature review. *International Journal of Advanced Technology and Engineering Exploration*, 9(92), 1028–1055. doi: 10.19101/IJATEE.2021.875704
- Karsten, R. (2011). An assessment of the potential of tidal power from Minas Passage, Bay of Fundy, using three-dimensional models. In *Proceedings of the international conference on offshore mechanics and arctic engineering - omae* (Vol. 5, pp. 377–384). doi: 10.1115/OMAE2011-49249
- Krogstad, H. E., & Barstow, S. F. (1999). Satellite wave measurements for coastal engineering applications. *Coastal Engineering*, 37, 283–307.
- Lawrence, J., Kofoed-Hansen, H., & Chevalier, C. (2009). High-resolution metocean modelling at EMEC's (UK) marine energy test sites. In *8th european wave and tidal energy conference (ewtec 2009)* (pp. 209–221). Uppsala, Sweden: European Tidal and Wave Energy Conference.
- Lentz, S. J., Kirincich, A., & Plueddemann, A. J. (2022, 1). A Note on the Depth of Sidelobe Contamination in Acoustic Doppler Current Profiles. *Journal of Atmospheric and Oceanic Technology*, 39(1), 31–35. doi: 10.1175/JTECH-D-21-0075.1
- Lewis, M., Neill, S. P., Robins, P. E., & Hashemi, M. R. (2015, 4). Resource assessment for future generations of tidal-stream energy arrays. *Energy*, 83, 403–415. doi: 10.1016/j.energy.2015.02.038
- Liu, X., Chen, Z., Si, Y., Qian, P., Wu, H., Cui, L., & Zhang, D. (2021, 7). A review of tidal current energy resource assessment in China. *Renewable and Sustainable Energy Reviews*, 145. doi: 10.1016/j.rser.2021.111012

- Lockwood, M. (2021). Routes to credible climate commitment: the UK and Denmark compared. *Climate Policy*, 21(9), 1234–1247. doi: 10.1080/14693062.2020.1868391
- Lyne, V., Condie, S. A., & Hallegraef, G. (2005). *Collation and analysis of oceanographic datasets for national marine bioregionalisation*. Retrieved from <https://www.researchgate.net/publication/274008249>
- Marcollo, H., & Efthimiou, L. (2024). *Floating Offshore Wind Dynamic Cables: Overview of Design and Risks* (Tech. Rep.). World Forum Offshore Wind e.V.
- MARIN. (n.d.). *Offshore Basin* (Tech. Rep.).
- Marsh, P., Penesis, I., Nader, J. R., Cossu, R., Auguste, C., Osman, P., & Couzi, C. (2021, 12). Tidal current resource assessment and study of turbine extraction effects in Banks Strait, Australia. *Renewable Energy*, 180, 1451–1464. doi: 10.1016/j.renene.2021.08.051
- McCann, G. N. (2007). Tidal current turbine performance and loading sensitivity to waves and turbulence – a parametric study. In *Proceedings of the 7th european wave and tidal energy conference*. Porto, Portugal.
- McNaughton, J., Harper, S., Sinclair, R., & Sellar, B. (2015). Measuring and modelling the power curve of a Commercial-Scale tidal turbine. In *Proceedings of the 11th european wave and tidal energy conference*. Nantes, France.
- Ministry of Petroleum and Energy. (2016). *Renewable energy production in Norway*. Retrieved from <https://www.regjeringen.no/en/topics/energy/renewable-energy/renewable-energy-production-in-norway/id2343462/>
- Miquelez-Madariaga, I., Lizarraga-Zubeldia, I., Diaz de Corcuera, A., & Elso, J. (2022, 7). Lidar-based feedforward control design methodology for tower load alleviation in wind turbines. *Wind Energy*, 25(7), 1238–1251. doi: 10.1002/we.2724
- Moore, T., & Boyle, C. (2014). The tidal energy potential of the Manukau Harbour, New Zealand. *Sustainable Energy Technologies and Assessments*, 8, 66–73. doi: 10.1016/j.seta.2014.07.001
- Morison, J., Johnson, J., & Schaaf, S. (1950, 5). The Force Exerted by Surface Waves on Piles. *Journal of Petroleum Technology*, 2(05), 149–154. doi: 10.2118/950149-G

- Mounet, R. E., Chen, J., Nielsen, U. D., Brodtkorb, A. H., Pillai, A. C., Ashton, I. G., & Steele, E. C. (2023, 8). Deriving spatial wave data from a network of buoys and ships. *Ocean Engineering*, 281, 114892. Retrieved from <https://linkinghub.elsevier.com/retrieve/pii/S0029801823012763> doi: 10.1016/j.oceaneng.2023.114892
- Mullings, H., & Stallard, T. (2021, 9). Assessment of dependency of unsteady onset flow and resultant tidal turbine fatigue loads on measurement position at a tidal site. *Energies*, 14(17). doi: 10.3390/en14175470
- Munk, W. H. (1950). Origin and generation of waves. In *First conference on coastal engineering*. Long Beach, California.
- Naberezhnykh, A., Ingram, D., Ashton, I., & Culina, J. (2023, 2). How Applicable Are Turbulence Assumptions Used in the Tidal Energy Industry? *Energies*, 16(4). doi: 10.3390/en16041881
- Nasab, N. M., Kilby, J., & Bakhtiaryfard, L. (2020, 3). The potential for integration of wind and tidal power in New Zealand. *Sustainability (Switzerland)*, 12(5), 1–21. doi: 10.3390/su12051807
- Norris, J. V., & Droniou, E. (2007). Update on EMEC activities, resource description, and characterisation of wave-induced velocities in a tidal flow. In *The 7th european wave and tidal energy conference*. Porto, Portugal.
- Nortek AS. (n.d.-a). *Aquadopp Profiler 1 MHz* (Tech. Rep.).
- Nortek AS. (n.d.-b). *Signature 500 Technical specifications* (Tech. Rep.). Retrieved from <https://www.nortekgroup.com/products/signature-500/pdf>
- Nortek AS. (2018). *Signature Principal of Operation* (Tech. Rep.). Rud, Norway: Nortek AS. Retrieved from https://www.nortekgroup.com/assets/software/N3015-025-Principles-of-Operation-Signature_0918.pdf
- Office for National Statistics. (2021). *Wind energy in the UK: June 2021* (Tech. Rep.).
- Orcina. (2014). *OrcaFlex Manual Version 9.6a* (Tech. Rep.). Retrieved from www.orcina.com
- Osalusi, E. (2010). *Analysis of Wave and Current Data in a Tidal Energy Test Site*.
- Osalusi, E., Side, J., & Harris, R. (2009, 5). Reynolds stress and turbulence estimates in bottom boundary layer of Fall of Warness. *International Communications in Heat and Mass Transfer*, 36(5), 412–421. doi: 10.1016/j.icheatmasstransfer.2009.02.004

- Pacheco, A., Ferreira, O., Carballo, R., & Iglesias, G. (2014, 7). Evaluation of the production of tidal stream energy in an inlet channel by coupling field data and numerical modelling. *Energy*, 71, 104–117. doi: 10.1016/j.energy.2014.04.075
- Palmer, D., Gottschalg, R., & Betts, T. (2019, 4). The future scope of large-scale solar in the UK: Site suitability and target analysis. *Renewable Energy*, 133, 1136–1146. doi: 10.1016/j.renene.2018.08.109
- Pao, L. Y., & Johnson, K. E. (2009). A Tutorial on the Dynamics and Control of Wind Turbines and Wind Farms. In *2009 american control conference* (pp. 2076–2089). St. Louis, MO, USA.
- Parkinson, S. G., & Collier, W. J. (2016, 12). Model validation of hydrodynamic loads and performance of a full-scale tidal turbine using Tidal Bladed. *International Journal of Marine Energy*, 16, 279–297. doi: 10.1016/j.ijome.2016.08.001
- Pierson, W. J., & Moskowitz, L. (1964, 12). A proposed spectral form for fully developed wind seas based on the similarity theory of S. A. Kitaigorodskii. *Journal of Geophysical Research*, 69(24), 5181–5190. doi: 10.1029/jz069i024p05181
- Quirapas, M. A. J. R., Lin, H., Abundo, M. L. S., Brahim, S., & Santos, D. (2015). Ocean renewable energy in Southeast Asia: A review. *Renewable and Sustainable Energy Reviews*, 41, 799–817. doi: 10.1016/j.rser.2014.08.016
- Ramos, V., Carballo, R., & Ringwood, J. V. (2016). Assessing the utility and effectiveness of the IEC standards for wave energy resource characterisation. In G. Soares (Ed.), *Progress in renewable energies offshore* (pp. 27–36).
- Ramos, V., & Ringwood, J. V. (2016). Implementation and evaluation of the International Electrotechnical Commission specification for tidal stream energy resource assessment: A case study. *Energy Conversion and Management*, 127, 66–79. doi: 10.1016/j.enconman.2016.08.078
- RealTide Consortium. (2019). *RLT-WP-1-2PDL-000-00-RAM Assessment Report* (Tech. Rep.).
- RealTide Consortium. (2020). *RLT-WP1-1-DEL-000-01 – D1.1 – FMEA Report* (Tech. Rep.).
- RealTide Consortium. (2021). *D2.2 – Next Generation Flow Measurements and Flow Classification (RLT-WP2-2-PDL-0000-04)* (Tech. Rep.).

- Rowell, D., Jenkins, B., Carroll, J., & McMillan, D. (2022, 12). How Does the Accessibility of Floating Wind Farm Sites Compare to Existing Fixed Bottom Sites? *Energies*, *15*(23). doi: 10.3390/en15238946
- Russell, A. J., Collu, M., McDonald, A. S., Thies, P. R., Keane, A., & Quayle, A. R. (2024). LIDAR-assisted feedforward individual pitch control of a 15 MW floating offshore wind turbine. *Wind Energy*. doi: 10.1002/we.2891
- Scottish Government. (2021). *Energy Statistics for Scotland-Q1 2021 Figures*. Retrieved from <https://scotland.shinyapps.io/Energy/?Section=RenLowCarbon&Subsection=RenElec&Chart=ElecGen>
- Sellar, B., Harding, S., & Richmond, M. (2015, 7). High-resolution velocimetry in energetic tidal currents using a convergent-beam acoustic Doppler profiler. *Measurement Science and Technology*, *26*. doi: 10.1088/0957-0233/26/8/085801
- Sellar, B., & Sutherland, D. (2015). *Technical Report on Tidal Site Characterisation During the ReDAPT Project* (Tech. Rep.). The University of Edinburgh. Retrieved from <http://redapt.eng.ed.ac.uk>
- Sellar, B., & Sutherland, D. (2016). *Tidal Energy Site Characterisation at the Fall of Warness, EMEC, UK v4.0* (Tech. Rep.). The University of Edinburgh.
- Sellar, B., Wakelam, G., Sutherland, D., Ingram, D., & Venugopal, V. (2018, 1). Characterisation of Tidal Flows at the European Marine Energy Centre in the Absence of Ocean Waves. *Energies*, *11*(1), 176. doi: 10.3390/en11010176
- Shadman, M., Roldan-Carvajal, M., Pierart, F. G., Haim, P. A., Alonso, R., Silva, C., ... Saavedra, O. R. (2023, 1). A Review of Offshore Renewable Energy in South America: Current Status and Future Perspectives. *Sustainability (Switzerland)*, *15*(2). doi: 10.3390/su15021740
- Shao, J., Chen, H., Li, J., & Liu, G. (2022, 1). An evaluation of the consumer-funded renewable obligation scheme in the UK for wind power generation. *Renewable and Sustainable Energy Reviews*, *153*. doi: 10.1016/j.rser.2021.111788
- SonTek. (2023). *RS5 ROBUST DATA FROM THE WORLD'S SMALLEST ADCP* (Tech. Rep.).


- Story, W. R., Fu, T. C., & Hackett, E. E. (2011, 6). RADAR MEASUREMENT OF OCEAN WAVES. In *Proceedings of the asme 2011 30th international conference on ocean, offshore and arctic engineering*. Rotterdam, The Netherlands. Retrieved from http://asmedigitalcollection.asme.org/OMAE/proceedings-pdf/OMAE2011/44380/707/4574855/707_1.pdf
- Sverdrup, H. V., & Munk, W. H. (1946). Empirical and theoretical relations between wind, sea, and swell. *Transactions American Geophysical Union*, 27(6), 823–827. doi: 10.1029/TR027i006p00823
- Teledyne RD Instruments. (2011a). *Acoustic Doppler Current Profiler Principles of Operation A Practical Primer* (Tech. Rep.). Retrieved from <http://www.rdinstruments.com>
- Teledyne RD Instruments. (2011b). *WavesMon v3.08 User's Guide* (Tech. Rep.).
- Teledyne RD Instruments. (2016). *Sentinel V Waves Array - Product datasheet* (Tech. Rep.). Retrieved from www.teledynemarine.com
- The Conservative Party. (2015). *The Conservative Party Manifesto 2015*.
- THEoREM. (2018). *Wave-Current flume tank*. Retrieved from <https://theorem-infrastructure.org/english-version/tank-facilities/wave-current-flume-tank>
- Thies, P. R., Johanning, L., Harnois, V., Smith, H. C., & Parish, D. N. (2014, 3). Mooring line fatigue damage evaluation for floating marine energy converters: Field measurements and prediction. *Renewable Energy*, 63, 133–144. doi: 10.1016/j.renene.2013.08.050
- TIGER. (2022). *T1.7.3 Test Procedure Report 2 IEC/TS62600-200 Feedback and Recommendations for Floating TEC Incident Resource Measurement for Power Performance Assessment* (Tech. Rep.).
- Todeschini, G., Coles, D., Lewis, M., Popov, I., Angeloudis, A., Fairley, I., . . . Masters, I. (2022, 1). Medium-term variability of the UK's combined tidal energy resource for a net-zero carbon grid. *Energy*, 238. doi: 10.1016/j.energy.2021.121990
- UNEP. (2016). *Adaptation Gap Report*. Retrieved from <http://www.unep.org/climatechange/adaptation/gapreport2016/>

- United Nations. (1997). *Kyoto Protocol to the United Nations framework convention on climate change*.
- United Nations. (2015). *The Paris Agreement*. Retrieved from https://unfccc.int/files/essential_background/convention/application/pdf/english_paris_agreement.pdf
- U.S. Department of Energy. (2023). *Notice of Intent to Issue Funding Opportunity Announcement No. DE-FOA-0002845*. Retrieved from <https://eere-exchange.energy.gov/Default.aspx#FoaId110aceb4-394b-4aa2-8c3e-1232302c0ab2>
- U.S. Integrated Ocean Observing System. (2019). *Manual for Real-Time Quality Control of In-Situ Current Observations* (Tech. Rep.). doi: 10.25923/sqe9-e310
- U.S. Integrated Ocean Observing System. (2020). *QARTOD - Prospects for Real-Time Quality Control Manuals, How to Create Them, and a Vision for Advanced Implementation* (Tech. Rep.). Retrieved from <https://ioos.noaa.gov/about/ioos-by-the-> doi: 10.25923/ysj8-5n28
- Valiente, N. G., Saulter, A., Gomez, B., Bunney, C., Li, J. G., Palmer, T., & Pequignet, C. (2023, 5). The Met Office operational wave forecasting system: the evolution of the regional and global models. *Geoscientific Model Development*, 16(9), 2515–2538. doi: 10.5194/gmd-16-2515-2023
- Waldman, S., Bastón, S., Nimalidinne, R., Chatzirodou, A., Venugopal, V., & Side, J. (2017, 10). Implementation of tidal turbines in MIKE 3 and Delft3D models of Pentland Firth & Orkney Waters. *Ocean & Coastal Management*, 147, 21–36. doi: 10.1016/j.ocecoaman.2017.04.015
- Walker, S., & Thies, P. R. (2021, 11). A review of component and system reliability in tidal turbine deployments. *Renewable and Sustainable Energy Reviews*, 151. doi: 10.1016/j.rser.2021.111495
- Wang, Y., Yu, B., Berto, F., Cai, W., & Bao, K. (2019, 11). Editorial: Modern numerical methods and their applications in mechanical engineering. *Advances in Mechanical Engineering*, 11(11). doi: 10.1177/1687814019887255
- Xu, T., Haas, K. A., & Gunawan, B. (2023, 5). Estimating annual energy production from short tidal current records. *Renewable Energy*, 207, 105–115. doi: 10.1016/j.renene.2023.02.107

- Yang, Z., Wang, T., Branch, R., Xiao, Z., & Deb, M. (2021, 7). Tidal stream energy resource characterization in the Salish Sea. *Renewable Energy*, *172*, 188–208. doi: 10.1016/j.renene.2021.03.028
- Yoro, K. O., Daramola, M. O., Sekoai, P. T., Wilson, U. N., & Eterigho-Ikelegbe, O. (2021, 10). Update on current approaches, challenges, and prospects of modeling and simulation in renewable and sustainable energy systems. *Renewable and Sustainable Energy Reviews*, *150*. doi: 10.1016/j.rser.2021.111506
- Young, I. R. (1999). Ocean Wave Measurement. In R. Bhattacharyya & M. E. McCormick (Eds.), *Wind generated ocean waves* (Vol. 2, pp. 227–254). Elsevier. doi: 10.1016/S1571-9952(99)80011-7

Article

On the Performance of a Horizontally Mounted ADCP in an Energetic Tidal Environment for Floating Tidal Turbine Applications

Jan Dillenburger-Keenan ^{1,2,*}, Calum Miller ¹ and Brian Sellar ² ¹ Orbital Marine Power, Kirkwall, Orkney KW15 1ZL, UK² School of Engineering, The University of Edinburgh, Edinburgh EH9 3BE, UK

* Correspondence:

Abstract: Incident flow measurement is key in the tidal industry for conducting power performance assessments. This paper explores the use of a horizontally mounted Nortek Signature 500 Acoustic Doppler Current Profiler (ADCP) as a means for incident flow measurement onboard a utility-scale tidal turbine. This study shows that the measurement range of an ADCP mounted horizontally in highly dynamic tidal flow (up to 4 m/s) is less than the maximum range stated by the manufacturer. The ability for the horizontal ADCP to accurately resolve velocities in a multi-beam configuration is also analysed. Effects from both vertical shear and beam selection result in incident flow velocities that differ from a single horizontal beam recording. The maximum measurement range of the instrument is found to depend on current speed and on the proportion of data loss that is acceptable to the user. The ability of the ADCP to record data from the free-stream velocity two equivalent diameters upstream of the O2, as set out by IEC TS 62600-200, is considered. It is found that at this distance, there is 90% data loss. Accepting only 10% data loss across all flow speeds resulted in a maximum range of 31 m for a Nortek Signature 500 in this study. While some limitations of an ADCP deployed horizontally in highly energetic tidal flow are identified, the benefits of mounting the sensor close to the rotor facing horizontally into the incoming flow mean that valuable data are still produced for tidal turbine operators.



Citation: Dillenburger-Keenan, J.; Miller, C.; Sellar, B. On the Performance of a Horizontally Mounted ADCP in an Energetic Tidal Environment for Floating Tidal Turbine Applications. *Sensors* **2024**, *24*, 4462. <https://doi.org/10.3390/s24144462>

Academic Editor: Christian Vollaire

Received: 24 April 2024

Revised: 31 May 2024

Accepted: 5 June 2024

Published: 10 July 2024

Keywords: ADCP range; floating tidal turbine; velocimetry; power performance assessment

1. Introduction

Tidal energy is an untapped renewable energy resource, one that is prevalent throughout the United Kingdom (UK) coastal waters. It is estimated that up to 11% of the UK electricity needs could be met by tidal energy, enough to displace a significant proportion of heavy fuel electricity generation within the UK [1]. Barriers to energy market entrance for tidal energy developers have seen a reprieve in recent years with government ring-fenced subsidies enabling early phase designs to avoid competing with established technologies [2,3]. In conjunction with market support, the tidal energy industry continues to innovate in order to bring costs down.

Tidal turbines have seen a division in design philosophy with the majority of globally deployed turbines opting for either a seabed-mounted or floating superstructure. Floating tidal turbines ensure that operations and maintenance costs are low as major components are accessible using small vessels. Placing sensors on a floating tidal turbine benefits from accessibility and the ability to intervene quickly to replace damaged or broken units. However, certain parameters are more difficult to record from a floating platform.

Incident flow velocity is a key parameter for a tidal turbine from both a control and performance perspective. The dominant sensor used in full-scale tidal environment velocimetry is the Acoustic Doppler Current Profiler (ADCP). ADCPs use multiple (typically 3–5) acoustic transducers whose acoustic *beams* diverge away from the instrument. The



Copyright: © 2024 by the authors. Licensee MDPI, Basel, Switzerland. This article is an open access article distributed under the terms and conditions of the Creative Commons Attribution (CC BY) license (<https://creativecommons.org/licenses/by/4.0/>).

Doppler shift in acoustic signal returning to the transducer gives the speed of flow along the axis of the transducer. Given the diverging multi-beam configuration of the sensors, the x , y , z components of flow relative to earth or sensor coordinates can be resolved [4,5]. This non-intrusive measuring technique allows for the flow speed to be calculated at defined distance-bins away from the sensor, enabling a 'profile' to be recorded.

Standard practice for the deployment of ADCPs in the tidal environment is to place them on the sea bed profiling the vertical water column [6–9]. Isolated ADCPs rely on battery power and, therefore, have a defined deployment period, after which they require collection for data extraction. Placing an ADCP onboard a tidal turbine, however, enables continuous sensor power and, therefore, a continuous measurement campaign. A number of studies have seen the deployment of ADCPs onboard a tidal turbine [10,11].

In order to record incident flow from onboard a tidal turbine, the ADCP must be placed horizontally profiling into the flow. The International Electrotechnical Commission (IEC) stipulates that true incident flow data must be obtained from beyond the influence of the turbine on the flow [12]. Turbine-mounted ADCPs for incident flow measurement are inhibited by an inability to be situated beyond the influence of the turbine on the flow. As a result, the ADCP must accommodate this requirement with an 'adequate profiling range'. The deployment of a horizontal ADCP has been suggested as an addition to the next iteration of the IEC guidance on incident resource measurement for power performance assessment [13].

Previous horizontal ADCP deployments on tidal turbines for inflow analysis include the DeepGen-IV [10], the Sabella D10 [11], and the DeltaStream 400 kW turbine [8]. The DeepGen-IV saw a horizontal single-beam Nortek Continental profiling behind the rotor, and a single-beam Nortek AD2CP placed on the rotating hub profiling forward of the rotor. The Sabella D10 saw the deployment of a 5-beam Nortek Signature 500 on the aft of the turbine profiling rearward: due to the fixed nature of the turbine, this constituted incident profiling on the ebb tide. The DeltaStream turbine saw a single-beam 1 MHz Nortek Aquadopp sensor placed in the rotating nose cone of the turbine profiling into the incident flow.

The deployment of ADCPs from onboard a tidal turbine enables a further reduction of seabed operations for a floating tidal turbine. To the authors' knowledge, the deployment of a horizontal ADCP at hub height on a floating, utility-scale, tidal turbine remains a research gap. While theoretical advantages include continuous sensor power and data collection, the envelope of application has not been tested. This study quantifies the range of a horizontal ADCP placed at hub height on a floating tidal turbine in relation to sensor manufacturer stated range, while also exploring advantages and shortcomings of sensor configurations.

2. Materials and Methods

This study outlines the operational envelope of a horizontally mounted 5-beam ADCP when placed at hub height on a utility-scale floating tidal turbine. Firstly, the study identifies the range of a single horizontal beam under a number of incident flow speeds in order to inform technology developers of expected range for the instrument used. Secondly, an assessment of horizontal flow measurement accuracy and range from divergent beams of a horizontally mounted ADCP is presented. The results are then discussed and conclusions are drawn.

2.1. The Floating Tidal Turbine

Orbital Marine Power is a long-standing sector leader in floating tidal energy. The third device deployed by Orbital is the O2. The O2 is a 2 MW tidal turbine composed of two separate 1 MW nacelles supported by legs attaching them to the main hull floating structure (see Figure 1). The two rotors have a diameter of 20 m each. The rotors are designed to be raised to above the water line for maintenance, and are lowered for power production, giving a clearance of 3 m between top-dead-center of the rotor and the sea surface during operation.

The O2 is kept on station using a catenary mooring system. Four mooring lines extend from the turbine to the sea floor, two from each end of the main hull. Given the catenary

nature of the mooring system, the turbine can move ≈ 25 m in any direction on the plane of the sea surface. The location of the turbine is dependent on wind direction, wave climate, and thrust imparted on the structure and rotors by the tide; however, the turbine does not vane between tides.

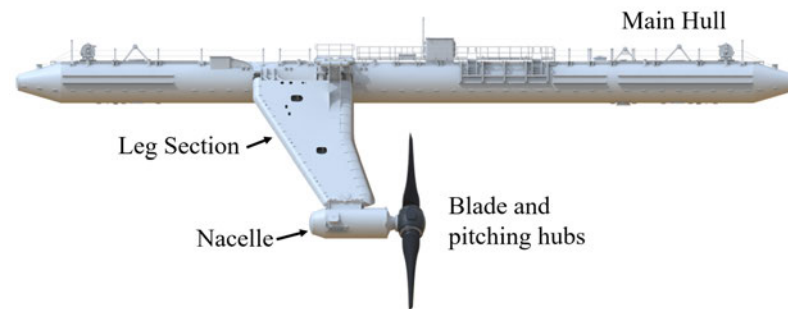


Figure 1. Side profile of the O2 2 MW tidal turbine designed, built, and installed by Orbital Marine Power.

2.2. The ADCP

A 500 kHz Nortek Signature 500 5-beam ADCP was placed on the port leg of the O2. The instrument was placed near the rotor centre, however, was offset as seen in Figures 2 and 3. The instrument was positioned horizontally pointing aft using a mounting bracket. The leg position of the ADCP avoids rotation that would be seen from a hub mounting.

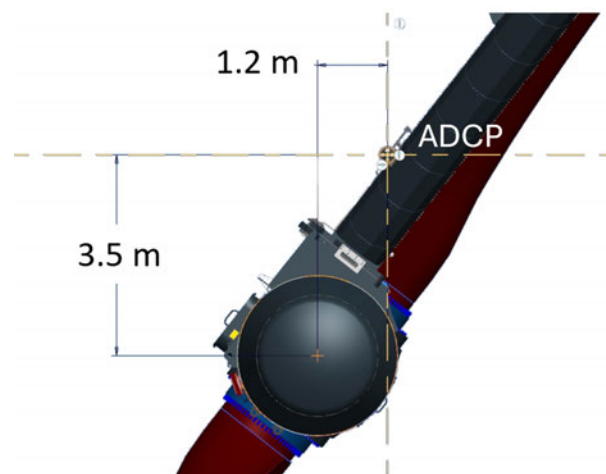


Figure 2. Leg ADCP location as viewed from aft of the O2 with distances to the hub center shown.

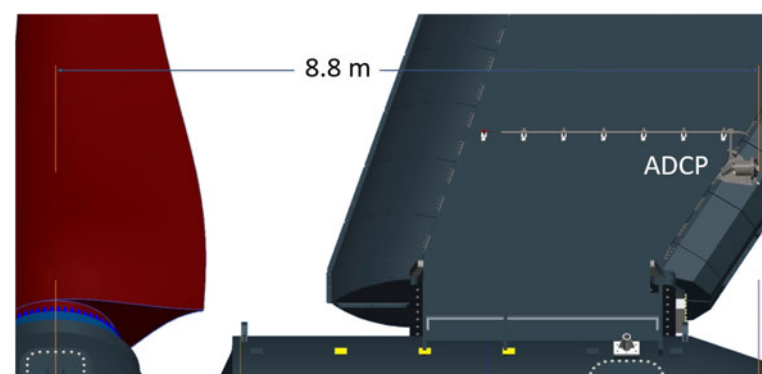


Figure 3. Leg ADCP location as viewed from the port side of the O2 with distance to the hub center shown.

The 5-beam ADCP was orientated with the central beam pointing horizontally aft with the other two pairs of diverging beams placed along the vertical and horizontal plane.

This resulted in a '+' shape when viewed from in front of the sensor head. All five of the transducers were activated, recording continuously at 4 Hz for the duration of the data set.

The coordinate system used in the analysis of horizontal ADCP data remained that of the instrument itself (see Figure 4). This results in the flow towards the sensors being on the z-axis, i.e., the turbine inline flow.

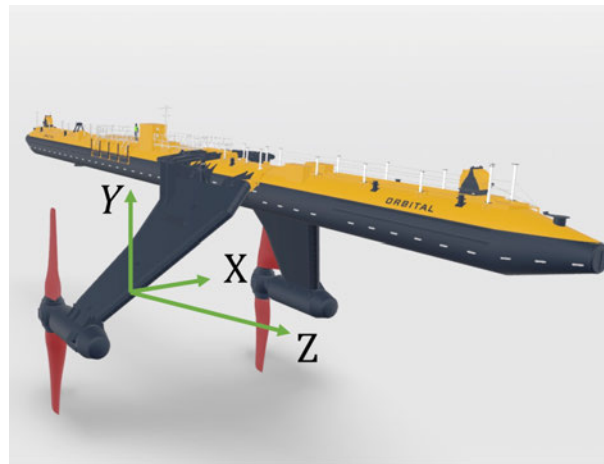


Figure 4. Leg ADCP coordinate system.

2.3. ADCP Data Set

Data were recorded using the horizontal ADCP from 1 March 2023 until 14 March 2023 representing seven tidal cycles. The horizontal ADCP logged 5 beams continuously in 1 m bins for 68 bins at 4 Hz. This time period represents a 14-day data set and covers the continuous logging of close to a full springs tidal cycle. Only flow towards the sensor was considered for this study as this represents incident resource. Flow away from the sensor was contaminated by the turbine rotor and instrument setup wake and so was not included in this study.

Figure 5 shows the environmental conditions during the data acquisition campaign. The wave height was recorded using Orbital Marine Power's in-house wave recording technique. It can be seen that the wave height remained below $H_s = 1.3$ m for the duration of the data acquisition period.

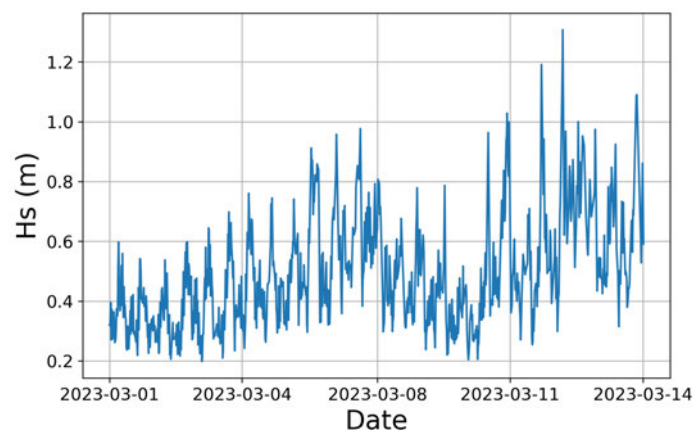


Figure 5. Significant wave height for the duration of the data set.

2.4. Data Quality Control Procedure

Quality Assurance/Quality Control of Real-Time Oceanographic Data (QARTOD) is a framework of quality control manuals for a range of oceanic measurement variables. Within QARTOD exists a framework for quality control for in situ current measurement

using an ADCP [14]. Quality control of ADCP data is used to ensure erroneous data are not included in processes performed post data collection.

The QARTOD process begins with the raw collection of data using an ADCP. Each datum in the recording is then evaluated with respect to tests and flagged as either passed, not evaluated, suspect, failed, or missing. Suspect data points are then investigated to determine their validity. Nonconformists within the data set to the QARTOD tests are removed or assigned a NaN value.

The data from the horizontal ADCP were filtered using a number of QARTOD filters (see Tables 1 and 2). Only points that passed all filters were used in the results section of this study.

Table 1. Beam filters applied to horizontal ADCP data set.

Test ID	Test Function
T6	Flag bin if amplitude is less than 30 dB
T8	Flag bin if correlation is less than 80%
T15	Flag all bins if pitch, heading, or roll rate is more than 2.5 °/s
T18	Flag if amplitude is not within 0.1 dB of previous bin
JDK1	Flag if velocity in bin is not within ± 0.5 m/s of the median of beam for that time

Table 2. Transformed filters.

Test ID	Test Function
T10	Flag bin if velocity is greater than 8 m/s
T20	Flag bin if magnitude of velocity is more than ± 0.8 m/s of the previous bin

2.4.1. Beam Quality Control—Application of QARTOD

Beam data recorded by the horizontal ADCP were filtered using QARTOD tests with constraints outlined in Table 1 with the addition of a bespoke filter for horizontal ADCP deployment. Filters were applied to each bin and each beam for the duration of the data set. Failure to meet filter criteria resulted in a flagged data point.

Filter JDK1 was applied only to the central beam of the horizontal ADCP to remove spikes from the data set. Under laminar flow conditions with streamlines parallel to a horizontal seabed, it is expected that the horizontal beam would record the same velocity at each bin distance from the sensor. This is because there are no shear profiles across the study domain as would be the case for an upward-facing, seabed-mounted ADCP. These conditions are not realised in the field; however, spikes away from the median value along the beam are considered suspect and are flagged by this filter.

Demonstration of successful data collection with stringent filters can act as a clear baseline of quality control for future studies.

2.4.2. Coordinate Transform

To convert beam velocity measurements to instrument coordinates, the beams were coordinate transformed. The output of this stage was instrument coordinate velocities from the sensor to the end of the measurement domain. The physical orientation of the beams used in the coordinate transformation determines the plane being recorded. Each opposite pair of divergent transducers can record in one plane while Beam 5 can only record directly in front of the ADCP.

One of the underpinning assumptions in the transformation of beam velocities to instrument coordinates is homogeneous flow at each bin distance from the sensor [4]. It is assumed that every beam measures the same velocity at each bin distance away from the sensor head.

2.4.3. Transformed Quality Control

The coordinate transformed flow speeds were further quality controlled with a second level of QARTOD filters (see Table 2). Each of these filters (T10 and T20) was used to de-spike the resolved data. Including a limit to velocity maximum and bin by bin velocity difference ensured that errors introduced by the transformation process were removed.

2.5. Single-Beam Range

The maximum range achievable by a horizontal ADCP in an energetic tidal environment is an important variable as it sets the domain limit for future studies with the sensor. This includes any studies using a horizontal turbine-mounted ADCP for a power performance assessment to measure the free stream tidal velocity. Developing an understanding of the ability for a horizontal ADCP to range to the free stream is important in this context.

The maximum distance to which data can be recorded is defined, in this case, as the quantity of data remaining post quality control filters. The aim of this study was not to define a maximum range but rather to demonstrate the effect of range on the volume of data remaining post quality control. It is then for the ADCP user to determine a suitable level of data rejection for their study and, therefore, the range they can expect.

2.6. Incident Flow from Divergent Beams

For a horizontal ADCP, the z -axis represents the inline flow to the turbine (see Figure 4). To record velocities along the z -axis using a 4-beam ADCP, a number of beams are combined as there is no beam directly in line with the z -axis and, therefore, no direct measurement [4]. Traditional 4-beam ADCP deployments use opposite beams to record two separate values for the z -axis velocity. The difference in these two values of z -axis velocity is then used as a quality control parameter often called the 'error velocity'. The issue with this method is that these derived values for z -axis velocity could be subject to the same error disguising them from a comparison filter.

Beam 5 of a 5-beam ADCP, like that used in this study, represents a direct measurement of the z -axis velocity (see Figure 4). As such, this study compares the direct measurement of the z -axis velocity (Beam 5) to the z -axis velocities from transformed divergent beams in a bid to quantify the true error in z -axis velocity from transformed beams when the ADCP is placed horizontally.

Due to the deployment characteristics as well as the orientation of the horizontal ADCP, Beam 4 is located closest to a boundary (the sea surface). As a result, the range of this beam is limited by surface strike. Given the depth of deployment as well as the angle of the beam to the horizontal, this beam can only reach 17 m. This can be seen in Figure 6, where the amplitude of Beam 4 increases as it strikes the sea surface. For this study, any data recorded by Beam 4 after 17 m from the sensor head were omitted.

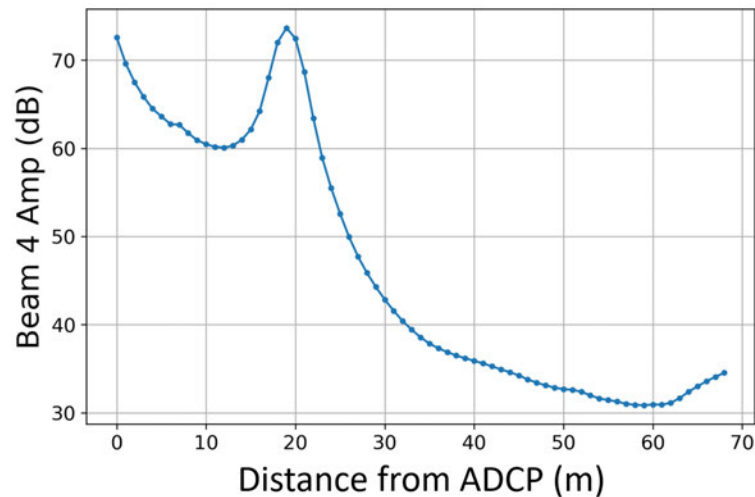


Figure 6. Mean amplitude of Beam 4 against distance in front of the horizontal ADCP showing sea surface strike around 17 m.

3. Results

3.1. Single-Beam Range

The data from Beam 5 were quality controlled using the filters outlined in Section 2.4.1. The percentage of data removed after the application of each filter can be seen in Figure 7 with negative flow speeds representing flow approaching the sensor. Positive flow speeds recorded were omitted in this study as discussed earlier.

Figure 7 shows that most of the data were able to pass through the amplitude filter (T6) in the initial 40 m of the study area. The T6 filter shows a sharp increase in data removed from 40 m to the end of the domain. This increase is seen most dramatically in the lower absolute flow speeds with less than 20% of data remaining when tide speed is between -1.5 m/s and 0 m/s beyond 50 m from the ADCP. The correlation based filter represented by T8 in Figure 7 shows a similar high pass rate for the initial study area. The decline in passing data for T8 begins at 30 m and accelerates at 40 m. Again, it can be seen that the filter removes more data at lower flow speeds. Filter T15 removes data as a result of high rates of pitch, roll, or yaw. Figure 7 shows that no data reached this threshold and so this filter had no effect on the data set. Filter T18 was designed as a method to remove spikes in amplitude due to suspended bodies in the water column. Figure 7 shows that very little data were removed by this filter. Filter JDK1 removed a large proportion of data from higher flow speeds in close proximity to the horizontal ADCP, as can be seen in Figure 7. JDK1 had a further small effect throughout the study domain with a noticeable removal of data from the mid-range region of around 25 m but a small amount when compared to T6 and T8.

Figure 7 shows the combined result of all filters used for the quality control of the beam data in this study. It is clear that between 5 m and 31 m, over 90% of data meet the requirements set out by the QARTOD filters for all flow speeds. Beyond 31 m, -2.5 m/s to -4.5 m/s sees a large removal of data. Lower speeds see a larger volume of data removal, over 90% removed, while higher absolute speeds see only around 60% of data removed by the end of the study domain.

Table 3 shows the range from the horizontal ADCP for a given acceptable data loss and flow speed. The value for acceptable data loss is to the discretion of the user and will have an impact on the uncertainty of the flow measurements. It can be seen that the full range of the sensor configuration (68 m) is reached if 60% data loss is accepted at -3.75 m/s. It can also be seen, as is shown in Figure 7, that slower flows inhibit the range of the horizontal ADCP.

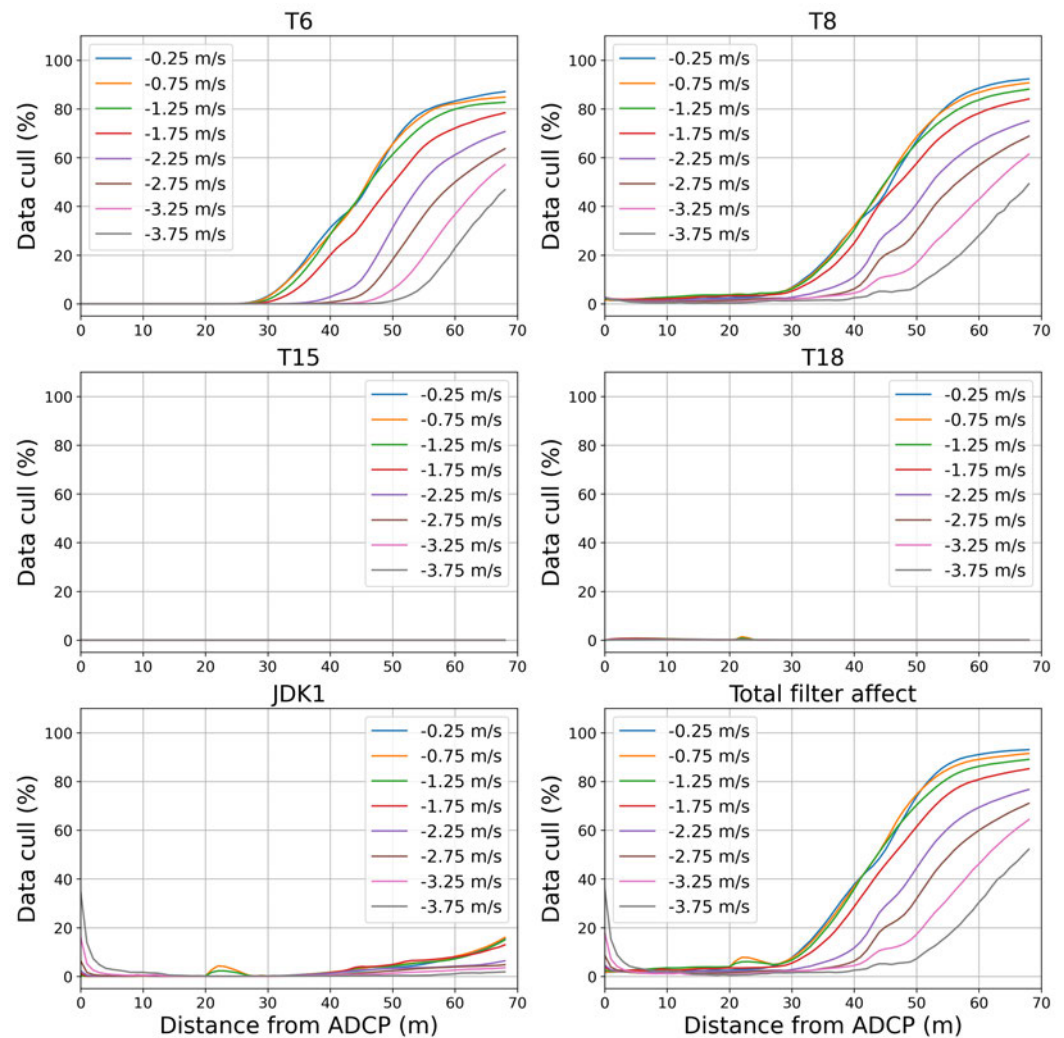


Figure 7. Percentage of data removed in Beam 5 after filters applied, as a function of distance in front of the horizontal ADCP for a range of flow speed brackets. Each sub-figure represents a different filter with each line representing a 0.5 m/s speed bracket with the bracket centre indicated. The total filter effect is shown in the bottom right sub-figure.

Table 3. Horizontal ADCP range in meters for a given acceptable data loss percentage and flow speed.

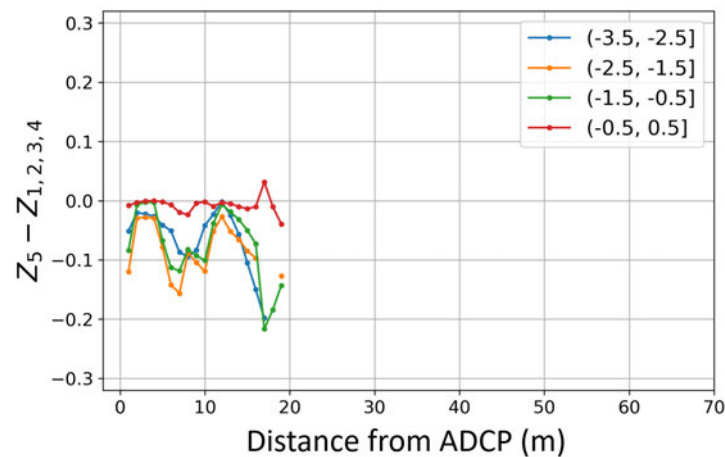
U (m/s)	Data Loss				
	90%	80%	70%	60%	50%
−0.25	57.9	51.9	49.1	46.8	44.5
−0.75	62.6	52.2	48.5	46.0	43.7
−1.25	68.0	54.3	49.9	46.5	43.7
−1.75	68.0	58.9	52.9	49.5	46.3
−2.25	68.0	68.0	60.6	54.8	51.5
−2.75	68.0	68.0	67.2	60.0	55.4
−3.25	68.0	68.0	68.0	65.7	61.4
−3.75	68.0	68.0	68.0	68.0	67.2

3.2. Incident Flow from Divergent Beams

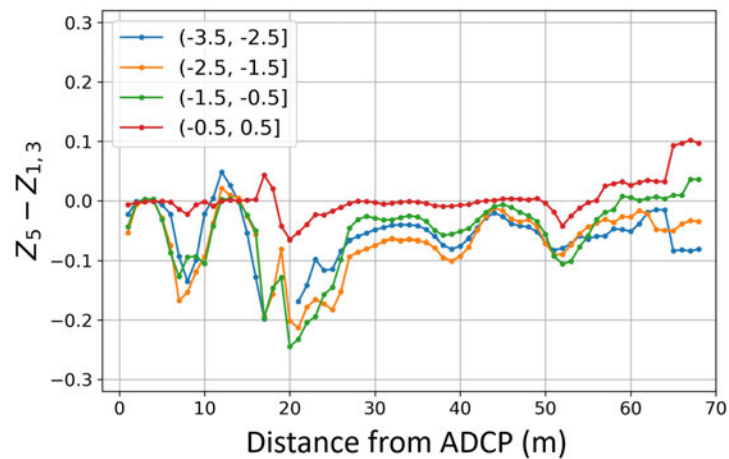
z -axis velocities recorded by Beam 5 were compared to a number of z -axis velocities derived from diverging beams. For simplicity of notation, z -axis velocities from Beam 5 will be written as Z_5 , while z -axis velocities from diverging beams will have the beam numbers

used as the subscript (e.g., z-axis velocity derived from Beams 1, 2, 3, and 4 will be written as $Z_{1,2,3,4}$).

Two different measurements of z-axis velocity were made using combinations of diverging beams: $Z_{1,3}$ and $Z_{1,2,3,4}$. The flow speed bin averages are displayed in Figure 8. Figure 8 represents the average velocity error compared to Z_5 for each distance bin. Quality control filters were applied as per Tables 1 and 2. Distance bins where more than 70% of data were removed by filters were considered beyond the range of the horizontal ADCP for this study.



(a) $Z_5 - Z_{1,2,3,4}$ against distance.



(b) $Z_5 - Z_{1,3}$ against distance.

Figure 8. Z velocity from beam combinations compared to Beam 5 against distance from the horizontal ADCP binned by flow speed.

Figure 8a shows the difference between Z_5 and $Z_{1,2,3,4}$. The absolute difference in velocity never goes beyond 0.1 m/s at low flow speeds, while higher flow speeds are responsible for more variation with distance as well as greater errors. This figure only extends to 17 m as Beam 4 strikes the sea surface after this distance, as discussed in Section 2.6.

Figure 8b shows the error in recording for $Z_{1,3}$. Using only Beams 1 and 3, $Z_{1,3}$ is able to record velocities to 68 m for slower flow speeds as well as higher speeds. The absolute error in measurement across all tide speeds is only momentarily greater than 0.2 m/s.

The majority of the span shown in the sub-figures of Figure 8 sees a negative value of Z velocity error. This suggests that the Z velocity recorded using beam transformations is higher than Z velocities recorded by Beam 5 directly, irrespective of the choice of beams.

4. Discussion

The Nortek Signature 500 data sheet indicates a maximum range of 70 m in average mode [15]. This study demonstrated that a horizontally mounted Nortek Signature 500 ADCP is not capable of profiling to the maximum range indicated by the manufacturer under every flow condition due to the high-energy nature of the environment. The range was, in fact, shown to be flow-speed-dependent for a Nortek Signature 500. Despite this dependency, 50 m represents the distance at which the horizontal ADCP could measure while maintaining over 50% of all data post rigorous quality control for all speeds for this study setup. The purpose of this study was to demonstrate a ‘percentage data rejection—range’ dependency for a single instrument, and so the percentage data rejection that correlates with ‘end of range’ is not explicitly identified. Rather, it is for the operator to determine the percentage rejection that is deemed appropriate given sensitivity and uncertainty requirements for a study on a case-by-case basis.

It is important to note that the choice of sensor frequency and power are also deciding factors in the range of an ADCP. Previous horizontal deployments of 1 MHz single-beam sensors have seen ranges much lower than this study. The 1 MHz Nortek Aquadopp single-beam ADCP placed in the nose cone of a seabed-mounted tidal turbine in [8] ranged 20.4 m, while a Nortek AD2CP 1 MHz single-beam sensor in [9] ranged 13 m upstream.

4.1. Horizontal ADCP for Power Performance Assessment

A power performance assessment is one major use-case of incident flow measurement with IEC Technical Specification (TS) 62600-200 being a major guidance document in the creation of a turbine power curve [12]. The document, in its current form, mandates incident flow measurement from a vertically profiling ADCP placed in the free stream flow. The document is very specific in the identification of incident-free stream measurement locations. For the recording of incident flow from in front of the turbine, an ADCP must be placed two to five rotor diameters upstream of, and inline with, the rotor [12]. The power performance assessment also requires flow measurement over the entire rotor capture area of the turbine.

4.1.1. Single-Beam Range

Given the required non-dimensional upstream distance for free stream flow recording according to TS 62600-200 [12], the range requirement for the use of a horizontal ADCP for incident flow recording is turbine specific. That said, the ADCP range found in [8] using a 1 MHz Nortek Aquadopp and in [9] using a 1 MHz Nortek AD2CP represented 1.75D and 0.72D of their respective turbines, where D is the turbine rotor diameter. This is much shorter than the TS 62600-200 prescribed distance of 2–5D.

The acoustic frequency of an ADCP has a bearing on the manufacturer stated range. There is, therefore, an effect on the total range when deployed horizontally as can be seen in Table 4. The values contained in Table 4 are not directly comparable, in part as the sensors were at different water column heights, but give an indication of the range achievable.

Table 4. Range of three horizontal ADCPs deployed on full-scale tidal turbines along with manufacturer-stated range including the Nortek Signature 500 studied in this paper [8,9,16].

Sensor	Manufacturer Stated Range (m)	Horizontal Range in an Energetic Tidal Environment (m)
1 MHz Nortek Aquadopp	25	20.4
1 MHz Nortek AD2CP	-	13
Nortek Signature 500	70	31 (with 10% data loss see Figure 7).

This study has shown that the range of the single central beam on the Nortek Signature 500 is flow speed specific. In order for a horizontal Nortek Signature 500 to reach the free

stream of an O₂ turbine according to the TS 62600-200 [12], the ADCP would have to range 56.6 m under all flow conditions. This is only possible with the acceptance of 90% data loss for the Nortek Signature 500 used in this study, according to Table 3.

4.1.2. Incident Flow from Divergent Beams

It is important that, within TS 62600-200, the incident flow measured represents an average of the flow speed experienced by the entire rotor diameter [12]. For a horizontal ADCP, this manifests as a beam cone the diameter of the rotor at the measurement bin. In the instance that a single ADCP beam ranges into the free stream for a specific tidal turbine, it is likely that the beam cone of a single beam will not diverge to the rotor diameter for larger turbines.

In these cases, in order to have a diverged acoustic cone the size of the rotor area, a multiple beam approach must be adopted. Figure 8 shows that beam combination is an important consideration when using a horizontally mounted ADCP in a multi-beam configuration. It is likely that one divergent beam will strike a boundary before the location of the free stream: either the sea surface (as seen in Figure 6) or the sea floor for turbines placed lower in the water column.

The transverse flow homogeneity assumed in the combination of multiple beams for instrument coordinate flow speed transformation is inherently flawed for a horizontally mounted ADCP. This is because vertical shear profiles through the water column ensure that the flow speeds across the measurement area differ. At the limit of $Z_{1,2,3,4}$, 17 m from the sensor head, the beam cone of the 25° divergent beams is 15.8 m in diameter. The difference in flow speed at the top and bottom of this beam cone can be assessed by looking at the shear profile, U , given by Equation (1), where U_{ref} is a reference velocity, h is the height above the seabed, h_{ref} is the height at which U_{ref} occurs, and α is the shear profile exponent. Assuming a $\frac{1}{5}$ th shear profile exponent [17] and a water depth of 35 m for the site, the flow speed difference between the top and bottom of the beam cone on the y -axis (see Figure 4) is as much as 14% 17 m in front of the sensor head. The shear profile has less effect on $Z_{1,3}$ as beam 1 and 3 are on the horizontal plane and so only diverge at the beam width on the y -axis (see Figure 4). In this case, only a 2% difference in flow speed between the upper and lower cone limits would be expected at 2D (56.6 m) in front of the sensor head. That said, $Z_{1,2,3,4}$ has diverged to ± 8 m on the x -axis and ± 8 m on the y -axis (see Figure 4) by 17 m, while $Z_{1,3}$ has diverged ± 26 m on the x -axis and only ± 1.4 m on the y -axis by 56.6 m. In both cases, the beam cone is not the same size and shape at the measurement location as the turbine rotor.

$$U(h) = U_{ref} \left(\frac{h}{h_{ref}} \right)^\alpha \text{ for } h \geq 0 \quad (1)$$

Figure 8 shows that the single-beam, Beam 5, measure of Z velocity (Z_5) is consistently lower than the transformed divergent beam recording in both the 4-beam and 2-beam case ($Z_{1,2,3,4}$ and $Z_{1,3}$). A power curve created using Beam 5 would, therefore, be more optimistic than a power curve using either of the divergent beam combinations presented.

4.2. Additional Applications of a Horizontal Hub Height ADCP

While a hub-mounted ADCP has been shown to provide a practical solution to floating tidal energy inflow measurement, the sensors setup can be leveraged for advancements in understanding in other areas. The O₂ does not vane between tides, resulting in the horizontal ADCP measuring the inflow on one tide and the wake on the next. Profiling along the axis of wake propagation enables a time domain view from a single profile. How this profile changes with incident flow speed, and between operating states, can also be analysed for array configurations and downstream turbine interactions.

The live and uninterrupted recording of incident flow towards a turbine from a horizontal hub height ADCP presents the possibility for controller applications. Feed

forward turbine control, like that already used in the wind industry [18,19], could reduce loads on a turbine, enabling a further reduction in costs for the developer.

5. Conclusions

The application of turbine-based sensors is key for floating tidal energy as it avoids the need for additional seabed operations. Incident flow measurement is, however, a difficult parameter to record from onboard a turbine due to the necessity for measurements to be outwith the influence of the turbine itself. Horizontal ADCPs represent a realistic means of turbine incident flow measurement.

This study shows that compliance with IEC-prescribed free stream range requirements for large tidal turbines is a challenge for horizontal ADCPs. Large turbines require a greater horizontal ADCP range as 'free-stream' location is a function of turbine diameter. As a result, more data are lost from a horizontal ADCP at the free stream of a larger tidal turbine. This has implications for uncertainty calculations. These findings pertain to the Nortek Signature 500 used in this study. Future work could apply the methodology contained in this paper to other ADCPs in order to determine a comparable metric as to how other sensors are affected by a horizontal deployment.

Standard compliant incident flow measurement for a tidal turbine power performance assessment requires flow averaged over the entire rotor diameter. This study shows that the use of divergent beams to obtain a 'rotor area-sized beam cone' can have implications on accuracy on flow speed measurements. The choice of beams is also important for divergent beam cone range.

Overall, while the deployment of horizontal turbine-mounted ADCPs offer a lower operational cost option for incident flow measurement as well as a number of additional potential use-cases, ADCP configuration and setup are important considerations prior to deployment.

Author Contributions: Conceptualization, J.D.-K., C.M. and B.S.; methodology, J.D.-K., C.M. and B.S.; formal analysis, J.D.-K.; investigation, J.D.-K.; data curation, J.D.-K.; writing—original draft preparation, J.D.-K.; writing—review and editing, J.D.-K., C.M. and B.S.; visualization, J.D.-K.; supervision, C.M. and B.S. All authors have read and agreed to the published version of the manuscript.

Funding: This work was funded by UK Research and Innovation as part of the EPSRC and NERC Industrial CDT for Offshore Renewable Energy (IDCORE), Grant EP/S023933/1.

Institutional Review Board Statement: Not applicable.

Informed Consent Statement: Not applicable.

Data Availability Statement: Restrictions apply to the availability of these data. Data were obtained from Orbital Marine Power and are available with the permission of Orbital Marine Power.

Conflicts of Interest: The authors declare no conflicts of interest. The funders had no role in the design of the study; in the collection, analyses, or interpretation of data; in the writing of the manuscript; or in the decision to publish the results.

Abbreviations

The following abbreviations are used in this manuscript:

ADCP	Acoustic Doppler Current Profiler
IEC	International Electrotechnical Commission
QARTOD	Quality Assurance / Quality Control of Real-Time Oceanographic Data
TS	Technical Specification
UK	United Kingdom

References

1. Coles, D.; Angeloudis, A.; Greaves, D.; Hastie, G.; Lewis, M.; Mackie, L.; McNaughton, J.; Miles, J.; Neill, S.; Piggott, M.; et al. A review of the UK and British Channel Islands practical tidal stream energy resource. *Proc. R. Soc. Math. Phys. Eng. Sci.* **2021**, *477*, 20210469. [CrossRef] [PubMed]
2. GOV.UK. Contracts for Difference Allocation Round 4 Results. 2022. Available online: <https://www.gov.uk/government/publications/contracts-for-difference-cfd-allocation-round-4-results> (accessed on 20 January 2024)
3. GOV.UK. Contracts for Difference Allocation Round 5 Results. 2023. Available online: <https://www.gov.uk/government/publications/contracts-for-difference-cfd-allocation-round-5-results> (accessed on 20 January 2024)
4. Nortek AS. *Signature Principal of Operation*; Technical report; Nortek AS: Rud, Norway, 2018.
5. Teledyne RD Instruments. *Acoustic Doppler Current Profiler Principles of Operation A Practical Primer*; Technical report; Teledyne RD Instruments: Poway, CA, USA, 2011.
6. Osalusi, E.; Side, J.; Harris, R. Reynolds stress and turbulence estimates in bottom boundary layer of Fall of Warness. *Int. Commun. Heat Mass Transf.* **2009**, *36*, 412–421. [CrossRef]
7. Yang, Z.; Wang, T.; Branch, R.; Xiao, Z.; Deb, M. Tidal stream energy resource characterization in the Salish Sea. *Renew. Energy* **2021**, *172*, 188–208. [CrossRef]
8. Harrold, M.; Ouro, P.; O'Doherty, T. Performance assessment of a tidal turbine using two flow references. *Renew. Energy* **2020**, *153*, 624–633. [CrossRef]
9. McNaughton, J.; Harper, S.; Sinclair, R.; Sellar, B. Measuring and modelling the power curve of a Commercial-Scale tidal turbine. In Proceedings of the 11th European Wave and Tidal Energy Conference, Nantes, France, 6–11 September 2015.
10. Sellar, B.; Wakelam, G.; Sutherland, D.; Ingram, D.; Venugopal, V. Characterisation of Tidal Flows at the European Marine Energy Centre in the Absence of Ocean Waves. *Energies* **2018**, *11*, 176. [CrossRef]
11. RealTide Consortium. *D2.2—Next Generation Flow Measurements and Flow Classification (RLT-WP2-2-PDL-0000-04)*; Technical report; The University of Edinburgh: Edinburgh, UK, 2021.
12. IEC/TS 62600-200; Marine Energy-Wave, Tidal and Other Water Current Converters-Part 200: Electricity Producing Tidal Energy Converters-Power Performance Assessment. IEC: Geneva, Switzerland, 2013.
13. TIGER. *T1.7.3 Test Procedure Report 2 IEC/TS62600-200 Feedback and Recommendations for Floating TEC Incident Resource Measurement for Power Performance Assessment*; Technical report; The Tidal Stream Industry Energiser: Cornwall, UK, 2022.
14. U.S. Integrated Ocean Observing System. *Manual for Real-Time Quality Control of In-Situ Current Observations*; Technical report; U.S. Integrated Ocean Observing System: Silver Spring, MD, USA, 2019. [CrossRef]
15. Nortek AS. *Signature 500 Technical Specifications*; Technical report; Nortek AS: Rud, Norway, 2024.
16. Nortek AS. *Aquadopp Profiler 1 MHz*; Technical report; Nortek AS: Rud, Norway, 2024.
17. Naberezhnykh, A.; Ingram, D.; Ashton, I.; Culina, J. How Applicable Are Turbulence Assumptions Used in the Tidal Energy Industry? *Energies* **2023**, *16*, 1881. [CrossRef]
18. Miquelez-Madariaga, I.; Lizarraga-Zubeldia, I.; Diaz de Corcuera, A.; Elso, J. Lidar-based feedforward control design methodology for tower load alleviation in wind turbines. *Wind Energy* **2022**, *25*, 1238–1251. [CrossRef]
19. Russell, A.J.; Collu, M.; McDonald, A.S.; Thies, P.R.; Keane, A.; Quayle, A.R. LIDAR-assisted feedforward individual pitch control of a 15 MW floating offshore wind turbine. *Wind Energy* **2024**, *27*, 317–424. [CrossRef]

Disclaimer/Publisher's Note: The statements, opinions and data contained in all publications are solely those of the individual author(s) and contributor(s) and not of MDPI and/or the editor(s). MDPI and/or the editor(s) disclaim responsibility for any injury to people or property resulting from any ideas, methods, instructions or products referred to in the content.